Stony Brook University

Solid-State NMR Spectroscopy Investigation of Phosphorus Incorporation In Calcium Carbonate

A Thesis Presented

by

Laura Marie Kubista

to

The Graduate School

in Partial Fulfillment of the

Requirements

for the Degree of

Master of Science

in

Geosciences

Stony Brook University

August 2011

Stony Brook University

The Graduate School

Laura Marie Kubista

We, the thesis committee for the above candidate for the

Master of Science degree, hereby recommend

acceptance of this thesis.

Dr. Brian Phillips- Thesis Advisor
Associate Professor, Department of Geosciences

Dr. Richard J. Reeder- Chairperson of Defense
Chair and Professor, Department of Geosciences

Dr. Troy Rasbury
Associate Professor, Department of Geosciences

This thesis is accepted by the Graduate School

Lawrence Martin
Dean of the Graduate School

Abstract of the Thesis

Solid-State NMR Spectroscopy Investigation of Phosphorus Incorporation In Calcium Carbonate

by

Laura Marie Kubista

Master of Science

in

Geosciences

Stony Brook University

2011

Phosphorus is an essential element to Earth's ecosystems its availability to organisms can depend on precipitation as a stable phosphate mineral, alone, as well as within other minerals as trace chemical or structural defects. Of these, calcium carbonate minerals are among the most reactive and abundant in many low temperature geochemical settings and often contain significant amounts of phosphorus. The concentration in which phosphorus is found in natural samples such as speleothems, corals and marine sediments has been used to create paleohydrology and paleonutrient proxies. Through the use of highly sensitive instrumental techniques it is now possible to identify individual phosphorus species in the presence of carbonate minerals to better understand phosphorus mobility and create paleoclimate proxies.

This work focuses on the uptake of phosphate during calcite precipitation using solid-state nuclear magnetic resonance (NMR) spectroscopy. The first study focuses on the speciation of phosphorus in a natural speleothem from Christmas Island, investigating the effect of

phosphorus extraction from calcite. Three phosphorus species were observed with ^{31}P NMR spectroscopy in the speleothem. The digestion of calcite by application of various acids, bases and chelating agents was used to selectively remove calcium carbonate and its effect on the distribution of the phosphate forms in the speleothem. Through the use of NMR it is possible to investigate if phosphorus species are preserved, specifically targeted, or re-precipitated as a secondary phosphorus species during dissolution treatments. Throughout these studies it was determined that none of the phosphorus species in the speleothem were specifically removed, nor were any secondary phosphorus forms precipitated; during treatment phosphorus bearing calcite appears to be removed along with phosphate-free calcite.

The second study focuses on the effects of temperature, initial phosphate concentration, pH, rate of reactant addition, and magnesium concentration on the uptake of dissolved phosphate during calcite precipitation in synthetic samples. It was determined with ^{31}P NMR spectroscopy that some variables did influence the solid in phosphorus species formed, their proportions, and the amount of phosphate included during calcite precipitation. As samples were synthesized with higher phosphate concentrations, faster reactant addition rates, higher magnesium concentrations and lower temperatures the proportion of crystalline calcium phosphates (monetite and an unidentified phase) to phosphate coprecipitated in the calcite structure decreased. Precipitation of crystalline calcium phosphates, including additional unidentified phases, and the number of species present increased at higher temperatures and slower reaction addition rates. These results suggest that the distribution of phosphate species in calcite deposits might provide insight into the conditions of calcite/phosphate coprecipitation in natural systems.

Table of Contents

List of Tables

List of Figures

Acknowledgments

I would like to thank…

...my advisor Dr. Brian Phillips for his guidance and patience throughout my time researching and writing my accompanying thesis. Furthermore for helping me discover many new personal strengths as I learned to become a better scientist…

…To my past and present lab mates Wei Li, Andrew Ilott, Harris Mason and Stacey Cochiara for teaching me instrumental techniques and being ever supportive…

…My friends in the geosciences who were sounding boards and collaborators, in particular Andrea Harrington, Alex Smirnov, and Millicent Schmidt…

..My parents and siblings, Rich and Gayle Kubista, Kristi and Kevin, their constant emotional and moral support is what kept me going. Without them I would never have found the passion for science, and would not have realized my potential…

..And finally I would like to thank my Fiancé, Richard Harrington, without your constant support and encouragement I never would have finished this work, you are my best friend.

I. Introduction to Calcium Phosphates and Solid State NMR

1.1. Overview of Phosphorus and Calcium Carbonates

Calcium phosphates have been extensively studied due to their environmental implications. Present in sediments, cave deposits, and bone the conditions on which calcium phosphates form is complex. Through the use of the concentration of phosphorus it is possible to determine past paleoclimate from natural samples [1]. In addition understanding the formation of each phosphate species can help with environmental remediation strategies [1]. The application of fertilizers and pesticides increases the phosphorus concentrations in soils and water systems, leading to eutrophication in which the increased bioactivity of certain organisms completely strips the ecosystem of other vital elements, causing a mass die off of all life [2]. Only by understanding how to make phosphorus precipitate in a phase that is stable and not biologically available can remediation in natural systems occur.

Another interest in phosphorus is its use in carbon sequestration. If introduced to algal plumes in the ocean, bioactivity would increase, consuming CO_2. The death of these microorganisms would eventually lead to a CO_2 sink. This can only work if phosphorus is readily available; phosphorus easily precipitates with calcium to form an inorganic fraction, for example calcium phosphate, that is no longer bioavailable [3]. Understanding the formation, reactivity and stability of calcium phosphates is crucial to maintain and promote ecosystem health.

Trace elements included in calcium carbonates exhibit trends that correspond to times of high/low precipitation and terrestrial changes [1, 4]. To better understand how these changes are recorded, it is imperative to understand the controls on phosphorus incorporation in low

temperature calcium carbonate deposits. Concentrations of phosphorus in calcium carbonate minerals vary depending on the amount of bioactivity that occurred during mineral precipitation, which can be linked to paleoclimate. Studies of recently formed speleothems can be matched to measured rainfall to determine the trends between phosphorus and past climates. Figure 1 shows data for the MND-S1 speleothem which formed on a boardwalk in a tourist cave in Moondyne Cave, Australia [5]. Fairchild and Treble (2009) were able to correlate the year with rainfall and other environmental variables. During times of high precipitation there were high concentrations of phosphorus. High rainfall promotes intense vegetation and bioactivity. Both magnesium and strontium were present in this speleothem; the relationship between them and other components in the minerals can be used to create a model of past conditions [6].

Stable isotopes such as those of carbon and oxygen reflect the soil dynamics and atmospheric phenomena. These systems have been extensively studied and the effects of temperature, concentration, and pH are understood. For example, it is possible to use the $\delta^{13}C$ and $\delta^{18}O$ ratio to model the age of the deposits [7]. Comparing carbon and oxygen isotope data to the concentration of trace elements, such as phosphorus and magnesium, enables scientists to delve deeper into the conditions at which the speleothems formed.

Calcium based speleothems require high pH, carbonate sources, and favorable evaporation conditions to form [8]. Figure 2 shows common conditions in which speleothems form. In caves, exposure to CO_2 in the air determines the amount of calcium carbonate precipitated at a given time along with the drip rate. Knowledge of the degree of precipitation of calcium carbonate can be used to extrapolate the CO_2 content in ancient systems. The chemical reaction of precipitation of carbonate with calcium is:

$Ca^{2+} + 2HCO_3^- \longleftrightarrow CaCO_{3(s)} + CO_{2\,(g)} + H_2O.$

There are two main calcium carbonate minerals in speleothems, calcite and aragonite. This thesis will concentrate on the formation of calcite since it is the most predominant in nature [9]. The saturation index of calcite in solution is defined as logarithmic:

$Log(SI_{calcite}) = log([Ca^{2+}][CO_3^{2-}]) - log(K_{calcite})$

$K_{calcite}$ is the solubility product of calcite for the temperature of the reaction (T) [9]. The solubility product at 25˚C is 4.5×10^{-9} [7]. Trace elements are also present in natural systems during calcite formation; depending on the conditions they can adsorb to the surface of calcite, substitute in the mineral structure during crystallization, or precipitate as a separate mineral.

Careful distinction between phosphorus and phosphate must be made. Phosphorus is an element that may combine with many other elements. In natural systems, the form of phosphorus that is bioavailable is organic or dissolved orthophosphate. Hence, it can be assumed that these forms would be present in phosphorus deposits [10]. In most common minerals phosphorus is found in its most oxidized form, phosphate (PO_4^{3-}). Dissolved phosphate can occur as a byproduct of phosphorus from plants from decomposition of organic phosphorus [9]. Common forms of organic phosphorus found in plants include phytin, phospholipids, and nucleic acid. This phosphorus anion easily associates with other elements such as calcium, iron and magnesium. Almost all the phosphorus present on earth is in an inorganic phosphate form. Phosphate minerals include wavellite, vivianite, and those of the apatite group [9]. The solubility of the minerals it forms depends on the coordination of the phosphorus and the chemical composition [11]. In the experiments conducted in this thesis, the phosphorus mentioned will be assumed to be in the phosphate form, unless otherwise mentioned because

dissolved inorganic phosphate is the most common form in fluids from which calcite precipitates. Phosphate present in natural systems comes from biogenic, marine, igneous, agricultural and metamorphic deposits; the weathering of this material provides the transportation and its re-precipitation of phosphate in environmental systems [9].

Phosphate can react directly with calcium to precipitate as calcium phosphate minerals or co-precipitate with calcite. Possible reactions for the substitution of carbonate with phosphate include:

$$3(CO_3^{2-})_S + 2(PO_4^{3-})_{aq} \rightarrow 3(CO_3^{2-})_{aq} + 2(PO_4^{3-})_S + \square$$

Where □ is a vacant carbonate site

Or $CO_3^{2-}{}_{(s)} + HPO_4^{2-}{}_{(aq)} = HPO_4^{2-}{}_{(s)} + CO_3^{2-}{}_{(aq)}$

[12]

There are many other reactions possibly, but they are simply not known. Depending on the condition, different calcium phosphate minerals can form [13]. A slight increase in phosphate concentration, temperature or precipitation rate can yield entirely different calcium phosphate species. By understanding how each type of calcium phosphate forms, it is possible determine the past environmental conditions [1]. Previous work on the synthesis of calcium phosphates will be discussed in Chapter 3.

Analysis of phosphate in natural samples is often difficult due to the low concentrations. Speleothems typically contain only trace amounts of phosphorus. The average speleothem has concentrations ranging from 30-100 μg P g^{-1}, but some samples have been discovered with 3,000-5,000 ppm phosphorus [14].

Phosphorus is not the only impurity that affects the precipitation of calcite. Other elements that are being studied include iron, magnesium and strontium [1, 15]. Precipitation of calcite in oceans is dominated by biological processes. It has been found that magnesium and phosphorus contribute to the inhibition of crystallization. Mucci (1986) determined that not only do the concentrations of phosphate and magnesium determine the rate of precipitation of calcite, but they also determine the amount of calcite precipitated [16-17].

Techniques such as X-ray Diffraction (XRD) and X-ray absorption spectroscopy (XAS) cannot detect the form of phosphorus at concentrations typically found in natural samples. In addition phosphate can occur in nonstoichiometric phases or solid solutions which are hard to distinguish with XRD and XAS [18]. Techniques such as inductively coupled plasma mass spectrometry (ICPMS) can only determine the concentration of phosphorus, providing no structural information [19]. Through the use of Solid State Nuclear Magnetic Resonance (NMR) it is possible to determine the form of phosphorus and structural information of calcium phosphates. Mason et al. (2007) obtained a stalagmite from Grotta di Ernesto, Italy and it was analyzed by NMR to determine the phosphate species present, Figure 3. The data exhibited three peaks, which were assigned to monetite, phosphate substitutions in calcite and a second crystalline phosphate phase that could not be identified. Phosphorus concentrations in this sample were average, 30-100 ppm [14].

1.2. Calcium Phosphate Phases

Common calcium phosphate phases include hydroxylapatite, monetite, brushite, octacalcium phosphate and amorphous calcium phosphate [13]. The following paragraphs are a

brief introduction to these forms, and the implications that they can give if found in the natural system.

Hydroxylapatite(HAP), $Ca_5OH(PO_4)_3$, is the most common calcium phosphate mineral found in natural systems [13]. The structural bonds between phosphorus, oxygen and calcium stabilize the mineral making it relatively insoluble at low pH and high temperatures. HAP is resistant to many chemical treatments, such as by chelators and acids. Evidence of this compound in natural samples suggests high concentrations of source phosphate and higher ambient temperatures. This insinuates periods of high bioactivity. The peak for HAP in ^{31}P NMR spectra is a distinct sharp peak located at 2.8 ppm [13, 20]. The saturation index of HAP is:

$$Log(SI_{HAP}) = 5log[Ca^{2+}] + 3log[H_2PO_4^-]$$

Owing to its small K_{HAP} (log K= -44.333) and slow rates of nucleation, many natural waters are oversaturated with respect to HAP if measurable concentrations of phosphate are present.

Monetite, $Ca(HPO_4)$, is the least stable of crystalline calcium phosphates. This triclinic structure provides three locations for the proton to move. Commonly found in cave deposits, it forms from bat guano deposited over time. Monetite is one of the lesser studied calcium phosphates with Solid State NMR spectroscopy due to its complexity. Due to the multiple locations available for the proton to move to, monetite can exhibit one or two peaks,$\delta_{P\text{-}31}$= -0.3 and $\delta_{P\text{-}31}$= -1.7, during ^{31}P NMR experiments depending on the strength of the ^{1}H decoupling applied [20].

Brushite, $CaHPO_4*2H_2O$, is the hydrated form of monetite. It is commonly found in damp caves, at low pH (<6), along with the bat guano [21]. Synthesis of this material is

completed using water, or exposing monetite to high humidity. Brushite has monoclinic symmetry, the phosphate being bonded to water creating a weak bond that is easily dissolved in solution. The ^{31}P NMR peak shift of Brushite is $\delta_{P\text{-}31}$= +1.4 ppm [20].

Octacalcium phosphate (OCP), $Ca_8H_2(PO_4)_6*5H_2O$, a precursor to HAP, is commonly found in tooth enamel, bones and dentine. This calcium phosphate has a similar structure to apatite, and when treated with heat easily decomposes to HAP. Due to its potential for biomedical application, such as bone grafting, it is being extensively studied. ^{31}P NMR spectra of poorly crystalline OCP show two broad peaks at 2.8 and -0.5 [13, 20]. While as Tsen et al. (2004) observed four ^{31}P peaks at -0.2, 2.0, 3.3 and 3.7 ppm using POST-C7 pulse sequence [22]. The tendency for OCP decomposing to HAP means that it is not commonly found in sediments or cave systems and was not studied in this thesis.

The least stable of calcium phosphates is amorphous calcium phosphate (ACP). It is non-crystalline, making it difficult to determine its properties with instrumental techniques. The formation and general stability of this compound is poorly understood. At times it seems to be highly reactive and crystallizes, while in other situations it remains stable for years [23]. ACP is believed to be the first step in the formation of any crystalline calcium phosphate from highly oversaturated solutions [2]. ACP is easily recognized with ^{31}P NMR, it yields a broad peak at $\delta_{P\text{-}31}$= 3.0 ppm. Yet, this peak location overlaps with peaks from other common phosphate minerals, and the use of multiple different pulse sequences is necessary to identify ACP with confidence.

1.3. Solid State Nuclear Magnetic Resonance (NMR) Spectroscopy

Nuclear Magnetic Resonance (NMR) spectroscopy is the application of a resonant magnetic field to change the orientation of the magnetic moment of a nucleus. Some isotopes of elements have nuclei that exhibit magnetic moments. The elements studied in this thesis (^{1}H, ^{31}P) have a spin of I=1/2 so they can take one of two orientations in an applied magnetic field. The energy difference between these orientations can be detected when a much larger static magnetic field is applied, this is called Zeeman interaction. The energy is:

$$E= -m\gamma\hbar B_0$$

Where γ is the magnetogyric ratio, m is the spin angular momentum quantum number (½ or -½) and B_0 is the external field applied to the sample. The energy difference between magnetic orientations is:

$$\Delta E= \gamma\hbar B_0 = \hbar\omega_0$$

Where ω_0 is the Angular Larmor frequency. This ΔE results in a slight population difference between the m= ½ and m= -½ orientations, that can be changed by application of radiation at frequency ω_0. This population difference gives rise to a net magnetic moment that can be observed. To collect signal using NMR, a short pulse is applied that rotates the net magnetic moment away from B_0, about which it ω_0 giving the free induction decay (FID) in which the nuclear magnetic moments relax down to their equilibrium population state. The signal is processed using a Fourier transformation (FT) to obtain a frequency spectrum. Each isotope has a specific value for γ, and ω_0 at a fixed B_0. By applying only the frequency (ω_0) that is correlated to the element being investigated, it is possible to collect element specific data. The frequencies detected back from the mineral are shifted slightly by interactions with electrons in a way that is

sensitive to bonding structure. This effect is called the chemical shift. The equation that describes the chemical shift is:

$\nu_{obs} = \nu_0(1+\delta) = (\omega_0/z\pi)(1 + \delta)$

Where ν_{obs} is the observed frequency of the peak, ν_0 is the Larmor frequency (ω_0 in angular units), and δ is the chemical shift in relative units (typically ppm). The frequencies observed are relative, and must be referenced to a standard. One limiting factor with solid state NMR is an element must have a net spin not equal to zero to produce signal when a magnetic field is applied. Other difficulties that arise include low concentration of elements or NMR-Active isotopes, and paramagnetic element.

1.4. NMR Techniques Used

Multiple techniques were used to analyze the samples. Through the use of multiple pulse programs it is possible to get an accurate representation of the chemical bond properties of minerals and the spatial proximity of different elements to each other.

1.4.1. Magic Angle Spinning (MAS)/Single Pulse

The most basic method of analyzing solid samples is through single-pulse excitation combined with magic angle spinning (MAS). Powder samples provide broad patterns because frequency shifts due to chemical shift and dipolar interactions depend on the orientation with respect to the magnetic field, B_0. In the 1950's it was discovered that if a sample was titled at a 54.74˚, also known as the magic angle, along the B_0 axis, and spun about this axis, it was

possible to eliminate some of the broadening that was caused by these anisotropic nuclear spin interactions. In addition to this narrowing of the peak, spinning side bands could be observed which are artifacts of the MAS technique and spaced at the spinning frequency. These bands can provide structural information such as the magnitude of the Chemical Shift Anisotropy (CSA). The most basic NMR experiment applies a single pulse (SP), after which one can detect all the forms of a particular element. Through comparison of intensity it is possible to quantify the proportions of each species if the magnetization is allowed to fully relax between each acquisition, and if the weight of the sample is known, when referenced to a standard it is even possible to determine the concentration of the element in the sample [24]. SP is acquired through the application of a 90˚ pulse in which the net magnetic moment is rotated 90˚ away from B_0. After which the net magnetic moment processes around B_0 at frequency ν_{obs}, which induces an alternating voltage at this frequency in a detection coil, see Figure 4.

1.4.2. Cross polarization (CP)

Under a strong external magnetic field spin flips of one type of nucleus does not cause spin flips in another type, because energy is not conserved. Hartmann and Hahn solved this issue by developing the pulse sequence cross polarization (CP) which allows magnetization to transfer among different types of nuclei. In this they use dipolar coupling which allows energy transfer-spin flips in the applied transverse (Rotating) magnetic fields. The Hartmann-Hahn conditions are:

$$\gamma_I B_{1,I} = \gamma_S B_{1,S}$$

or

$\nu_{1,I} = \nu_{1,S}$

[25]

Where I and S are two different types of nuclei (e.g., ^{31}P and ^{1}H) γ_I, γ_S are magnetogyric ratios, and $B_{1,I}$ and $B_{1,S}$ are the applied transverse fields, which result in precession about the applied fields at rates ν_1. Figure 5 shows the CP pulse sequence. A pulse is applied to the secondary element, typically ^{1}H, after which a contact pulse is applied. This contact pulse allows the elements, ^{1}H and ^{31}P, to "communicate" and transfer spin in such a way that signal is observed only from ^{31}P that are near ^{1}H nuclei. Finally the proton is decoupled and signal from the ^{31}P is detected. The contact time needed varies depending on the distance between the elements. It is possible to get structural information by plotting contact time versus intensity of signal [26]. The rate at which ^{31}P signal builds-up is a measure of the dipole coupling-which depends on the spatial proximity between nuclei as the sum of $d(I\text{-}S)^{-3}$. CP revolutionized the detection of different elements, in that it was possible to detect the relative proximity of two different elements to each other. In addition, some single elements have a long T_1-spin lattice relaxation time. Through the use of CP it is possible to indirectly observe the element by applying the pulse on something that has a much shorter T_1, thus dramatically decreasing the acquisition time [27].

1.4.3. Heteronuclear Correlation (HETCOR)

Correlation of specific peaks from nucleus I (e.g. ^{31}P) with those of nucleus S (e.g. ^{1}H) based on spatial proximity can be obtained as 2-D data through a manipulation of the CP sequence called Heteronuclear Correlation (HETCOR). Figure 6 shows the HETCOR pulse sequence. The only manipulation of the sequence is the addition of a t_1 delay on the ^{1}H source

spin. This delay allows the ^{1}H magnetic moment to rotate around B_0 at a rate determined by its chemical shift before the contact pulse transfer the polarization from ^{1}H to the ^{31}P. Fourier transformation $t_2 \rightarrow F_2$ and $t_1 \rightarrow F_1$ gives a 2-D map of $^{1}H(F_1)$ and $^{31}P(F_2)$ chemical shifts with cross-peaks between them corresponding to the specific ^{1}H from which magnetization was transformed to ^{31}P. The data from this experiment can be used to create a map of proton relationship with ^{31}P, giving information on relationship to water and other associated protons.

1.4.4. Rotational Echo Double Resonance (REDOR)

The use of Rotational Echo Double Resonance (REDOR) provides clearer structural information on the distance between nuclei than does that of CP. In addition, it is possible to measure the interatomic distance between different nuclei, not limiting the acquisition to that of ^{1}H. For example one can observe the proximity between ^{13}C and ^{31}P. Figure 7 shows the pulse sequence. A series of π pulses are applied during each rotor period to ensure that the dipole coupling is not averaged to zero over each rotor period.

The Spin Echo experiment applies two pulses to the ^{1}H channel. The first, 90˚, is followed by a period in which spin-spin relaxation and inhomogeneous effects can occur. The application of a second pulse, 180˚, refocuses the magnetization by inverting the magnetization vectors. The second pulse must is applied after time τ, and signal is collected after 2τ. Figure 8 shows this pulse sequence. If the dipolar coupling is fully averaged, then the signal intensity (S_0) is completely recovered at time 2τ. To determine the REDOR effect the signal intensity of a spin echo experiment (S_0) is compared to that of the REDOR in which the π pulses on the second (non-observed) nucleus prevent averaging of the dipolar coupling. The difference (S0-S)

depends on the interatomic distances, number of nearby nuclei, and the length of the dephasing period.

1.4.5. Specific Elemental Analysis with NMR Spectroscopy

This thesis analyses three elements with NMR spectroscopy, ^{31}P, ^{13}C, and ^{1}H. Both ^{13}C and ^{1}H analysis was performed only after determining phosphate phase, it is not necessary to discuss common peak shifts and forms for this study. The only naturally occurring isotope of phosphorus is ^{31}P, spin ½, enabling all the phosphorus species in a sample to be detected by NMR [28]. Most of the phosphorus compounds give rise to a singlet at a well-defined position. The protonation of calcium phosphates distinctly changes the peak location, in that it moves the isotropic chemical shift upfield [13]. Peak locations for species of phosphorus tend to fall between 25 to -25 ppm in reference to environmental samples [28]. The ^{31}P NMR reference is 85% H_3PO_4 which is set to 0 ppm and all peaks are shifted in respect to this. This thesis concentrates on the region in which orthophosphates are found, between 5 to -1 ppm, yet this region overlaps with other forms of phosphorus, and is not inclusive. Other regions for phosphorus include 30 to 15 ppm phosphonates, 12 to 0 ppm Monester phosphates, 1 to -5 ppm Diester phosphates and -10 to -25 ppm Tri- & Tetraphosphates. Chemical shifts depend primarily on molecular shielding around the phosphorus nuclei but pH, ionic strength, and probe temperature can slightly change the signal [29].

1.5. Summary of Chapters

This thesis investigates the inclusion of trace amounts of phosphate in calcite in both natural and synthetic samples. In chapter 2 the digestion and preservation of calcium phosphates in a natural sample is studied. In chapter 3, the investigation of the effects of phosphate and magnesium concentration on the form of phosphate in precipitates of calcite is investigated. In addition chapter 3 uses solid state NMR to determine if changes in temperature, rate, pH, and concentration of phosphate affects the distribution of phosphate coprecipitated with calcium carbonate.

1.6. References

1. Huang, Y., et al., *Seasonal variation in Sr, Mg and P in modern speleothems (Grotta di Ernesto, Italy).* Chemical Geology, 2001. **175**: p. 429-448.

2. Griffin, R.A. and J.J. Jurinak, *The Interaction of Phosphate with Calcite.* Soil Sci. Soc. Amer. Proc, 1973. **37**: p. 847-850.

3. House, W.A. and L. Donaldson, *Adsorption and Coprecipitation of Phosphate on Calcite.* Journal of Colloid and Interface Science, 1986. **112**(2): p. 309-324.

4. Baldini, J.U., F. McDermott, and I.J. Fairchild, *Structure of the 8200-Year Cold Event Revealed by a Speleothem Trace Element Record.* Science, 2002. **296**(5576): p. 2203-2206.

5. Fairchild, I.J. and P.C. Treble, *Trace elements in speleothems as recorders of environmental change.* Quaternary Science Reviews, 2009. **28**: p. 449-468.

6. Fairchild, I.J., et al., *Annual to sub-annual resolution of multiple trace-element trends in speleothems.* Journal of Geological Society, 2001. **158**(5): p. 831-841.

7. Frisia, S. and A. Borsato, *Developments in Sediments*. Carbonates in Continental Settings, ed. A.J. Van Loon. Vol. 61. 2010, Netherlands: Elsevier.

8. Brasier, A.T., *Searching for travertines, calcretes and speleothems in deep time: Processes appearances, predictions and the impact of plants.* Earth-Science Reviews, 2011. **104**: p. 213-239.

9. Aydin, I., et al., *Determination of mineral phosphate species in sedimentary phosphate rock in Mardin, SE Anatolia, Turky by sequential extraction.* Microchemical Journal, 2009. **91**: p. 63-69.

10. Sykes, G.A., M.J. Collins, and D.I. Walton, *The significance of a geochemically isolated intracrystalline organice fraction within biominerals.* Org. Geochem., 1995. **23**(11/12): p. 1059-1065.

11. Morse, J.W. and R.S. Arvidson, *The dissolution kinetics of major sedimentary carbonate minerals.* Earth-Science Reviews, 2002. **58**: p. 51-84.

12. Ishikawa, M. and M. Ichikuni, *Coprecipitation of phosphate with calcite.* Geochemical Journal, 1981. **15**: p. 283-288.

13. Rothwell, W.P., J.S. Waugh, and J.P. Yesinowski, *High-Resolution Variable-Temperature ^{31}P NMR of Solid Calcium Phosphates.* Journal of the American Chemical Society, 1980. **102**(8): p. 2637-2644.

14. Mason, H.E., et al., *Phophorus Speciation in Calcite Speleothems Determined from Solid-State NMR Spectroscopy.* Earth and Planetary Science Letters, 2007. **254**: p. 313-322.

15. Meyer, H.J., *The influence of Impurities on the growth rate of calcite.* Journal of Crystal Growth, 1984. **66**: p. 639-646.

16. Mucci, A., *Growth kinetics and composition of magnesium calcite overgrowths precipitated from seawater: Quantitative influence of orthophosphate ions.* Geochemica et Cosmochimica Acta, 1986. **50**: p. 2255-2265.

17. Zhong, S.J. and A. Mucci, *Calcite precipitation in seawater using a constant addition techinique: a new overalll reaction kinetic expression.* Geochimica et Cosmochimica Acta, 1993. **57**: p. 1409-1417.

18. Yesinowski, J.P. and H. Eckert, *Hydrogen Environments in Calcium Phosphates: ^{1}H MAS NMR at High Spinning Speeds.* J. Am. Chem. Soc., 1987. **109**: p. 6274-6282.

19. Glimcher, M.J., et al., *Recent studies of bone minerals: Is the amorphous calcium phosphate theory valide?* J. Crystal Growth, 1981. **53**: p. 100-119.

20. Aue, W.P., et al., *Solid-State Phosphorus-31 Nuclear Magnetic Resonance Studies of Synthetic Solid Phases of Calcium Phosphate: Potential Models of Bone Mineral.* Biochemistry, 1984. **23**: p. 6110-6114.

21. Hill, C.A., *Mineralogy of Kartchner Caverns, Arizona.* Journal of Cave and Karst Studies, 1999. **61**(2): p. 73-78.

22. Tseng, Y.-H., et al., *High resolution ^{31}P NMR study of octacalcium phosphate.* Solid State Nuclear Magnetic Resonance, 2004. **26**(2): p. 99-104.

23. Tropp, J., N.C. Blumenthal, and J.S. Waugh, *Phosphorus NMR study of solid amorphous calcium phosphate.* J. Am. Chem. Soc., 1983. **105**(1): p. 22-26.

24. Mason, H.E., et al., *Phosphate defects and apatite inclusions in coral skeletal aragonite revealed by solid-state NMR spectroscopy.* Geochemica et Cosmochimica Acta, In review.

25. Hartmann, S.R. and E.L. Hahn, *Nuclear Double Resonance in the Rotating Frame.* Phys. Rev., 1962. **128**(5): p. 2042-2053.

26. Kolodziejski, W. and J. Klinowski, *Kinetics of cross-polarization in solid-state NMR: A guide for chemists.* Chemical Reviews, 2002. **102**: p. 613-628.

27. Feng, J., et al., *NMR Spectroscopy of Citrate in Solids: Cross-Polarization Kinetics in Weakly Coupled Systems.* Magnetic Resonance in Chemistry, 2008. **46**: p. 408-417.

28. Cade-Menun, B., *Characterizing phosphorus in environmental and agricultural samples by 31P nuclear magnetic resonance spectroscopy.* Talanta, 2005. **66**: p. 359-371.

29. Turner, B.L., N. Mahieu, and L.M. Condron, *Phosphorus-31 Nuclear Magnetic Resonance Spectral Assignments of Phosphorus Compounds in Soil NaOH-EDTA Extracts.* Soil Sci. Soc. Am. J., 2003. **67**: p. 497-510.

1.7. Figures

Figure 1. Rainfall relationship with trace and minor elements [1].

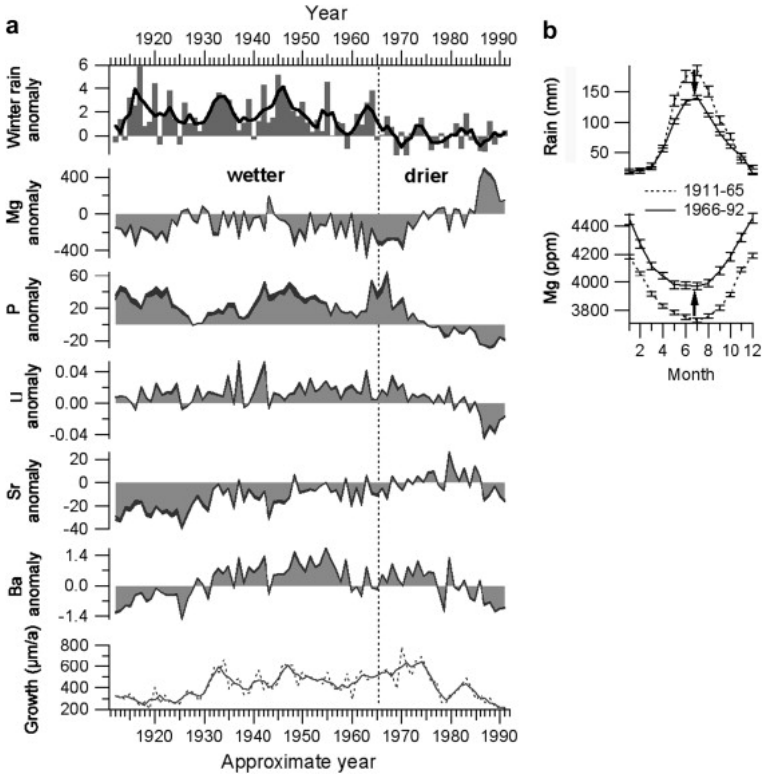

Figure 2. Formation of carbonate in caves diagram.

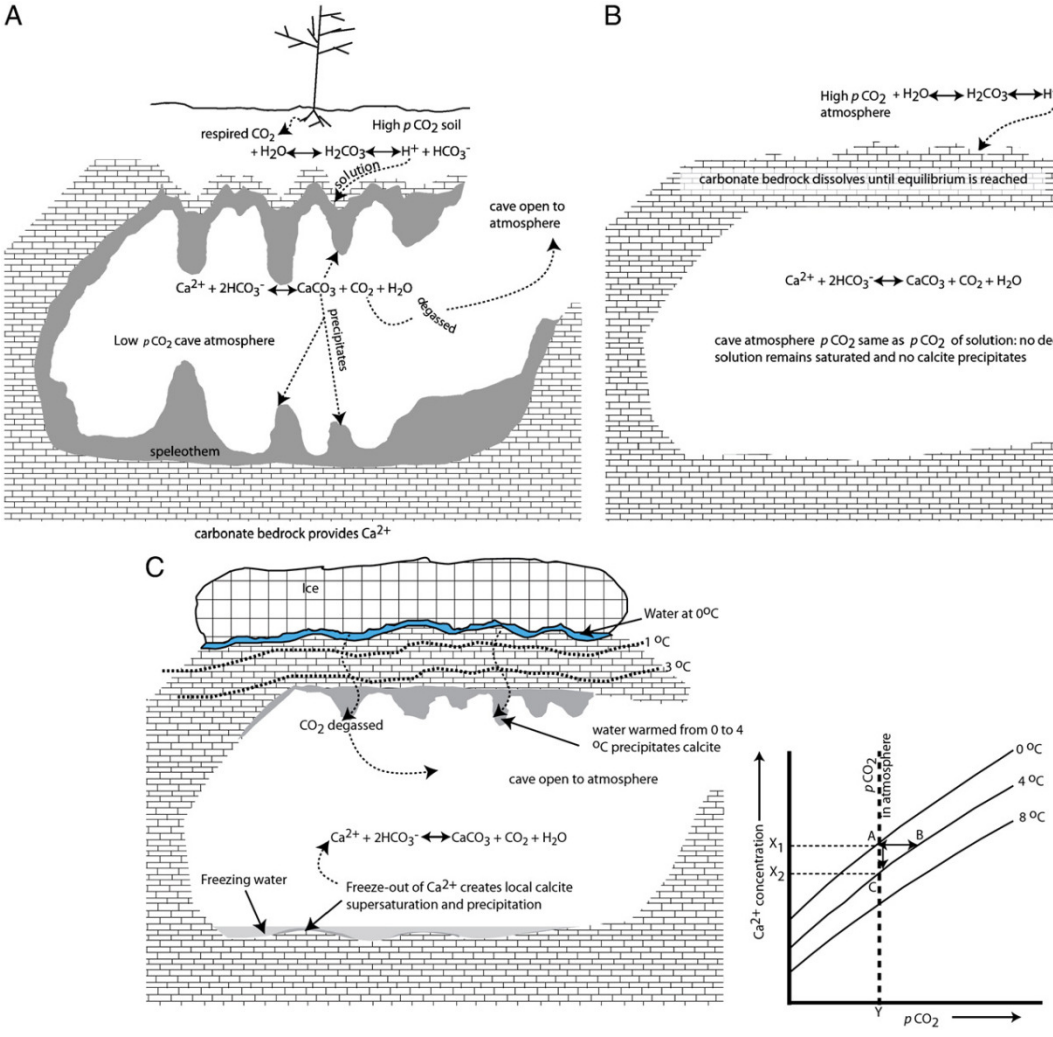

[8].

Figure 3. ^{31}P Single Pulse Spectra of Stalagmite from Grotto di Ernesto, Italy analyzed by Harris Mason [14].

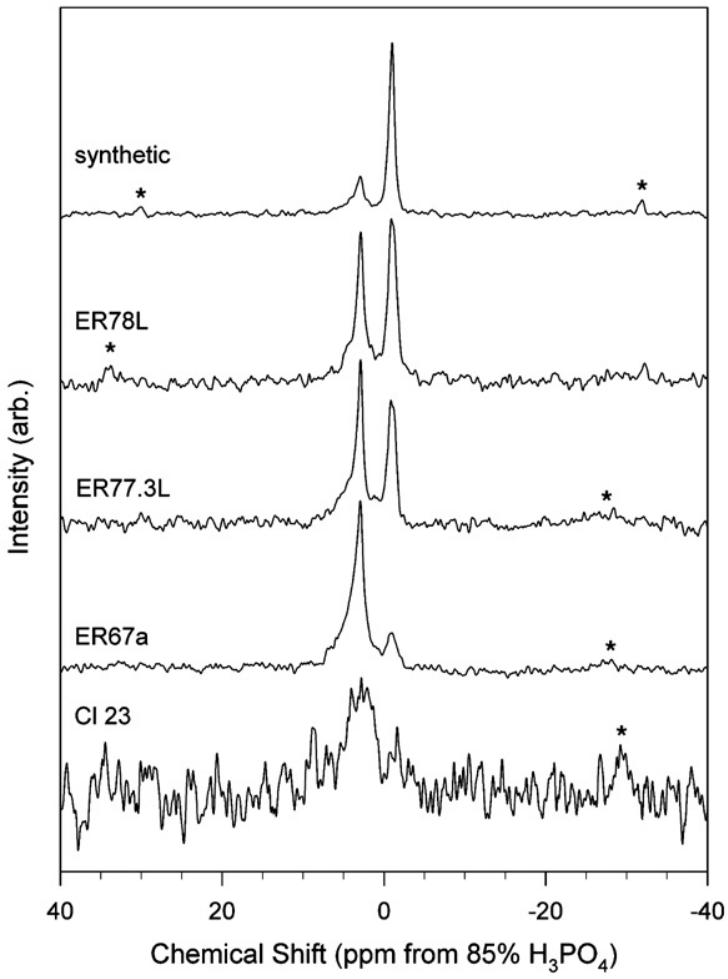

Figure 4. Single Pulse Program for observing an NMR signal. Horizontal axis is time, vertical axis is voltage for excitation and signal.

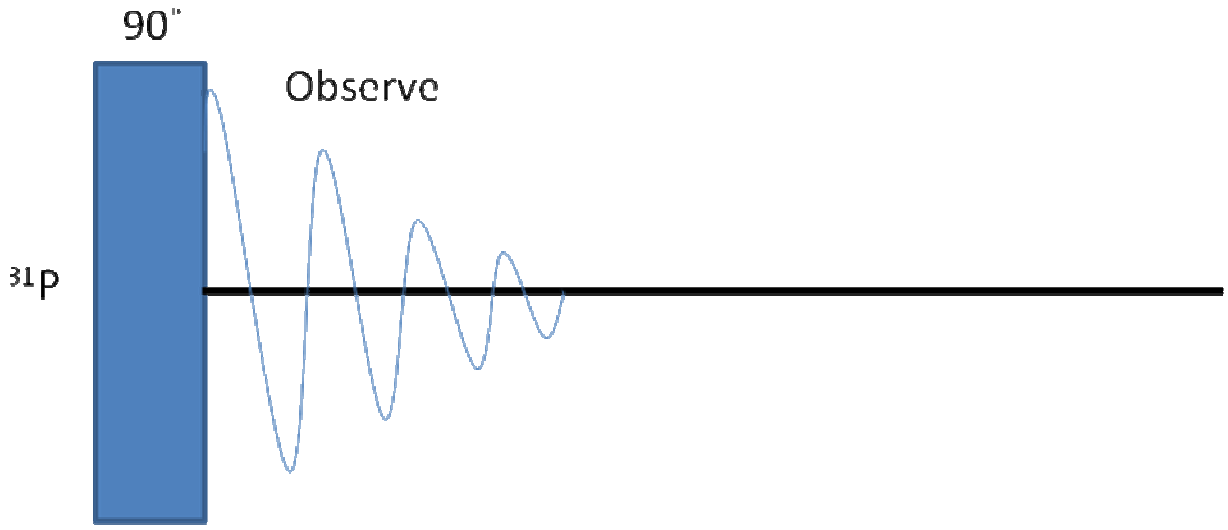

Figure 5. Cross Polarization Pulse Program for observing an NMR signal. Horizontal axis is time, vertical axis is voltage for excitation and signal.

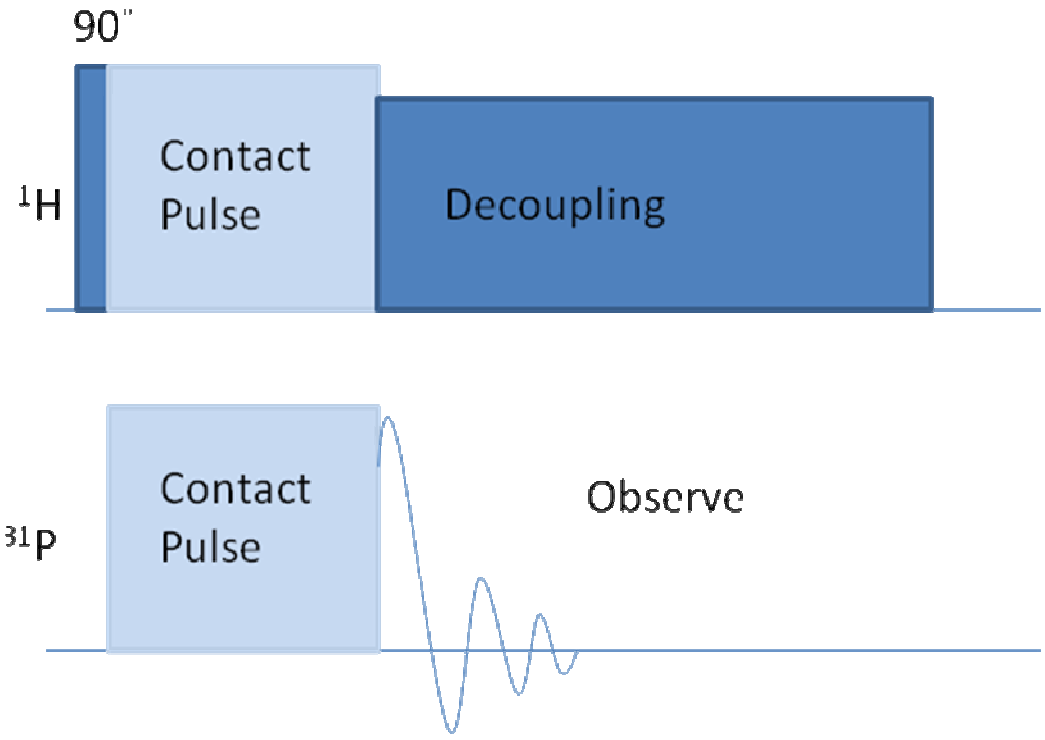

Figure 6. Hetcor Pulse Program for observing an NMR signal. Horizontal axis is time, vertical axis is voltage for excitation and signal.

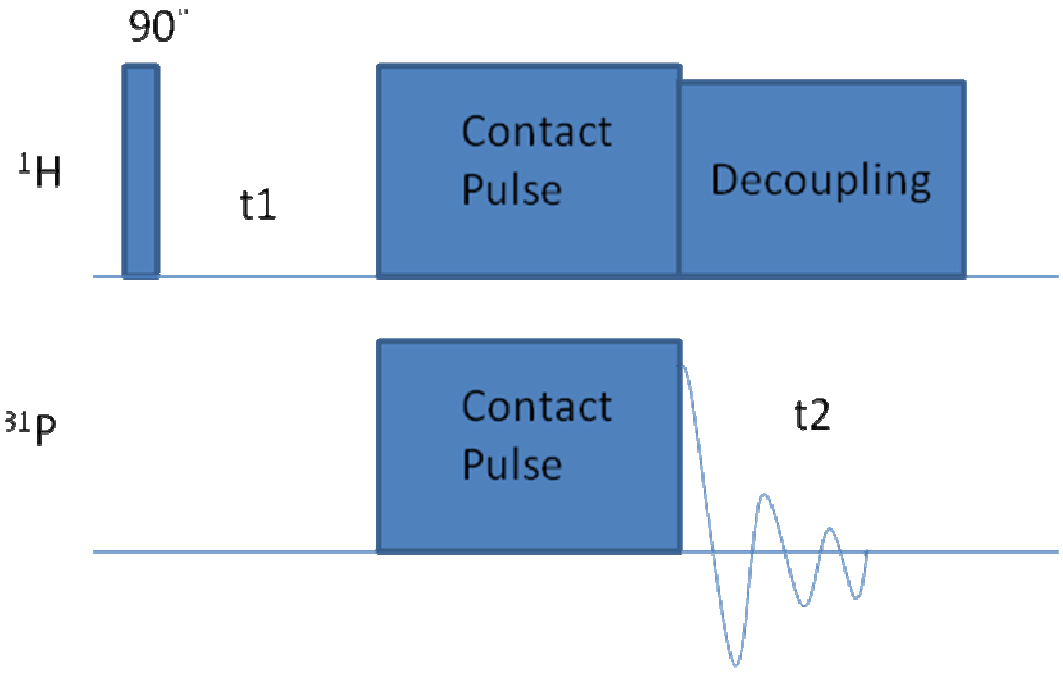

Figure 7. REDOR Pulse Program for observing an NMR signal. $\omega_{D,H\text{-}P}$ is the frequency of dipolar coupling between ^{1}H and ^{31}P. Note that the average is different between the ^{1}H 90˚ and the 180˚ pulses, and after the 180˚ pulse. Compare to Figure 8. Horizontal axis is time, vertical axis is voltage for excitation and signal.

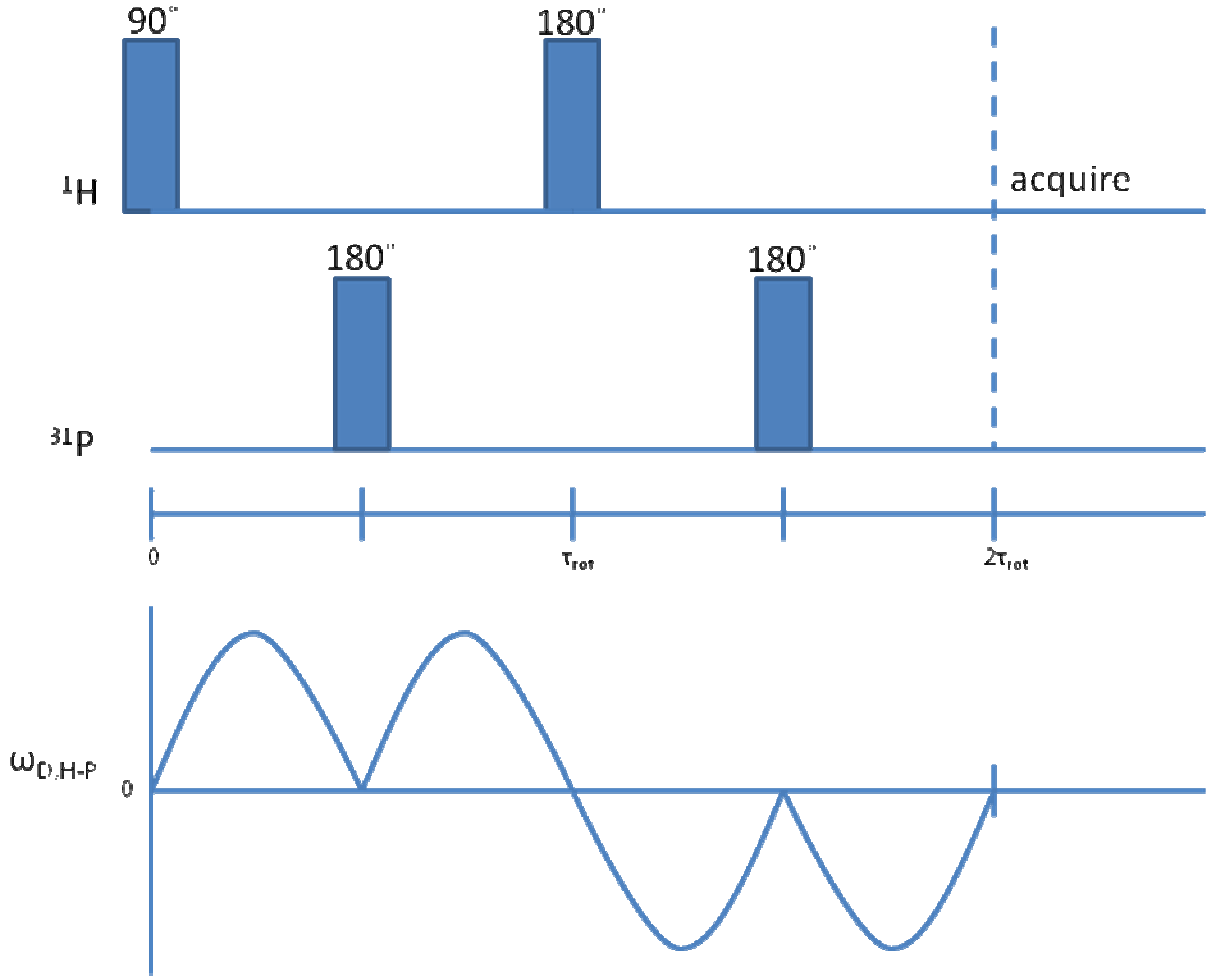

Figure 8. Spin-Echo Pulse Program for observing an NMR signal. $\omega_{D,H\text{-}P}$ is the frequency of dipolar coupling between ^{1}H and ^{31}P. Note that the average of $\omega_{D,H\text{-}P}$ is zero between the ^{1}H 90° and the 180° pulses, and after the 180° pulse. Horizontal axis is time, vertical axis is voltage for excitation and signal.

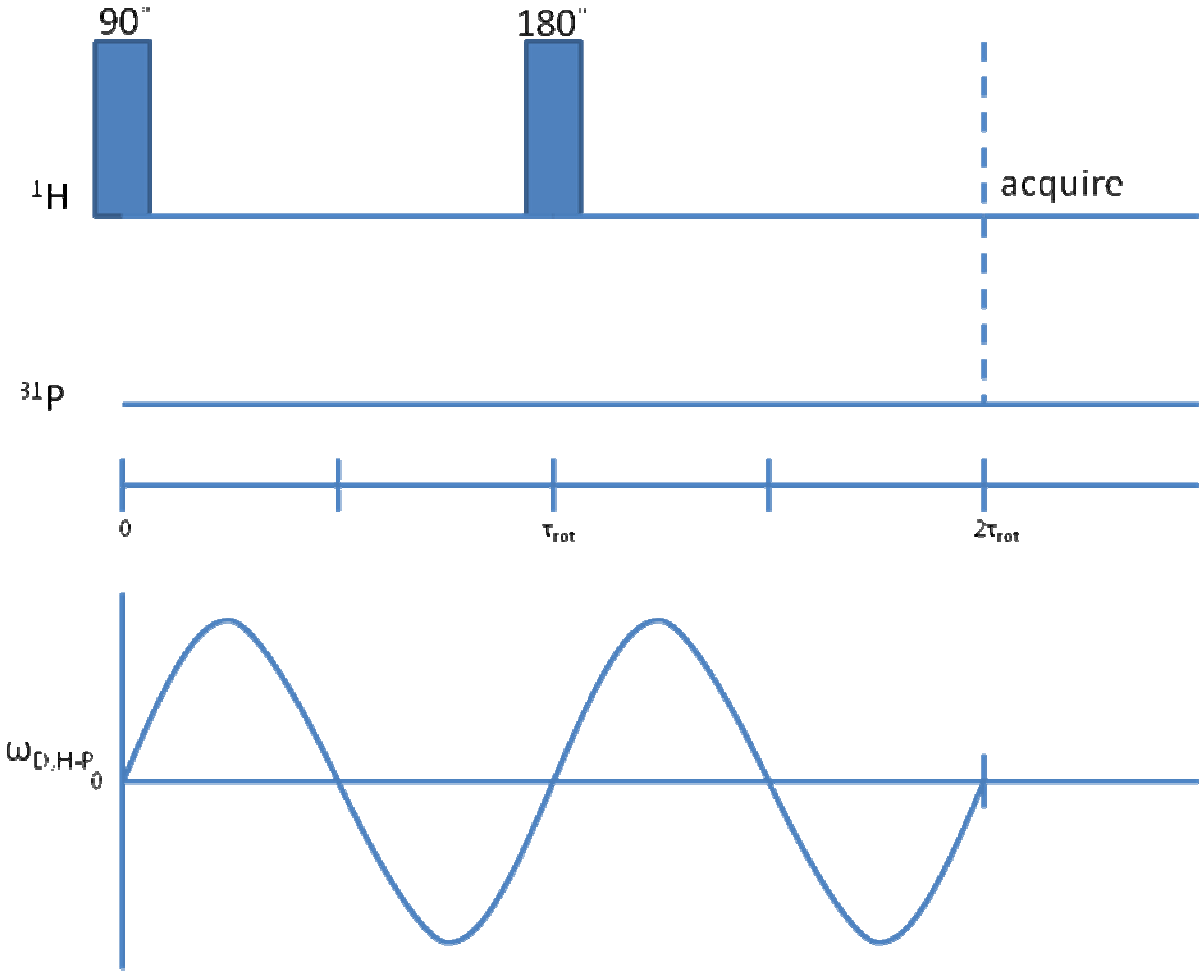

II. NMR Spectroscopic study of Phosphorus Extraction from a Calcite Speleothem

2.1. Abstract

A speleothem from Christmas Island, Australia, containing, 3,000-6,000 μg P g^{-1}, was subjected to digestion experiments then analyzed by ^{31}P NMR spectroscopy to determine if phosphate forms were altered. The caves that this sample came from are rich in phosphorus from bat guano. The sample exhibits three different forms of phosphorus, monetite, calcite with phosphate inclusions and an unidentified anhydrous calcium phosphate. Dissolution experiments were conducted to remove phosphate substituting into the calcite structure that accounted for 45% of the phosphorus in the sample. The use of hydrochloric acid, acetic acid, Na-EDTA, Shen and Boyle (1988) multistep cleaning procedure and sequential extraction method (SEDEX) for dissolution of calcite preserved the distribution of phosphate forms found in the speleothem. Our findings emphasize the need to use a dissolution experiment that does not precipitate a new phosphate phase if one is trying to conduct phase specific analysis.

2.2. Introduction

Trace element concentrations in minerals and their spatial variation have been extensively studied for their potential in determining past paleoclimates. During the precipitation of calcium carbonate minerals small amounts of other elements can be included within the matrix. These elements exhibit trends in concentration and species formed that correlate with climate phenomena; including phosphorus, a trace element, magnesium and strontium, minor elements, exhibit cycles associated with the temperature, hydrology, and the precipitation with calcium carbonates [1-2].

Phosphorus can be found in natural systems in multiple forms, organic, or inorganic [3]. Calcite systems, such as speleothems, are thought to contain mainly inorganic phosphorus due to the conditions in which they form and the sources of phosphorus. In cave systems phosphorus can be supplied by terrestrial material, such as decaying plants, or from phosphorus rich minerals found in the sediment [4]. Solution containing phosphorus from plant material undergoes decomposition, normally altering the phosphorus to phosphate, PO_4^{3-} [5]. In the presence of calcite, phosphate in solution can coprecipitate as a structural defect or as a separate phosphate mineral [6]. In some cases organic phosphorus is preserved and can be found in speleothems as occluded organic matter. Other forms in which phosphorus is found are phosphorus as defects in the mineral structure, surface adsorbed phosphate, coprecipitated phosphate (such as iron-bound and calcium-bound phosphate), and exchangeable or loosely sorbed phosphorus.

House and Donaldson studied the affect of initial phosphate concentration and temperature on the uptake of phosphate during calcite precipitation [7]. They determined that concentrations >20 μmol L^{-1} inhibited the formation of calcite and that within the first two minutes of the experiment 80% of the phosphorus was removed from solution. House and Donaldson created a model for the process of phosphate coprecipitation in which phosphate can react with calcium either in the forms of PO_4^{3-} to $CaPO_4^{3-}$ or HPO_4^{2-} to $CaHPO_4^{0}$. Solid state ^{1}H and ^{31}P NMR was used to investigate the reaction of dissolved phosphate with calcite, it was determined that in solutions with phosphate loadings of 0.002 to 1.0 P nm^{-2} there was sorption of unprotonated phosphate groups, whereas at higher concentrations of phosphate, 1.9 to 3.5 P nm^{-2}, brushite formed [8]. These studies emphasized the need to fully understand how phosphate reacts as calcite precipitates before it can be applied as a paleoenvironmental indicator [9].

Studies using atomic force microscopy have determined the presence of calcium phosphates and amorphous phosphate phases in phosphate and calcite coprecipitation studies [10]. Common crystalline calcium phosphates could be present as small inclusions in the calcite of speleothems, and in the coprecipitation studies include hydroxylapatite (HAP), $Ca_5OH(PO_4)_3$, brushite, $CaHPO_4*2H_2O$ and monetite, $Ca(HPO_4)$, all of which yield distinct ^{31}P NMR signals [11]. In addition the previously described amorphous phase was determined to be phosphate adsorbed to the surface of calcite, or incompatibly coprecipitating [8, 12].

Eventually, it may be possible to determine the climatic conditions in which a speleothem precipitated from the form of phosphorus precipitated after the depends on temperature, pH, and initial phosphorus concentrations is understood [5]. Phosphorus concentrations in natural samples, such as speleothems and corals, are low, often below 100 μg P g^{-1}, out of the range for most structure-sensitive techniques [13]. In the past, to accurately analyze the samples for the phases of phosphorus present, calcite needed to be removed while preserving the original phosphorus species. Through the use of acid digestion procedures it is possible to eliminate the excess calcite, leaving only the phosphorus species such as calcium phosphate for analysis [14]. Dilute acid solutions can be used to remove calcite from organic and inorganic fractions, yet, these methods can also create byproducts such as HAP, monetite, or phosphate sorbed to mineral surfaces [8, 15-16]. Some methods remove specific phosphorus forms so the remaining phosphorus species can be studied [17].

The dissolution of calcite and hydroxylapatite has been extensively studied. Fulmer and Ison (2002) showed that the solubility of hydroxylapatite varies depending on stoichiometry. Results showed that as ionic substitution in the apatite lattice increases and the crystallinity decreases, the solubility of the apatite increases. Hydroxylapatite can spontaneously precipitate

in a solution if its saturation index (logk/logI_{AP}) exceeds 10.93 [18]. During calcite precipitation phosphorus can loosely attached to the surface [8, 13]. The attraction between phosphorus and calcite is weak, and will dissolve very easily in acids. After dissolution of the surface sorbed phosphorus, even in low concentrations, the phosphorus can recombine with the calcium in solution and precipitate as a new phosphorus or phosphate precipitate depending on what other cations and anions are present in solution. Numerous reactions can cause the precipitation of phosphate, for example: [19]

$CaHPO_4(s) \leftrightarrow Ca^{2+} + H^+ + PO_4^{3-}$ log K=-19.275

$H^+ + PO_4^{3-} \leftrightarrow HPO_4^{2-}$ log K= 12.375

$CaHPO_{4(s)} = Ca^{2+} + HPO_4^{2-}$ =-6.90 = $1.26*10^{-7}$

K values were calculated from Visual MINTEQ ver. 2.53, 2007.

There have been no spectroscopic studies of the structure and composition of the precipitates or insoluble residues that are released by the dissolution of calcium carbonate. Fulmer and Ison et al.[20] observed a precipitate form during the dissolution of hydroxylapatite, but reported no structural analysis. The affinity of phosphorus to react with calcium is extremely high and crystalline calcium phosphate solids are highly insoluble (e.g. HAP), so as calcium concentrations increase any trace amount of phosphate can precipitate as calcium phosphate.

Crystalline calcium phosphates are less soluble in weak acids than calcite [17]. Each form of phosphorus has a different affinity to extraction. This allowed scientists to develop methods to remove each fraction of phosphorus in a stepwise process from a sample containing calcite and multiple forms of phosphorus.

2.2.1. Digestion and cleaning methods for P extraction from Calcite

Digestion is used to remove calcite and other components from a sample to increase the concentration of a trace element species. Samples commonly treated this way include fossils, corals, speleothems, marine formanifera, bone and other calcium carbonate deposits for investigating phosphate-rich inclusions [3, 14, 17, 21]. Calcite can be preferentially dissolved by acid because it is more soluble than crystalline calcium phosphates such as apatite [15, 22]. Common methods used to investigate the dissolution of calcite and calcium phosphates include:

2.2.1.1. Digestion in Hydrochloric Acid

One of the most common procedures used to extract apatite is the use of a strong acid in low concentrations over time [23]. Since the 1980's the use of HCl and NaOH to remove excess calcium carbonate has been used, but there is some question as to the effectiveness of the procedure [24]. The reaction commonly creates solutions with high calcium concentrations which can precipitate first calcium phosphate, and eventually calcium carbonate if not replaced frequently; this is one reason scientists prefer to not use this method. Precipitation of secondary phosphate species has been observed, but there has been no analysis of the species that precipitates out of the solution [25]. If there are organic phosphorus ions in solution they can be hydrolyzed to phosphate which easily precipitates with calcium to form a calcium phosphate [25]. The use of 0.5 M HCl is the general procedure used to extract apatite, but it underestimates the residual phosphate [14, 26]. The reaction takes place by the following net reaction:

$2H^+ + CaCO_3 \rightarrow CO_2(g) + H_2O + Ca^{2+}$

2.2.1.2. Acetic Acid Digestion

Previous studies have shown that removal of calcite from phosphorite can be accomplished with a dilute acetic acid solution [23]. The conjugate base, acetate, can complex with the calcium without destroying the crystalline calcium phosphates [27]. Acetic acid solutions are also used to dissolve diagenetic carbonates from marine precipitates such as coccoliths and other calcium carbonate sediments found in nature [15]. Contradictory results from Bryant et al. (1996) provided evidence that during the dissolution of HAP, the precipitation of brushite can be detected by Fourier Transform Infrared Spectroscopy (FTIR) but no explanation of why this happens can be provided [28-29]. Other techniques that have been used to analyze samples treated with acetic acid include x-ray diffraction and high-power cathodoluminescence microscopy (CL) which determined that some aragonite and calcite clusters were preserved after acetic acid treatment [30]. Previous to using acetic acid, HCl was commonly used, but in 1895 acetic acid was used to extract graptolites from carbonates, since then it has been the preferred method for dissolution [26]. The reactions include [23]:

$CH_3COOH \leftrightarrow CH_3COO^- + H^+$ $\quad$ $Ka= 1.75*10^{-5}$ [31]

$CaCO_3(s) = Ca^{2+} + CO_3^{2-}$ $\quad$ $Ksp= 3.36 \text{ X } 10^{-9}$

$H^+ + CO_3^{2-} \rightarrow HCO_3^-$ $\quad$ $-pKa_2= 10.33$ [31]

$Ca^{2+} + 2CH_3COO^- \rightarrow Ca(CH_3COO^-)_2$ $\log K_{assoc} = 17.38$ [31]

$HCO_3^- + H^+ \leftrightarrow H_2CO_3^0$ $-pka_1 = 6.35$

$H_2CO_3^0 \rightarrow CO_2(g) + H_2O$ $-\log(K_H) = 31.62$

Acetate binds with the calcium directly, preventing free calcium concentrations from increasing- then precipitating out of the solution with freed phosphates or carbonates. The consumption of calcium both ensures the inhibition of secondary phosphorus species from forming, and the precipitation of calcium carbonate [27, 32].

2.2.1.3. Dissolution by Ethylenediaminetetraacetic acid (EDTA)

Inorganic phosphorus found in natural samples, such as sediments, is commonly classified in two major fractions, iron bound and calcium bound [25]. Ethylenediaminetetraacetic acid (EDTA), $C_{10}H_{16}N_2O_8$, is a hexadentate chelator with high affinity to bind to metal cations. It binds to a cation, such as calcium or iron, with six bonding sites, two amines and four carboxylates; the process of binding with the cation envelops it, preventing it from dissociating back into solution or reacting with other ligands or anions.

Golterman (1996) presented a method to remove iron- and calcium- bound phosphorus through the use of EDTA [33-34]. Removal of the phosphorus loosely sorbed to the surface of calcite was done by soaking the sample in 0.1 M Na_2EDTA for 1.5 hours. EDTA is commonly used to remove heavy metal contaminants from sediments, such as Pb, with weaker solutions ranging from 0.02 to 0.08 M.[35-36] Fredd and Fogler (1998) developed a method for the dissolution of calcite disks using solutions with higher concentrations of Na_2EDTA, 0.25 M with

KCl. Results showed that there is a significant increase in the rate of dissolution of calcite in the presence of EDTA versus just KCl at a pH of 3.21, suggesting that the chelating agent played a major role in the surface reactions [32]. Another method developed soaked the sample in 0.5 M EDTA solution over seven days [15]. De Groot and Golterman (1990) extracted inorganic phosphate from organic phosphate by applying EDTA which prevents the hydrolysis of the organic phosphate [14]. To determine if all the inorganic phosphate was removed, total phosphorus concentrations were analyzed in the studies by de Groot and Golterman (1990) using IBP Manual NR 8, a treatment of H_2SO_4 and H_2O_2, heating, centrifuging and neutralization. Other studies were specifically looking at calcite dissolution and solutions were analyzed using a atomic absorption spectrophotomer (AAS) [25, 32]. The reaction stoichiometry for the dissolution of calcium carbonate with Na-EDTA can be represented by: [37]

$$CaCO_3(s) \rightarrow Ca^{2+}(aq) + CO_3^{2-}(aq)$$

$$Na_4EDTA + 4H^+ \rightarrow H_4EDTA + 4Na^+$$

$$Ca^{2+}(aq) + H_4EDTA(aq) \rightarrow Ca\text{-}EDTA^{2-}(aq) + 4H^+ \qquad \log K_f = 10.69 \text{ [31]}$$

$$CO_3^{2-} + H^+ \rightarrow HCO_3^-$$

$$HCO_3^- + H^+ \leftrightarrow H_2CO_3^0$$

$$H_2CO_3^0 \rightarrow CO_2(g) + H_2O$$

2.2.1.4. Multi-step Cleaning

Dissolution methods are used on a multitude of natural materials, including corals, to remove contaminants that include detrital and organic material adsorbed to the surface of the sample and to remove calcium carbonate [21]. Minor constituents such as strontium and magnesium substitute directly into the calcium sites of calcite and aragonite, the variations in the concentration acquired from these samples can help reconstruct paleoclimate. Through the removal of calcium carbonate it is possible to provide samples that contain high enough concentrations to be analyzed with conventional instrumentation [21].

Shen and Boyle [21] developed a procedure specifically to clean corals, to remove the detrital and organic material adsorbed to the surface of coral; this process consumes most of the sample, but is believed to preserve all the minerals and fractions, besides pure calcium carbonate, present in the coral. This method includes many solutions of acids and bases in heat baths and sonicators that specifically remove the contaminants through a series of oxidation, reduction, and leaching treatments. Through the use of Graphite Furnace Atomic Absorption Spectroscopy (GFAAS) they determined that the trace elements of interest, mainly Pb, were preserved in the sample and did not go into solution. It is widely assumed that all trace elements are preserved, and no further instrumental characterization is typically done on the samples to determine if there was a change in the structure of the trace element species. This procedure is still used today, and was found to be the best way to clean coral samples from Panama to calculate the P/Ca ratios [38].

2.2.1.5. Sequential Extraction Method (SEDEX)

Selective dissolution of sedimentary materials has been used by many scientists to determine the concentration of phosphorus in each separate component. Ruttenburg [17] developed the sequential extraction method (SEDEX) to separately remove five sedimentary phosphorus reservoirs for analysis. These reservoirs include loosely sorbed phosphorus, ferric iron-bound phosphorus, authigenic carbonate fluoroapatite (including biogenic apatite) and $CaCO_3$-associated P, detrital apatite, and organic phosphorus. This procedure has become one of the most widely used methods for phosphorus extraction. Through the use of this method it is thought to be possible to identify and quantify different forms of phosphorus in samples that have phosphorus concentrations too low to detect with standard techniques such as XRD. This method can effectively isolate fractions as low as 0.005 wt % phosphorus, while typical detection limits for conventional powder XRD is about 1% [17]. Different solid phases have different a reactivity in solutions which is the basis of sequential extraction methods.

SEDEX comprises of a series of chemical treatments, each step removing a specific form of phosphorus. Some of the steps are from previously reported extraction schemes. The first step consists of a wash with $MgCl_2$ and citrate bicarbonate solution to remove exchangeable or loosely sorbed phosphorus as phosphate without dissolving carbonates. The reaction results in the formation of $MgPO_4^-$ complexes while Cl^- creates a mass action displacement. Step two is a treatment in citrate-bicarbonate-dithionite (CBD) solution, previously described by Lucotte and d'Anglejan (1985) [39] and Tessier et al. (1979) [40] which removes iron-bound phosphorus. The CBD reaction is driven by the reduction of Fe^{3+} by dithionite followed by chelation by citrate and the release of phosphate to the solution. The third extraction step was created to remove authigenic apatite, $CaCO_3$-bound P, and biogenic apatite, using acetic acid/acetate

buffer. This third step is a combination of acid dissolution and chelation of calcium with the acetate similar to that described above in section 2.2.2. The final chemical treatment is acid dissolution with 1 M HCl to remove detrital apatite and any other inorganic phosphorus. The residue remaining after the chemical treatments is assumed to contain only organic phosphorus. Studies have been done to ensure that the correct phases are removed in each step through the use of standards, but no studies have been conducted on the evolution of the species in the solid with each step. Solutions were analyzed for phosphorus concentration using the single-solution phosphomolybdate blue method [17, 34].

Treatment of calcium carbonates with HCl, acetic acid, EDTA, Shen and Boyle's multistep cleaning, and SEDEX have been extensively applied, but there have been few studies of the solid residues to determine if any byproducts were created or changes to the speciation of phosphorus [25]. Analysis with XRD and FTIR can identify predominant species, but may miss trace amounts of other species [15]. Other techniques used to analyze the preservation of species included Ultraviolet-visible spectroscopy (UV-Vis) and GFAAS [21, 34]. These methods can only quantify the amounts of an element either left in the sample or in solution, and cannot characterize the species removed. Studies employing these methods assume that phosphate species were preserved in their initial form, yet this cannot be certain unless analyzed with a highly specific technique. Here, we apply solid state ^{31}P NMR spectroscopy to investigate the effects of the various digestion and cleaning methods on phosphate species present in a calcite speleothem from Christmas Island that contains exceptionally high phosphorus concentrations.

2.3. Experimental

Portions of a calcite stalagmite from Christmas Island, Australia that formed in the Holocene under tropical climate was provided by Dr. Silvia Frisia. This specimen is being investigated by collaborators using isotope and trace element geochemistry for paleoclimate application. Phosphorus concentrations range from 3000 to 6000 μg P g^{-1}, measured by inductively coupled plasma mass spectrometry (ICP-MS), which was originally thought to come from bat guano contamination. Upon further investigation it was determined that the specimen was not contaminated due to its transparency and absence of color. Synchrotron radiation generated micro x-ray fluorescence (XRF) maps that showed phosphorus is concentrated along boundaries of dense needles throughout the speleothem. The high concentrations of phosphorus present, without the bat guano, suggests the phosphorus came from some other source, such as the soil zone where volcanic rocks rich in phosphorus were leached or from decomposition of organic matter. Very little trace element information has been collected on tropical speleothems, further analysis of the phosphorus in this sample would expand our understanding of the phosphorus distribution in calcium carbonate deposits. Portions of this speleothem were ground with a mortar and pestle to a grain size of <125 microns for further studies on the phosphorus in the sample.

2.3.1. Extraction Techniques

2.3.1.1. Dissolution in Hydrochloric Acid

Five grams of ground sample was placed in a dialysis bag. This sample was soaked in two liters of pH 4 HCl solution for 3 weeks, replacing solution every other day. The solution

pH was then decreased to a pH of 3 and soaked for 1 ½ months. A Metrohm model 718 STAT Titrino was used to maintain the solution pH with automated additions of a 1 molar HCl solution. At the end of the experiment only enough acid was added to consume 50% of the calcium carbonate. The sample was removed, rinsed with distilled water, and dried. See Table 1 for initial masses and final masses of sample.

2.3.1.2. Dissolution in Acetic Acid

Five grams of speleothem was stirred in 10 mL of 2 M Acetic Acid for one hour. The reaction was quenched with the addition of 500 mL of de-ionized water and filtered immediately. The sample was then dried and weighed. The procedure was repeated from Economou and Vaimakis's method [41] See Table 1 for starting and ending weights.

2.3.1.3. Dissolution by EDTA

The method was derived that described by Fredd and Fogler (1998), excluding the iron bound phosphorus removal due to the lack of iron in the Christmas Island Speleothem [27]. A total of 100 mL of 0.2 M solution of Na_2EDTA was added to 5 g of speleothem and stirred. The pH was kept constant at 4.86 by hand titrating in 100 mL more EDTA in five mL increments, at two hours titrating was stopped and the reaction was quenched by the addition of 500 mL of deionized water. The final pH was 5.68. The sample was then rinsed, dried, and weighed.

2.3.1.4. Multi-Step Cleaning

A series of acid and base reactions were used following the procedure described by Shen and Boyle (1988) to clean the speleothem. Three solutions were prepared for the reaction: 0.15 M HNO_3, a 50-50 mixture of 30% H_2O_2 and 0.2 M NaOH; and finally a solution containing 1 part hydrazine, 6 parts concentrated (7 M) NH_4OH and 3 parts 0.3 M citric acid. For each step of this procedure 1 gram of speleothem, crushed to <125 μm, was added to 4.17 mL of solution. The cleaning procedure was completed as follows: 4.17 mL of deionized H_2O was added to the sample in a 10 mL centrifuge tube and agitated in a sonicator for 10 minutes. The sample was then allowed to settle and the water was decanted, taking care to preserve the fine material. Step two consisted of the addition of 4.17 mL of the HNO_3 solution to the sample. The tube was inverted and placed in the sonicator for 2 minutes with occasional inversions to ensure settling did not occur. The HNO_3 solution was then decanted. Third, the 50:50 mixture of H_2O_2 and NaOH solutions was added and placed in boiling water for 2 minutes, followed by 2 minutes in the sonicator. This alternating process was repeated for 20 minutes, after which the solution was removed and rinsed twice with deionized water. The 1:3:6 mixture of hydrazine + NH_4OH + citric acid solution was added to the speleothem and placed in an 80˚C water bath for two minutes followed by the sonicator for another 2 minutes, alternating for 30 minutes. The solution was removed, and rinsed twice with distilled water. Steps 2 and 3 were repeated followed by three-two minute rinses with 0.15 M HNO_3. The sample was then filtered and dried in an oven at 60˚C overnight; 24% of the sample was consumed.

2.3.1.5. SEDEX

Sequential dissolution of the Christmas Island Speleothem was completed following the procedure described by Ruttenberg (1992) and the CBD treatment of Mehra and Jackson (1960) [42-43]. After each step the solid residue was dried and analyzed by NMR spectroscopy except for the third step which consumed all the remaining material.

In a 50 mL centrifuge tube 50 mL of 1M $MgCl_2$ was added to 0.5 g of speleothem crushed to pass a 125 μm sieve. The sample was hand-shaken and placed in shaker for 2 hours to maintain the particles in suspension. The residue was separated by centrifuge for 10 minutes at 3,900 rpm and the solution filtered on 0.2 μm filters. This $MgCl_2$ procedure was repeated and then the residue was washed with 50 mL H_2O for 2 hours in the shaker. The sample was dried at 60˚C overnight and weighed. Only 11% of the sample was consumed

In the second step of the SEDEX procedure, the CBD treatment included preparation of a solution that contained 45 mL of 0.3 M Na_3-citrate and 1 M $NaHCO_3$ added to 1.125 g Na-dithionite, yielding a pH of 7.71. This solution was added to the speleothem in a 50 mL centrifuge tube and shaken at a low speed for eight hours, then centrifuged, and filtered. The sample was placed in a new 50 mL centrifuge tube with 50 mL of 1 M $MgCl_2$ (pH 8) and shaken for 2 hours, centrifuged at 3900 rpm for 10 minutes, and filtered. The sample was then washed by adding it to 50 mL distilled water and shaken for 2 hours, filtered, and dried over night at 70˚C in the oven. The CBD treatment removed 50% of the sample.

The final step of the SEDEX procedure is treatment of the sample with acetate buffer to remove all the inorganic material. The acetate buffer was prepared by adding 50 mL of 1 M sodium acetate drop-wise with 10 M acetic acid to a pH of 4. This solution was added to the

residue from step two (CBD treatment) and shaken for 6 hours. At the end of designated time, no residue was observed, indicating absence of a significant amount of organic matter. The solution was centrifuged at 3900 rpm and filtered to ensure no trace amount of sample remained.

2.3.2. NMR Spectroscopy

All ^{31}P NMR spectra were collected using a Varian Inova 400 MHz NMR spectrometer under magic-angle-spinning (MAS) conditions at operating frequencies of 161.8 MHz and 399.8 MHz for ^{31}P and ^{1}H, respectively. Samples were contained in a 7.5 mm (o.d) Si_3N_4 rotor and spun at spinning rates between 1.5 and 6 kHz. ^{31}P single pulse experiments were completed with a relaxation delay of either 2 or 1000 seconds and 8 μs (90˚) pulse lengths. CP/MAS employed typical contact times of 0.2, 2, 10 ms, with ^{1}H 7 μs 90˚ pulse length. Measurements of chemical shift anisotropy (CSA) were done using Herzfeld-Berger analysis using the WinSolids HBA32 software program [44]. The ^{31}P NMR chemical shifts ($\delta_{P\text{-}31}$) are referenced with respect to 85% phosphoric acid, using hydroxylapatite as a secondary reference set to $\delta_{P\text{-}31}$=2.65 ppm. Heteronuclear correlation (HETCOR) spectroscopy experiments used a Chemagnetics probe assembly configured for 3.2 mm (o.d.) rotors. The spinning rate was 10 kHz with a ^{31}P pulse width of 4 μs, ^{1}H pulse width 4.5, 2 ms contact time, and 1280 acquisitions. The spectral window in the ^{1}H dimension (F1) was 50 kHz, with acquisition of 80 hyper complex points. Linear prediction methods were used to complete the free-induction signal in F1 to prevent truncation artifacts. The ^{1}H NMR chemical shifts ($\delta_{H\text{-}1}$) are referenced with respect to tetramethylsilane (TMS) using adamantane as a secondary reference set to $\delta_{H\text{-}1}$=2.0 ppm.

2.3.3. X-ray Diffraction

Powder x-ray diffraction (XRD) was used to analyze all samples with a Scintag PADX diffractometer using copper radiation. Samples were scanned from 15˚ to 50˚ 2θ, step size if 0.2˚, 1 degree per minute with a voltage of 45 kV and 25 mA. Further analysis with XRD was done on at a slow scan rate on one sample from 26 to 27 degrees (2θ) with a step size of 0.00050 per 250 seconds in an attempt to observe trace fractions of monetite in the sample.

2.4. Results and discussion

2.4.1. Christmas Island Speleothem

2.4.1.1. ^{31}P single-pulse NMR

Solid state ^{31}P NMR spectra of the Christmas Island Speleothem are shown in Figure 1. Three peaks are observed in the single pulse experiment (Fig. 1a); a broad peak near $\delta_{P\text{-}31}$= 3.2 ppm, (4 ppm full width at half-maximum; FWHM), a narrow resonance at $\delta_{P\text{-}31}$=2.9 ppm (0.8 ppm FWHM), and a narrow peak at $\delta_{P\text{-}31}$= -1.1 ppm (1.2 ppm FWHM). The spectrum collected for determining relative intensity was obtained under quantitative conditions, with a pulse delay of 1000 s to ensure all phosphorus signal was present and fully relaxed before each acquisition so that the integrated signal intensity is proportional to the number of corresponding nuclei. The relative intensity of each peak was calculated from least squares fits of the spectra to a sume of Gaussian curves. For the peaks at 3.2, 2.9 and -1.1 ppm the relative intensities were 0.50, 0.16, and 0.38, respectively. Of the 3,000-6,000 μg P g^{-1}, assuming phosphate was roughly 3% of the sample, 50% of the phosphorus was determined to be the peak at 3.1 ppm, followed by the peak at -1.1 ppm consisting of 34%, and the peak at 2.9 ppm consisting of 16%. Figure 1b shows a

spectrum collected with a pulse delay of 2 s dramatically changing the relative intensities of each phosphorus species. The peak observed at -1.1 ppm became the predominant species. The increase relative intensity of the peak at -1.1 ppm in relation to the peaks at 3.2 and 2.9 ppm shows that the peak at -1.1 ppm has a shorter spin-lattice relaxation time (T_1). Both the peaks at 3.2 and 2.9 have longer T_1 which mean they need a longer time to re-establish equilibrium magnetization by the magnetic field after each pulse, and will be under-represented in spectra unless given time to fully relax.

The appearance of the single pulse spectra varied substantially with varying ^1H decoupling power from 4.4 kHz to 35 kHz ($\nu_{1,H}=\gamma_H*B_{1,H}$). At lower decoupling powers the peak at -1.1 ppm was observed to split (decoupling power of 35 kHz) into 2 peaks at $\delta_{P\text{-}31}$= -0.2 ppm (1.7 ppm FWHM) and -2.2 ppm (1.6 ppm FWHM) (decoupling power of 9 kHz), which split further apart with decreasing decoupling power (Figure 2). This splitting of the -1.1 ppm peak is due to heteronuclear dipole coupling. There are two different directions available for the proton magnetic moment which affects the magnetic field at the ^{31}P nucleus. The peak at -0.2 ppm is correlated to the spin up and the peak at -2.2 ppm is correlated to the ^1H spin down. Application of sufficient ^1H field flips the ^1H between these orientations so that each ^{31}P is affected by the average.

2.4.1.2. $^{31}P\{^1H\}$ CP/MAS NMR

Spectra obtained by CP/MAS exhibited two peaks, a broad peak at $\delta_{P\text{-}31}$= 3.1 ppm, (3.7 ppm FWHM) and a peak at $\delta_{P\text{-}31}$= -0.9 ppm, (2.0 ppm FWHM) (Figure 1c-e). The CP/MAS spectra differed from single pulse spectra principally through the absence of the peak at 2.9 ppm

in CP spectra. Otherwise the peaks near 3.1 and -1.1 ppm exhibit similar positions and widths in both SP and CP spectra.

The contact time in CP/MAS was varied between 0.1 and 10 ms to investigate CP/MAS intensity variation with contact time, Figure 3. The peak observed at -1.1 ppm exhibited a maximum intensity at a contact time of 5 ms, the peak at 3.1 ppm had a ma106885826ximum intensity at a contact time of 1 ms. Intensity of the peak at -1.1 ppm at 5 ms was 15 times that of the peak at 3.1 ppm. The CP kinetics curves were fit to the classical bi-exponential function to yield values for T_{P-H} (time constant for $^{1}H \rightarrow ^{31}P$ polarization transfer) and $T_{1\rho,H}$ (relaxation of ^{1}H during the contact period) have been calculated for each phosphorus species. The broad peak at 3.1 ppm exhibited a T_{P-H}= 0.6 ms and $T_{1\rho,H}$= 13 ms the narrow peak at -1.1 ppm exhibited a T_{P-H}= 1.2 ms and $T_{1\rho,H}$= 52 ms. This result suggests that the interaction between protons and phosphorus (number of H at short distances) is stronger for the phosphorus corresponding to the 3.1 ppm peak than for those giving the peak at -1.1 ppm. The ^{1}H associated with -1.1 ppm peak, phosphorus takes longer to relax, $T_{1\rho,H}$, indicating more rigid ^{1}H environments, as could be expected for well-ordered crystalline structure. Two curves were fit to the data to show the energy build up and relaxation. Some of the misfit for the curve for the peak at -1.1 ppm, at long contact time potentially could arise from an oscillating curve (dashed curve), which could be attributed to quasi-isolated ^{31}P-^{1}H spin pairs.

2.4.1.3. Chemical Shift Anisotropy

Single pulse spectra collected at spinning rates of 2, 3, and 5 kHz exhibited in the center bands no change in peak positions or intensities (Figure 4). For CP spectra collected with

varying spinning speed, the proportion of the peak at -0.9 versus 3.1 changed for the center peaks (Figure 4). For the CP spectra at slower spinning speeds, such as 2 kHz, the relative intensity of the center peak at -0.9 ppm decreased in relation to the peak at 3.1 ppm, decreasing from 49% at 5 kHz to 46% at 3 kHz, and 32% at 2 kHz. A slightly less dramatic change in intensities was observed when peak intensities were integrated from the addition intensity from the side bands and the center bands, at a spinning rate of 3 kHz peak relative intensity of the peak at -0.9 ppm is 42% and 58%, at a spinning rate of 2 kHz the intensity at -0.9 ppm decreased to 37% and 3.1 ppm increased to 63%. It was expected that the values would remain constant over all spinning speeds due to the transfer of signal from the center band to the side bands as spinning speed decreases, but CP signal might be reduced if the peak at -0.0 ppm is more sensitive to the Hartmann-Hahn match condition, which varies with spinning rate.

Table 2 shows the Chemical Shift Anisotropy (CSA) for the ^{31}P peaks of the Christmas Island Speleothem obtained at a spinning speed of 3 kHz. The chemical shift is a tensor property for which the three principal values (δ_{11}, δ_{22},δ_{33}) can be estimated from the distribution of spinning side band intensity. The center band peak position corresponds to the average of the principal values ($\delta_{P\text{-}31}$= 1/3[δ_{11}+ δ_{22}+δ_{33}]). The CSA's were estimated from analysis of the spinning side band intensities using the HBA software package [44] collected on the CP/MAS spectra of the Christmas Island Speleothem shows that the anisotropy of the peak at -0.9 ppm is δ_{11}=13±2 ppm, δ_{22}=-8±3 ppm δ_{33}=-9±2 ppm. The CSA value for the 3.1 ppm peak were δ_{11}=16 ±2 ppm, δ_{22}=-3±1 ppm δ_{33}=-4±1 ppm. These CSA's are small and are consistent with orthophosphate groups [45].

2.4.1.4. HETCOR

Use of $^{31}P\{^{1}H\}$ HETCOR shows the direct relationship of phosphorus with neighboring protons, forming a 2-dimensional map of the peak position of the phosphorus with cross-peaks for protons they are close enough (<4Å) that polarization can be transferred during CP. Spectra exhibited two peaks in the ^{31}P side, a peak at $\delta_{P\text{-}31}$= 3.1 ppm and $\delta_{P\text{-}31}$= -0.9 ppm. ^{1}H spectra exhibited at peak at $\delta_{H\text{-}1}$= 13.9 ppm and a peak at $\delta_{H\text{-}1}$= 7.4 ppm. The ^{1}H peak at 13.9 ppm correlates to the peak at -0.9, and the ^{1}H peak at 7.4 ppm corresponded to the ^{31}P peak at 3.1 ppm (Figure 5).

2.4.1.5. Peak Assignments

The peak position and width of the peak observed in all ^{31}P spectra at 3.1 ppm are similar to peaks reported from a calcite speleothem from Grotta di Ernesto and from deep sea coral aragonite, which were assigned to phosphate defects in the crystal structure [13, 46]. Also, a strong $^{31}P\{^{13}C\}$ REDOR effect was observed for a similar peak from a synthetic aragonite/phosphate coprecipitate that indicates the phosphorus corresponding to this peak occur in close proximity to carbonate groups [46]. In this sample phosphate likely sorbed onto the surface and was included as a defect as the crystals continued to grow. This assignment further supported by the results of Hinedi et al. (1992) who assigned a similar peak to an unprotonated phosphate group sorbed onto the surface of calcite but which could have been incorporated during surface during surface reorganization [8]. In addition the ^{1}H peak near 7 ppm associated with the ^{31}P peak at 3.1 ppm matches that previously reported for bicarbonate defects within the calcite structure and for rigid molecular water near phosphate defects in aragonite [13, 46-47].

A narrow peak at 2.9 ppm is observed in the ^{31}P single pulse experiments at all spinning speeds and decoupling powers, but the peak does not occur during CP/MAS. The peak position and width almost match those previously reported for hydroxylapatite [11, 48-49], but the lack of signal in CP/MAS negates the possibility that it arises from HAP. HAP has a distinct proton group that provides signal during $^{31}P\{^{1}H\}$ CP/MAS, but the absence of the peak at 2.9 ppm means there are no neighboring proton to the corresponding phosphorus. The peak at 2.9 ppm was previously observed in a speleothem from Grotta di Ernesto and in phosphate coprecipitated with calcite following a constant addition method, studied by Mason et al. (2007) [13], and was tentatively attributed to an anhydrous Ca-orthophosphate due to the lack of closely associated protons and ^{31}P chemical shift [13]. The material which gives this peak is likely to be highly crystalline, because its narrow line shape and long spin lattice relaxation time (T_1) indicates a well ordered phosphorus environment. No other crystalline phosphate phase that has been investigated gives ^{31}P NMR peaks that match the 2.9 ppm peak position. To determine if the peak at 2.9 ppm could be attributed to phosphate dissolved in fluid inclusions, a portion of the sample was heated in a muffle furnace to 200˚C overnight. Single pulse ^{31}P NMR data showed that the peak at $\delta_{P\text{-}31}$= 2.9 ppm does not change in intensity or peak width when heated, indicating that this phosphorus species is not dissolved in a fluid inclusion.

The ^{31}P peak located at -0.9 ppm exhibits the same position and width of previously reported values for monetite. Presence of two peaks at lower decoupling power agrees with previous data for crystalline monetite [11, 47]. The occurrence of only one peak was observed by Mason et. al.[13] and was determined to be an averaging of the two peaks that normally occur at $\delta_{P\text{-}31}$= -0.5 ppm and -1.8 ppm which are split due to magnetic interactions with the ^{1}H [11, 48]. This ^{31}P peak correlates in the $^{31}P\{^{1}H\}$ HETCOR spectra to a ^{1}H peak at $\delta_{H\text{-}1}$= 13.9 ppm. This

result indicates that the phosphorus giving rise to the peak at -1.1 ppm and the ^{1}H for the peak at 13.9 ppm are in close proximity and in the same phase. This ^{1}H chemical shift is in good agreement with that previously reported for the acidic protons of monetite [50].

CSA data is sensitive to the local symmetry of a solid. That for the peak at -0.9 ppm which is attributed to monetite does not match the values previously reported [11, 49, 51]. Literature values note much higher CSA for monetite due to the two proton locations which create anisotropy. Values previously reported by Hartmann et al. are δ_{11}=11.9±2 ppm, δ_{22}=49.8±2 ppm δ_{33}=-65.3±2 ppm [52]. One possible explanation for the difference is presence of a contribution from dipolar coupling due to insufficient ^{1}H decoupling power. The peak at 3.1 ppm assigned to phosphate coprecipitated with calcite has similar values suggesting that it is relatively asymmetrical and possibly protonated. The asymmetry along with broad line width for this peak indicates a range of local configurations for phosphate substituted in the calcite structure.

2.4.2. X-ray Diffraction (XRD)

Intense peaks, corresponding to calcite reflections, were observed at 29.57˚, 43.14˚, and 47.66˚ 2θ (Figure 6-table) in addition to others expected for this mineral. All reflections observed in the conventional XRD patterns could be indexed to calcite. A region was selected for slow scanning in which calcite reflections are not present but contains major reflections for monetite (020), at 26.45˚ 2θ, and (-220), at 26.61˚ 2θ, confirming the presence of a small amount of monetite in the speleothem, and assignment of the ^{31}P peak at -0.9 ppm to this mineral. Two peaks were observed at 26.47˚, and 26.63˚ 2θ (Figure 6, inset).

2.4.3. NMR spectra of Chemically Treated Christmas Island Speleothem

2.4.3.1. Residue from HCl treatment

Figure 7 shows ^{31}P NMR spectra of the residue remaining after dissolution of 93% of a sub-sample of the Christmas Island Speleothem. The SP spectrum contains the same three peaks that were observed in the as-received sample (c.f. Fig 7 a and b) including a broad peak at $\delta_{P\text{-}31}$= 3.2, (3.0 ppm FWHM), a narrow resonance at $\delta_{P\text{-}31}$=2.9 ppm (1.3 ppm FWHM), and a narrow peak at $\delta_{P\text{-}31}$= -0.9 ppm (1.0 ppm FWHM). The CP/MAS spectra exhibited two peaks, at $\delta_{P\text{-}31}$= 3.1 ppm, (3.6 ppm FWHM) and at $\delta_{P\text{-}31}$= -0.9 ppm, (1.6 ppm FWHM). These data also closely match those of the original sample (c.f. Fig. 7c and 7d), which contained monetite, -0.9 ppm, phosphate coprecipitated in calcite, 3.1 ppm, and an unidentified anhydrous phosphate phase, 2.9 ppm.

Only slight differences in the SP relative intensities were observed between the as-received sample and the residue remaining after dissolution in the HCl. The HCl-treated sample exhibited a slight increase in the proportion of the 3.1 ppm peak, from 50% to 56%; the 2.9 ppm peak decreased from 16% to 12% and the total -1.1 ppm peak decreased from 34% to 32%. Table 1 lists the relative intensities of ^{31}P NMR peaks for all treatments to the speleothem. No new ^{31}P peaks were observed in the solid remaining after dissolution in HCl, in addition changes in peak intensities are within the uncertainties in the spectral fits. This result indicates that HCl preferentially dissolves phosphate-free calcite by a small fraction and that no significant amount of phosphate released by dissolution re-precipitates as a new phase.

2.4.3.2. Residue from Dissolution in Acetic Acid

Treatment of the Christmas Island Speleothem with acetic acid consumed 88% of the sample, the solid residue of which was analyzed by solid state NMR. The acetic acid-treated sample exhibits three peaks in the single pulse spectra that closely resemble those observed for the parent material (cf. Fig. 8a,b). A broad peak at $\delta_{P\text{-}31}$= 3.2, (3.0 ppm FWHM), a narrow resonance at $\delta_{P\text{-}31}$=2.9 ppm (1.3 ppm FWHM), and a narrow peak at $\delta_{P\text{-}31}$= -0.9 ppm (1.0 ppm FWHM). CP/MAS spectra exhibit two peaks, at $\delta_{P\text{-}31}$= 3.1 ppm, (3.2 ppm FWHM) and a peak at $\delta_{P\text{-}31}$= -0.9 ppm, (1.2 ppm FWHM). All of these ^{31}P NMR closely match the positions previously seen in the as-received sample, which were assigned to monetite (-0.9 ppm), phosphate coprecipited into calcite (3.1 ppm), and an unidentified material (2.9 ppm). Decoupling power was varied for CP/MAS experiments on the sample treated with acetic acid to verify that the peak at -0.9 ppm arises from monetite (Figure 9). The splitting of the peak at -0.9 ppm with decreased decoupling field is consistent with that of the original sample (cf. Fig. 2). With acetic acid treatment sample the 3.1 ppm peak's relative intensity increased to 56%, that at 2.9 ppm decreased to 12% and that of the monetite peak (-1.1 ppm) decreased to 32% (Table 2). All of the ^{31}P peaks observed in the as-received sample occur for the solid treated with acetic acid as well, with only minor changes in the relative intensities. Dissolution with acetic acid had a similar effect as HCl treatment with slight preference for the dissolution of phosphorus poor regions of the calcite, but congruently removed the phosphorus while preventing the re-precipitation of a solid.

2.4.3.3. EDTA-treated samples ^{31}P

A portion of the Christmas Island Speleothem was treated with 0.2 M EDTA solution, which consumed 84% of the sample. Single pulse spectra collected for the speleothem treated with EDTA, show no significant differences from that of the as-received sample (Figure 10; cf. Fig. 10a and b). The three peaks observed are a broad peak at $\delta_{P\text{-}31}$= 3.2, (3.4 ppm FWHM), a narrow resonance at $\delta_{P\text{-}31}$=2.9 ppm (0.8 ppm FWHM), and a narrow peak at $\delta_{P\text{-}31}$= -0.9 ppm (1.4 ppm FWHM). The CP/MAS spectra of this sample exhibit two peaks, at $\delta_{P\text{-}31}$= 3.1 ppm, (3.6 ppm FWHM) and a peak at $\delta_{P\text{-}31}$= -0.9 ppm, (1.2 ppm FWHM). The EDTA-treated sample's relative intensities exhibited a slight decrease for the peak at 3.1 ppm from 50% to 46%, and increases for the 2.9 ppm peak, from 16% to 18%, and the -1.1 ppm peak, to 36% (Table 2). Relative peak intensity changes observed are within the uncertainties of fitting the peaks and subjective data processing decisions (e.g. phase correction); treatment of the speleothem with EDTA dissolves a large fraction of the solid but preserves the relative distribution of phosphorus and appears to prevent re-precipitation phosphate released by dissolution of the solid.

2.4.3.4. Speleothem treated by Multistep Cleaning

The speleothem sample treated with the multistep cleaning procedure described by Shen and Boyle (1988) consumed 24% of the sample and exhibits three peaks in the SP spectra (Figure 11b), a broad peak at $\delta_{P\text{-}31}$= 3.2, (3.2 ppm FWHM), a narrow resonance at $\delta_{P\text{-}31}$=2.9 ppm (1.0 ppm FWHM), and a narrow peak at $\delta_{P\text{-}31}$= -0.9 ppm (1.4 ppm FWHM). The CP/MAS spectra (Fig. 12d) exhibited two peaks, at $\delta_{P\text{-}31}$= 3.1 ppm, (3.6 ppm FWHM) and a peak at $\delta_{P\text{-}31}$= -0.9 ppm, (1.6 ppm FWHM). These results closely match those of the parent sample material (cf. Fig 11a and b, and Fig. 11c and d), which contains monetite (-0.9 ppm), phosphate

coprecipited into calcite (3.1 ppm), and an unidentified phosphate component (2.9 ppm). Within uncertainty, this multi-step cleaning procedure did not change the relative proportions of resolved phosphorus species. In least squares fits to the SP spectrum, the proportion of -1.1 ppm peak decreased to 33% from 34%, the 2.9 ppm peak decreased to 15% from 16% and the 3.1 ppm peak increased to 53% (Table 1). Cleaning the Christmas Island Speleothem with the multistep procedure preserves the relative distribution of phosphorus in the sample while slightly preferentially consuming phosphorus-poor calcite.

2.4.3.5. Sequential Extraction (SEDEX) samples

Single pulse ^{31}P NMR spectra of the Christmas Island Speleothem after the $MgCl_2$ (Figure 12b) and CBD (Figure 12c) treatments contain three peaks similar to those of the parent material although 15% and 51% of the sample was consumed in these treatments, respectively (Table 1). No solid remained after the treatment with acetate. The peaks consisted of a broad peak at $\delta_{P\text{-}31}$= 3.1, (2.9 – 3.0 ppm FWHM), a narrow resonance at $\delta_{P\text{-}31}$=2.9 ppm (0.8 ppm FWHM) and a narrow peak at $\delta_{P\text{-}31}$= -0.9 ppm (1.2 – 1.4 ppm FWHM). CP/MAS data yielded a peak at $\delta_{P\text{-}31}$= 3.1, (3.4 – 3.6 ppm FWHM) and a narrow peak at $\delta_{P\text{-}31}$= -0.9 ppm (1.7 – 1.8 ppm FWHM). The peak at 2.9 ppm was not observed by CP/MAS, as was found for the parent speleothem (Figure 12d-f). The relative intensities of the ^{31}P peaks for the sample remaining after treatment with $MgCl_2$ were determined to be: 52% of the phosphorus related to the peak at 3.1 ppm, 16% to the peak at 2.9 ppm and 32% attributed to monetite (-0.9 ppm). After application of CBD on the sample 50% of the phosphorus was associated with the 3.1 ppm peak, 15% with the 2.9 ppm peak and 35% with the peak at -0.9 ppm (monetite). These relative intensities are the same within uncertainty as those observed for the parent speleothem calcite.

Peak positions and widths in both SP and CP ^{31}P spectra match closely those seen for the original Christmas Island Speleothem. After the $MgCl_2$ treatment 15% of the sample remained. Exchangeable or loosely sorbed phosphorus would have been removed in this step; since there was no change in the phosphorus distribution this result indicates that none of the sample consists of loosely sorbed phosphorus. An additional 51% of the sample was removed after the solid was treated with the CBD method, which should have removed easily reduced or reactive ferric Fe-bound phosphorus. Since no changes were observed in the relative intensities of the ^{31}P peaks, none of the sample consisted of iron bound phosphorus. Dissolution of all the sample after the acetate treatment suggests that all the phosphorus in the sample is inorganic, since organic material should have remained after this step. No significant changes in the distribution of phosphorus species was observed after the $MgCl_2$ and CBD treatments, suggesting that dissolution in both steps released phosphorus congruently with the calcite.

2.5. Conclusions

Analysis of the Christmas Island Speleothem by solid state ^{31}P NMR indicates the presence of three main forms of phosphorus, two of which correspond to crystalline phases monetite and an unidentified, likely anhydrous mineral. The remaining half, 1500-3000 μg P g^{-1}, of the phosphorus in the Christmas Island speleothem is contained as phosphate defects in the calcite structure.

The use of hydrochloric acid, acetic acid and EDTA digestion methods all preserved distribution of phosphorus among the three phosphate specie in the speleothem. Complete digestion of calcium carbonate with only the phosphate species remaining was not accomplished.

The use of these methods is suggested for dissolution of calcite while trying to preserve phosphate species. Use of HCl for the gentle dissolution of calcite is not suggested due to the length of the experiment.

Both the multistep cleaning and SEDEX preserved the distribution of phosphate species in the residue. Organic phosphorus or phosphate sorbed to the surface of the calcium carbonate would have been removed during the multistep procedure; since there was no evidence for selective removal of any phosphorus signal in the NMR spectra it is assumed there is no significant fraction of loosely sorbed phosphate or organic phosphorus in the Christmas Island Speleothem. Complete dissolution of the Christmas Island Speleothem after the removal of the inorganic phase in the SEDEX method suggests that all phosphate species are inorganic. Organic phosphorus should have remained after the third treatment, supporting the concept that the Christmas Island Speleothem contains no significant fraction of phosphorus as organic material. Further analysis of the peak at 2.9 ppm needs to be completed to determine the relationship with carbon and possibly identify the mineral phase.

All of the dissolution methods investigated suggested that phosphorus species were preserved and that the re-precipitation of calcium phosphates or other phosphorus species did not occur during treatment. The application of HCl, acetic acid and EDTA can continue to be used to remove calcium carbonate; SEDEX can continue to be used to remove each individual type of phosphorus. Application of Shen and Boyle's multistep cleaning procedure preserves phosphorus species while removing some of the calcium carbonate present in the sample. Solid state NMR supported previous research that the use of acids and bases can be used to remove calcium carbonate without altering the phosphorus forms and re-precipitate secondary phosphorus species.

2.6. References

1. Treble, P.C., J. Chappell, and J.M.G. Shelley, *Complex speleothem growth processes revealed by trance element mapping and scanning electron microscopy of annual layers.* Geochemica et Cosmochimica Acta, 2005. **69**: p. 4855-4863.

2. Huang, Y., et al., *Seasonal variation in Sr, Mg and P in modern speleothems (Grotta di Ernesto, Italy).* Chemical Geology, 2001. **175**: p. 429-448.

3. Koch, P.L., *Isotopic reconstruction of past continental environments.* Annual Review of Earth and Planetary Sciences, 1998. **26**: p. 573-613.

4. Hill, C.A., *Mineralogy of Kartchner Caverns, Arizona.* Journal of Cave and Karst Studies, 1999. **61**(2): p. 73-78.

5. Fairchild, I.J., et al., *Annual to sub-annual resolution of multiple trace-element trends in speleothems.* Journal of Geological Society, 2001. **158**(5): p. 831-841.

6. Frisia, S. and A. Borsato, *Developments in Sediments*. Carbonates in Continental Settings, ed. A.J. Van Loon. Vol. 61. 2010, Netherlands: Elsevier.

7. House, W.A. and L. Donaldson, *Adsorption and Coprecipitation of Phosphate on Calcite.* Journal of Colloid and Interface Science, 1986. **112**(2): p. 309-324.

8. Hinedi, Z.R., et al., *A ^{31}P and ^{1}H MAS NMR study of phosphate sorption onto calcium carbonate.* Journal of Colloid and Interface Science, 1992. **152**(1): p. 141-160.

9. Montagna, P., et al., *Phosphorus in cold-water corals as a proxy for seawater nutrient chemistry.* Science, 2006. **312**: p. 1788-1791.

10. Dove, P.M. and F.J. Hochella, *Calcite precipitation mechanisms and inhibition by orthophosphate: In situ observations by Scanning Force Microscopy.* Geochimica et Cosmochimica Acta, 1993. **57**: p. 705-714.

11. Aue, W.P., et al., *Solid-State Phosphorus-31 Nuclear Magnetic Resonance Studies of Synthetic Solid Phases of Calcium Phosphate: Potential Models of Bone Mineral.* Biochemistry, 1984. **23**: p. 6110-6114.

12. Mason, H.E., et al., *Phosphorus speciation in calcite speleothems determined from solid-state NMR spectroscopy.* Earth and Planetary Science Letters, 2007. **254**(3-4): p. 313-322.

13. Mason, H.E., et al., *Phophorus Speciation in Calcite Speleothems Determined from Solid-State NMR Spectroscopy.* Earth and Planetary Science Letters, 2007. **254**: p. 313-322.

14. de Groot, C.J., *Some remarks on the presence of organic phosphates in sediments.* Hydrobiologia, 1990. **207**: p. 303-309.

15. Koch, P.L., N. Tuross, and M.L. Fogel, *The Effects of Sample Treatment and Diagenesis on the Isotopic Integrity of Carbonate in Biogenic Hydroxylapatite.* Journal of Archaelogical Science, 1997. **24**: p. 417-429.

16. McDowell, R.W., et al., *Analysis of Potentially Mobile Phosphorus in Arable Soils Using Solid State Nuclear Magnetic Resonance.* J. Environ. Qual., 2002. **31**: p. 450-456.

17. Ruttenberg, K.C., *Development of a sequential extraction method for different forms of phosphorus in marine sediments.* Limnology and Oceanography, 1992. **37**(7): p. 1460-1482.

18. Houwen, J.A.M.V.D. and E. Valsami-Jones, *The Application of Calcium Phosphate Precipitation chemistry to Phosphorus Recovery: The Influence of Organic Ligands.* Environmental Technology, 2001. **22**(11): p. 1325-1335.

19. Sheikh, M.S., et al., *Reduction of dietary phosphorus absorption by phosphorus binders. A theoretical, in vitro, and in vivo study.* The Journal of Clinical Investigation, 1989. **83**(1): p. 66-73.

20. Fulmer, M.T., et al., *Measurements of the solubilities and dissolution rates of several hydroxyapatites.* Biomaterials, 2002. **23**: p. 751-755.

21. Shen, G.T. and E.A. Boyle, *Determination of lead, Cadmium and other trace metals in annually-banded corals.* chemical Geology, 1988. **67**(1-2): p. 47-62.

22. Krueger, H.W., *Exchange of carbon with biological apatite.* Journal of Archaelogical Science, 1991. **18**: p. 355-361.

23. Economou, E.D., T.C. Vaimakis, and E.M. Papmichael, *Kinetics of Dissolution of the Carbonate Minerals of Phosphate Ores Using Dilute Acetic Acid Solutions.* Journal of Colloid and Interface Science, 1998. **201**: p. 164-171.

24. Hieltjes, A.H.M. and L. Lijklema, *Fractionation of Inorganic Phosphates in Calcareous Sediments.* Journal of Environ Qual., 1980. **9**: p. 405-407.

25. de Groot, C.J. and H.L. Golterman, *Sequential fractionation of sediment phosphate.* Hydrobiologia, 1990. **192**: p. 143-148.

26. Jeppsson, L., R. Anehus, and D. Fredholm, *The Optimal Acetate Buffered Acetic Acid Technique for Extracting Phosphatic Fossils.* Journal of Paleontology, 1999. **73**(5): p. 964-972.

27. Fredd, C.N. and H.S. Fogler, *The kinetics of calcite dissolution in acetic acid solutions.* Chemical Engineering Sciences, 1998. **53**(22): p. 3863-3874.

28. Bryant, J.D., et al., *Oxygen isotope partitioning between phosphate and carbonate in mammalian apatite.* Geochemica et Cosmochimica Acta, 1996. **60**(24): p. 5145-5148.

29. Lee-Thorp, J.A. and J.v.d.M. Nikolaas, *Aspects of the chemistry of modern and fossil biological apatites.* Journal of Archaelogical Science, 1991. **18**(3): p. 343-354.

30. Koch, P.L., J.C. Zachos, and D.L. Dettman, *Stable isotope stratigraphy and paleoclimatology of the Paleogene Bighorn Basin (Wyoming, USA).* Paleogeography, Paleoclimatology, Palaeoecology, 1995. **115**(1-4): p. 61-69.

31. Harris, D.C., *Quatitiatve Chemical Analysis*. 6 ed, ed. J. Fiorillo. 2003, New York: W.H. Freeman and Company. 744.

32. Fredd, C.N. and H.S. Fogler, *The Influence of chelating Agents on the Kinetics of Calcite Dissolution.* Journal of Colloid and Interface Science, 1998. **204**: p. 187-197.

33. Saavedra, C., et al., *Effects of Tillage on Phosphorus Release Potential in a Spanish Vertisol.* Soil Sci. Soc. Am. J., 2007. **71**p. 56-63.

34. Golterman, H.L., *Fractionation of sediment phosphate with chelating compounds: a simplification, and comparison with other methods.* Hydrobiologia, 1996. **335**: p. 87-95.

35. Elliott, H.A. and G.A. Brown, *Comparative evaluation of NTA and EDTA for extractive decontamination of Pb-polluted soils.* Water, Air & Soil Pollution, 1989. **45**: p. 361-369.

36. Papassiopi, N., S. Tambouris, and A. Kontopoulos, *Removal of heavy metals from calcareous contaminated soils by EDTA leaching.* Water, Air & Soil Pollution, 1997. **109**(1-4): p. 1-15.

37. Kallay, N., et al., *Calorimetric Investigation of Kinetics of Solid Phase Dissolution: Calcium Carbonate Dissolution in Aqueous EDTA Solution.* Journal of Colloid and Interface Science, 1997. **188**: p. 68-74.

38. LaVigne, M., et al., *Skeletal P/Ca tracks upwelling in Gulf of Panama coral: Evidence for a new seawater phosphate proxy.* Geophysical Research Letters, 2008. **35**(L05604).

39. Lucotte, M. and B. D'Anglejan, *A comparison of several methods for the determination of iron hydroxides and associated orthophoshates in estuarine particulate matter.* Chem. Geol., 1985. **48**: p. 257-264.

40. Tessier, A., P.G.C. Campbell, and M. Bisson, *Sequential extraction procedure for the speciation of particulate trace metals.* Anal. Chem., 1979. **51**: p. 844-851.

41. Economou, E.D. and T.C. Vaimakis, *Benefication of Greek Calcareous Phosphate Ore Using Acetic Acid Solutions.* Ind. Eng. Chem. Res., 1997. **36**: p. 1491-1497.

42. Mehra, O.P. and M.L. Jackson, *Iron oxide removal from soils and clays by a dithionite-citrate system buffered with sodium bicarbonate.* Clays Clay Miner., 1960. **7**: p. 317-327.

43. Hunt, C.P., et al., *Effect of citraate-bicarbonate-dithionite treatment on fine-grained magnetite and maghemite.* Earth and Planetary Science Letters, 1995. **130**: p. 87-94.

44. Eichele, K., *HBA32*, in *WinSolids*. 1995.

45. Tseng, Y.-H., et al., *High resolution ^{31}P NMR study of octacalcium phosphate.* Solid State Nuclear Magnetic Resonance, 2004. **26**(2): p. 99-104.

46. Mason, H.E., et al., *Phosphate defects and apatite inclusions in coral skeletal aragonite revealed by solid-state NMR spectroscopy.* Geochemica et Cosmochimica Acta, In review.

47. Feng, J., et al., *Observation of bicarbonate in calcite by NMR spectroscopy.* Am. Mineral, 2006. **91**: p. 957-960.

48. Belton, P.S., R.K. Harris, and P.J. Wilkes, *Solid-state 31P NMR studies of synthetic inorganic calcium phosphates.* J. Phys. Chem. Solids, 1988. **49**: p. 21-27.

49. Rothwell, W.P., J.S. Waugh, and J.P. Yesinowski, *High-Resolution Variable-Temperature ^{31}P NMR of Solid Calcium Phosphates.* Journal of the American Chemical Society, 1980. **102**(8): p. 2637-2644.

50. Yesinowski, J.P. and H. Eckert, *Hydrogen Environments in Calcium Phosphates: ^{1}H MAS NMR at High Spinning Speeds.* J. Am. Chem. Soc., 1987. **109**: p. 6274-6282.

51. Herzfeld, J. and A.E. Berger, *Sideband intensities in NMR spectra of samples spinning at magic angle.* J. Chem. Phys., 1980. **73**(12): p. 6021-6030.

52. Hartmann, P., J. Vogel, and B. Schnabel, *The Influsence of Short-Range Geometry on the ^{31}P Chemical-Shift Tensor in Protonated Phosphates.* Journal of Magnetic Resonance, Series A, 1994. **111**(1): p. 110-114.

2.7. Figures

Figure 1. ^{31}P Single Pulse (SP) and $^{31}P\{^{1}H\}$ Cross Polarization (CP) MAS NMR spectra of Christmas Island Speleothem. a) SP with 1000s pulse delay, 5 kHz spinning rate; b) SP with 2s pulse delay, 5 kHz spinning rate; c) CP with 10 ms contact time, 3 kHz spinning rate; d) CP with 2 ms contact time, 3 kHz spinning rate; e) CP with 0.5 ms contact time, 3 kHz spinning rate. Spectra were collected with a ^{1}H decoupling power of 35 kHz for (from bottom to top) 2000, 2000, 2000, 2400, 86 acquisitions.

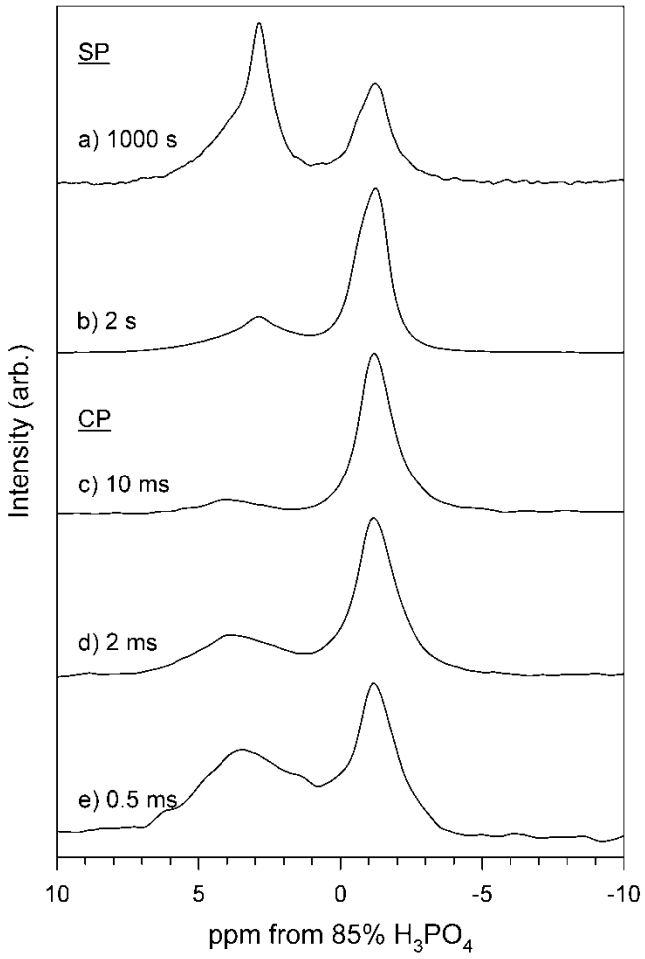

Figure 2. ^{31}P SP NMR spectra of Christmas Island Speleothem with varying continuous wave (CW) ^{1}H decoupling power (as $\nu_{1,H-1}$). a) 35 kHz; b) 26 kHz; c) 18 kHz; d) 9 kHz; f) 4.4 kHz. Spectra were collected at a spin rate of 2 kHz and a pulse delay of 2 s for 2200 acquisitions.

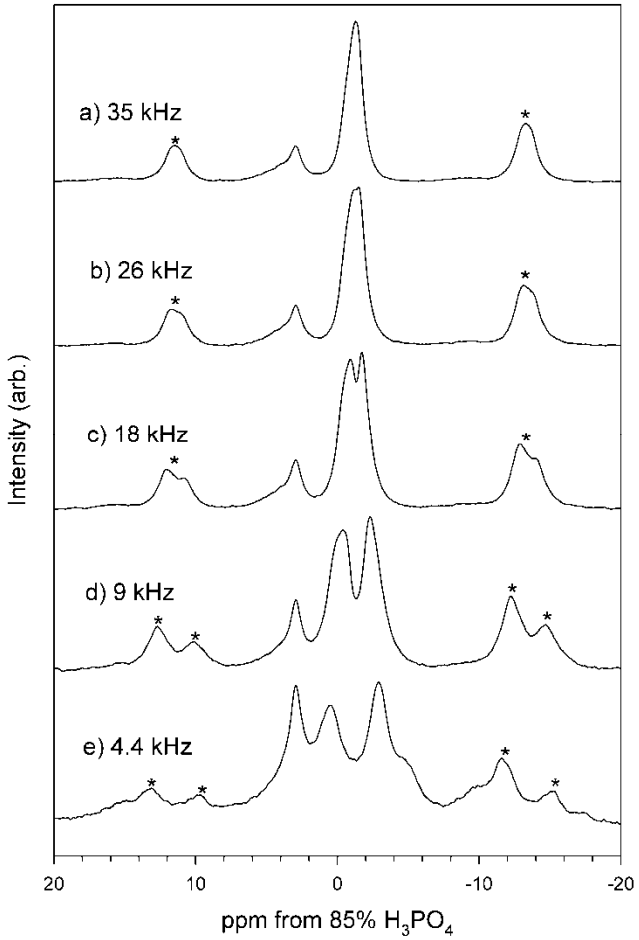

Figure 3. CP Kinetics of Christmas Island Speleothem from continuous wave (CW) $^{31}P\{^{1}H\}$ Cross Polarization (CP) MAS NMR spectra collected with varying contact times. Original spectra were collected at 10 kHz spinning rate, $\nu_{1\text{-}H}$=3.5, and 2 s pulse delay for 1000 acquisitions. Symbols represent the integrated intensity from center peaks for the ^{31}P sites at $\delta_{31\text{-}P}$=-1.1 ppm (○) and $\delta_{31\text{-}P}$= 3.2 (●)

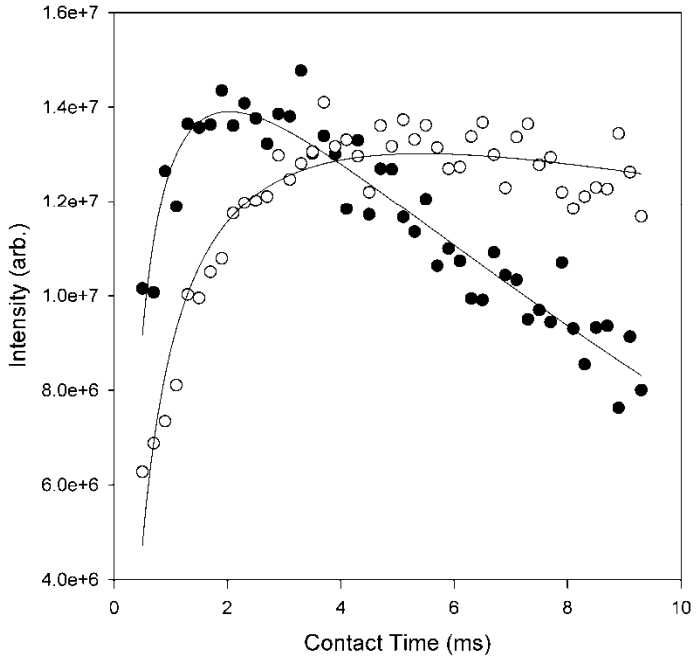

Figure 4. Comparison of ^{31}P Single Pulse (SP) NMR and $^{31}P\{^{1}H\}$ Cross Polarization (CP) MAS spectra of as-received Christmas Island Speleothem with spinning rate. a-d center bands only: a) SP with a spinning rate of 5 kHz; b) SP with a spinning rate of 2 kHz; c) CP with a spinning rate of 5 kHz; d) CP with a spinning rate of 2 kHz. e-h full spectra: e) SP with a spinning rate of 3 kHz; f) SP with a spinning rate of 2 kHz; g) CP with a spinning rate of 3 kHz; h) CP with a spinning rate of 2 kHz. Spectra were collected with a pulse delay of 2 s for (from bottom to top) SP 8000, CP 2000 acquisitions. CP spectra were collected with a contact time of 2 ms.

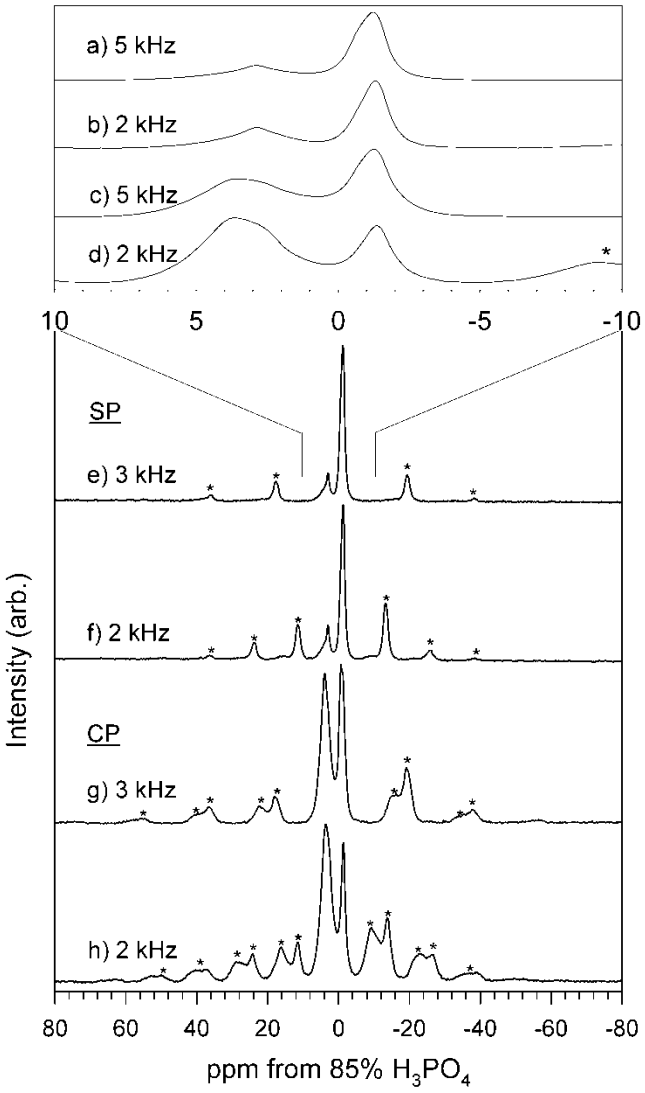

Figure 5. $^{31}P\{^{1}H\}$ HETCOR spectrum of the Christmas Island Speleothem. The spectrum was collected at a spin rate of 10 kHz, ^{31}P pulse width of 4 and ^{1}H pulse width of 4.5 and a pulse delay of 2 s for 1280 acquisitions for each point in t_1. The F1 spectral window was 50 kHz with 80 hyper complex points in t_1. The spectrum at the top of the 2D plot corresponds to the ^{1}H summed projection, the spectrum on the right side corresponds to the ^{31}P summed projection. Slices of the dimension ^{1}H were created corresponding to the two peaks observed in the ^{31}P spectrum. The top slice corresponds to the $\delta_{P\text{-}31}$= -1.1 ppm and the bottom corresponds to $\delta_{P\text{-}31}$= 3.2 ppm.

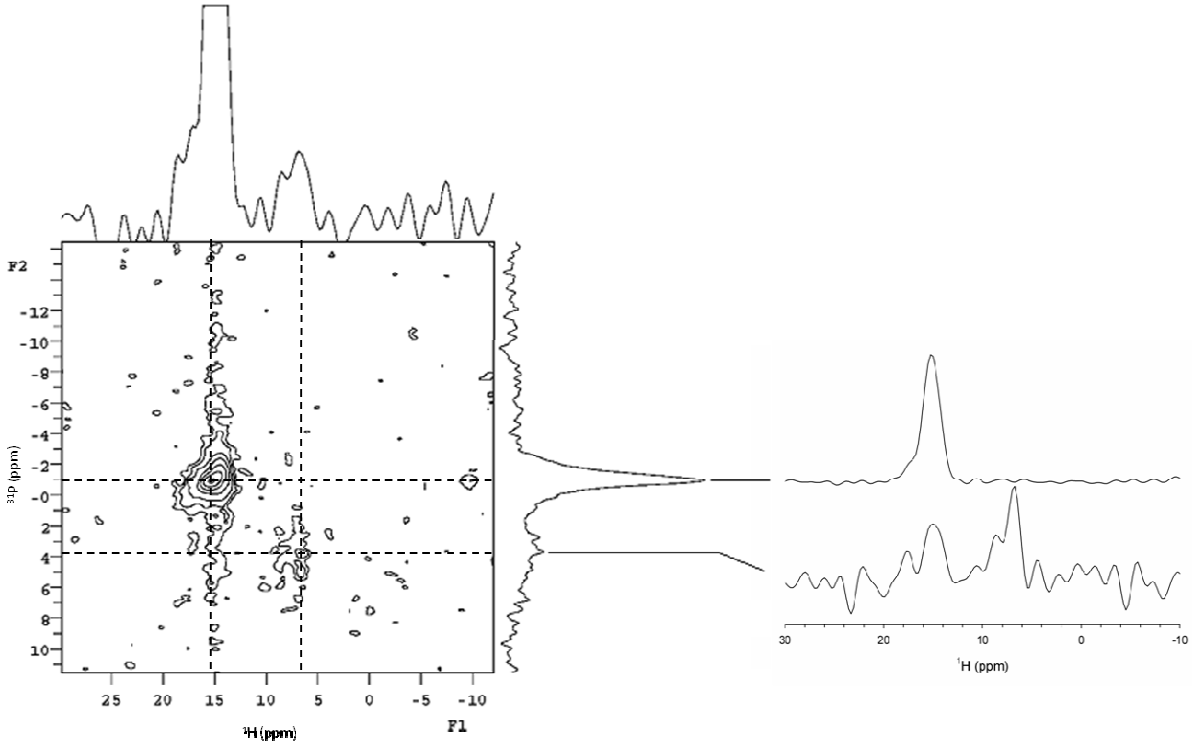

Figure 6. Powder x-ray diffraction pattern of Christmas Island Speleothem collected from 15˚ to 50˚ 2θ. Inset shows data collected at a slow scan rate from 26˚-27˚ 2θ in a region where peaks associated with monetite occur, but not for calcite. "C" indicates calcite reflections, "M" are for monetite.

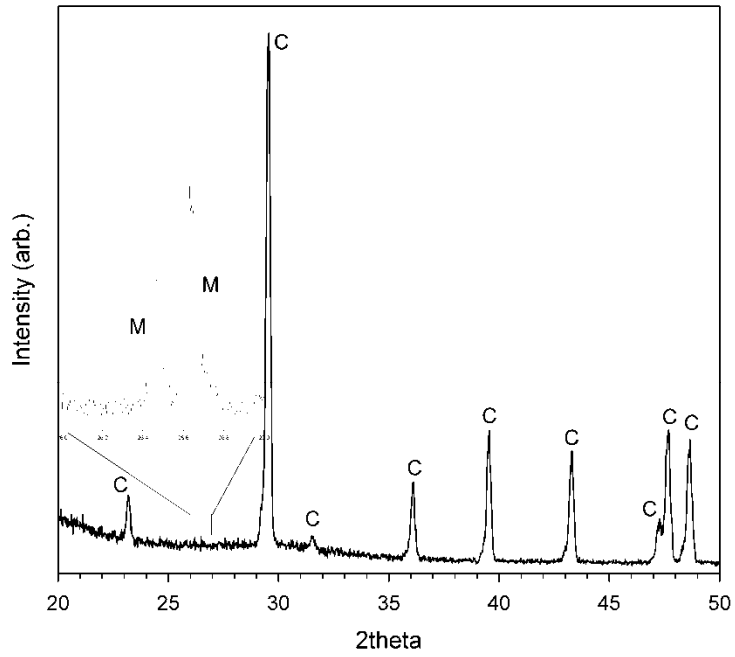

Degrees 2θ	hkl
23.19	C(012)
20.56	C(104)
31.57	C(006)
36.11	C(110)
39.56	C(113)
43.3	C(202)
47.21	C(024)
47.69	C(018)
48.66	C(116)
Slow Scan	
26.45	M(020)
26.63	M(-220)

Figure 7. Center band region of ^{31}P SP NMR and CP/MAS NMR spectra of solid residue of Christmas Island Speleothem dissolved in HCl. a) SP, As-received; b) SP, HCl treated; c) CP, As-received; d) CP, HCl treated. Spectra were collected at a spin rate of 5 kHz, decoupling power of 35 kHz, pulse delay of 1000 s (SP) and 2 ms contact time with 2 s pulse delay (CP) for (from bottom to top) 29696 and 15232 (CP) and 86 and 86 (SP) acquisitions.

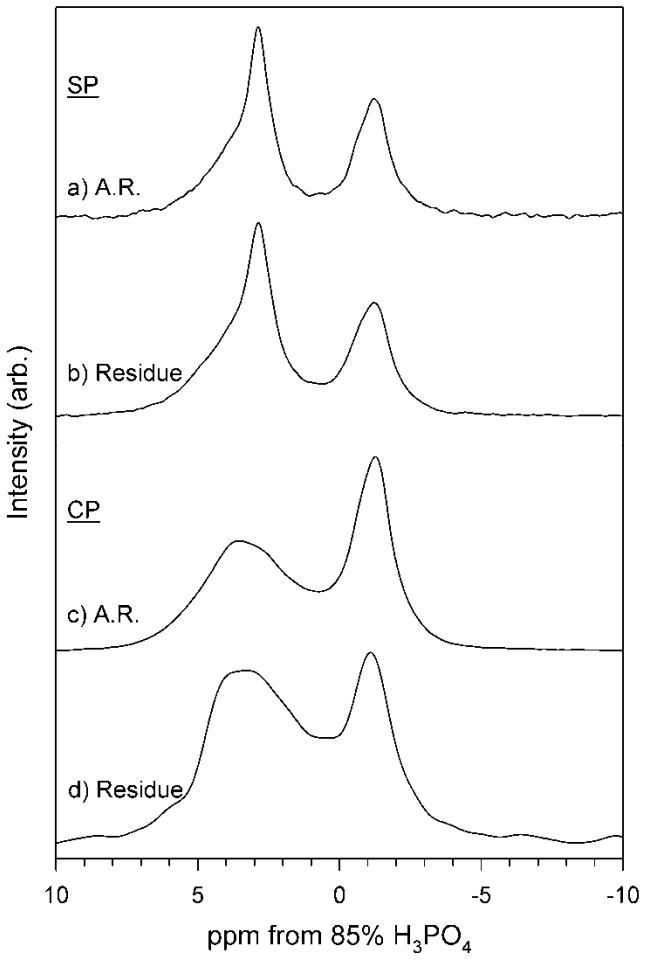

Figure 8. Center band region of ^{31}P SP NMR and CP/MAS NMR spectra of solid residue of Christmas Island Speleothem dissolved in Acetic Acid. a) SP, As-received; b) SP, Acetic Acid treated; c) CP, As-received; d) CP, Acetic Acid treated. Spectra were collected at a spin rate of 5 kHz, decoupling power of 35 kHz, pulse delay of 1000 s (SP) and 2 ms contact time with 2 s pulse delay (CP) for (from bottom to top) 29696 and 22496 (CP) and 86 and 86 (SP) acquisitions.

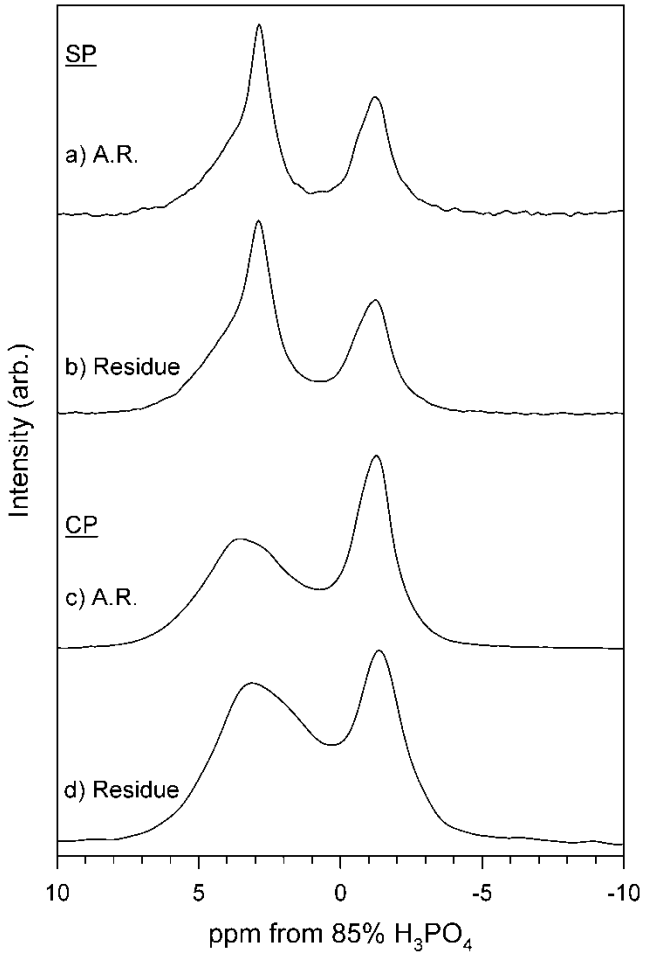

Figure 9. ^{31}P CP/MAS NMR spectra of acetic acid-treated Christmas Island speleothem with varying ^{1}H decoupling powers (as $\nu_{1,H-1}$). a) 35 kHz; b) 26 kHz; c) 18 kHz; d) 9 kHz; e) 4.4 kHz. Spectra were collected at a spin rate of 3 kHz and a pulse delay of 2 s for 4496 acquisitions each.

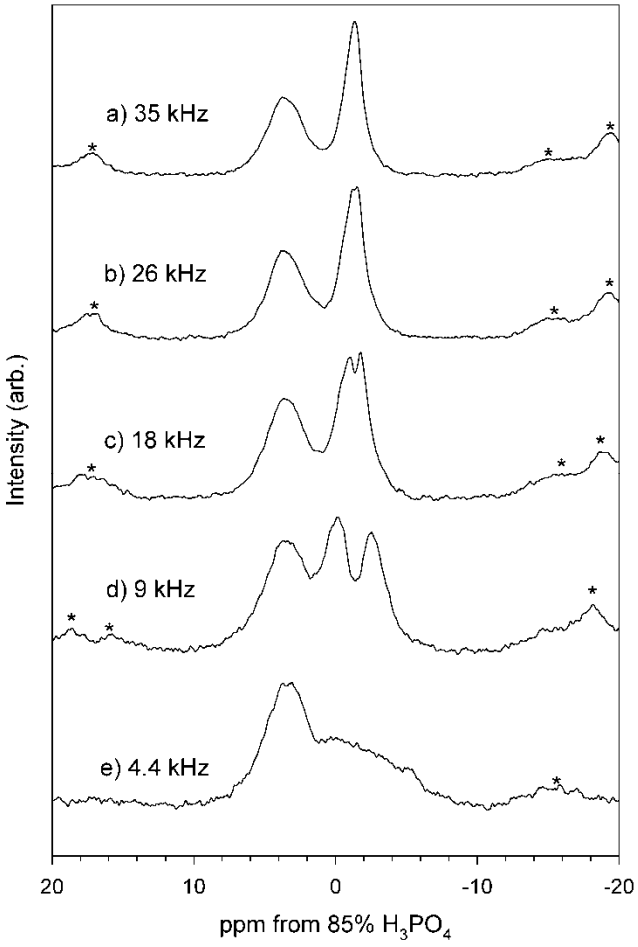

Figure 10. Center band region of ^{31}P SP NMR and CP/MAS NMR spectra of solid residue of Christmas Island Speleothem dissolved in EDTA solution. a) SP, As-received; b) SP, EDTA treated; c) CP, As-received; d) CP, EDTA treated. Spectra were collected at a spin rate of 5 kHz, decoupling power of 35 kHz, pulse delay of 1000 s (SP) and 2 ms contact time with 2 s pulse delay (CP) for (from bottom to top) 35624 and 29696 (CP) and 86 and 86 (SP) acquisitions.

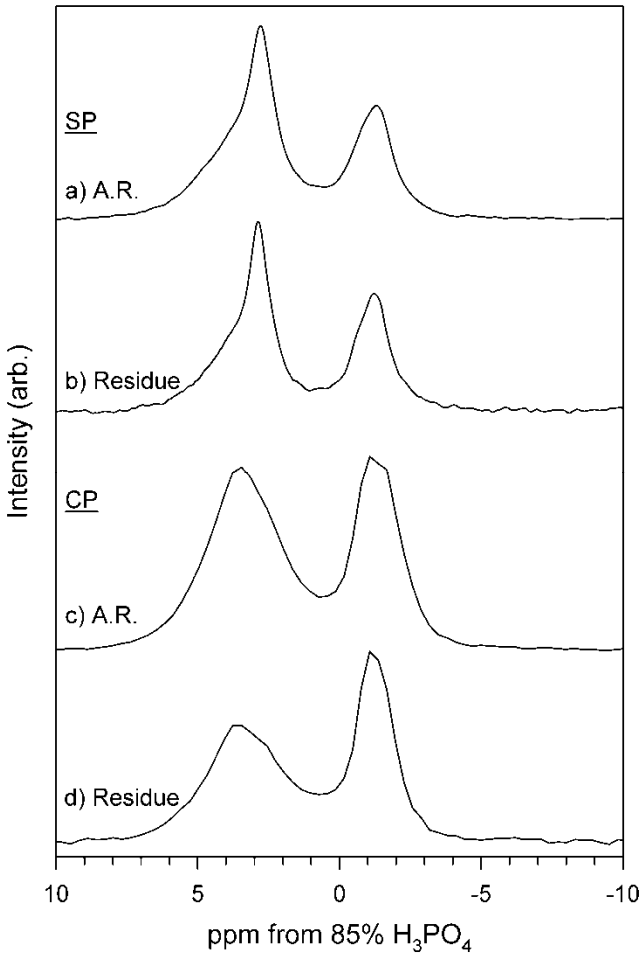

Figure 11. Center band region of ^{31}P SP NMR and CP/MAS NMR spectra of solid residue of Christmas Island Speleothem treated with the Multistep procedure. a) SP, As-received; b) SP, Multistep treated; c) CP, As-received; d) CP, Multistep treated with a decoupling power of 25 kHz. Spectra were collected at a spin rate of 5 kHz, decoupling power of 35 kHz, pulse delay of 1000 s (SP) and 2 ms contact time with 2 s pulse delay (CP) for (from bottom to top) 35624 and 29696 (CP) and 86 and 86 (SP) acquisitions.

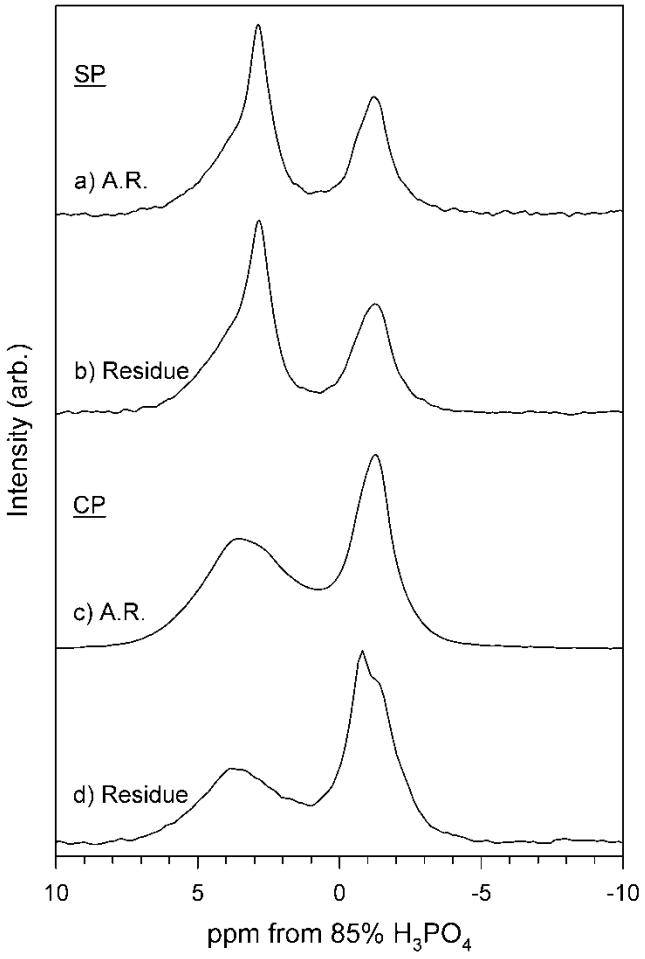

Figure 12. Center band region of ^{31}P SP NMR and CP/MAS NMR spectra of solid residue of Christmas Island Speleothem treated with the SEDEX method. a) SP, As-received; b) SP, Step 1, $MgCl_2$-treated; c) SP, Step 2, CBD-treated; d) CP, As-received; e) CP, Step 1, $MgCl_2$-treated; f) CP, Step 2, CBD-treated. Spectra were collected at a spin rate of 5 kHz, decoupling power of 25 kHz, pulse delay of 1000 s (SP) and 2 ms contact time with 2 s pulse delay (CP) for (from bottom to top) 3328, 5445 and 29696 (CP) and 86 and 86 (SP) acquisitions.

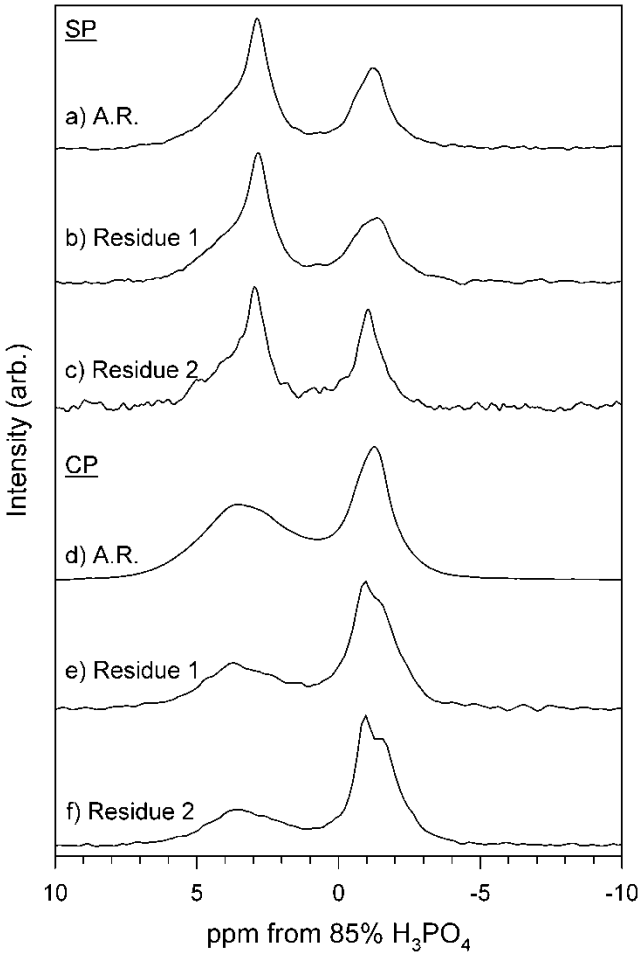

2.8. Tables

Table 1. SP experimental data on digestion of the Christmas Island Speleothem including sample consumed and relative integrated intensities of ^{31}P NMR peaks in quantitative SP spectra. *Dilution of dissolved samples was done using volume, not mass.

					Relative Intensities for ^{31}P NMR peaks centered at: (±0.04)		
Treatment	Starting weight (g)	Final weight (g)	Solid Consumed (%)	Final [P] in sample (μg P g^{-1} sample)	3.1 ppm (PO_4 in calcite)	2.9 ppm (unidentified)	-0.9 ppm (monetite)
As Received (none)	-	-	-	1641	50	16	34
HCl	4.93	0.36	93	2492	56	12	32
Acetic Acid	5.06	0.60	88	4530	56	12	32
EDTA	4.99	0.82	84	2939*	46	18	36
Multi-Step	1.00	0.76	24	3283	52	15	33
SEDEX-$MgCl_2$	0.50	0.44	15	1725*	52	16	32
SEDEX-CBD	0.44	0.22	51	1686*	50	15	35
SEDEX-Acetate Buffer	0.22	0.00	100	-	-	-	-

Table 2. Chemical Shift Anisotropy ^{31}P NMR peaks from the Christmas Island Speleothem estimated from analysis of the side band intensities of a $^{31}P\{^{1}H\}$ Cross Polarization (CP) MAS NMR spectrum acquired at spinning rate of 3 kHz.

δ_p=3.1	
D11	16.957
D22	-3.441
D33	-3.765
Red. Anisotropy	13.707
Anisotropy	20.56
Asymmetry	0.024
Span	20.722
Skew	-0.969
Monetite (-0.9 ppm)	
D11	13.333
D22	-8.432
D33	-8.747
Red. Anisotropy	14.615
Anisotropy	21.923
Asymmetry	0.022
Span	22.08
Skew	-0.971

III: Phosphate Speciation in Phosphate/Calcium Carbonate Coprecipitations Determined from Solid State NMR Spectroscopy

3.1. Abstract

Natural calcium carbonate samples contain defects from minor elements, such as phosphorus, that can be used as a paleoproxy. To understand the formation of phosphorus defects during calcium carbonate precipitation synthetic samples were prepared to investigate the effects of environmental factors such as pH, phosphorus concentration, temperature, and rate of reactant precipitiation. Through the use of ^{31}P solid state nuclear magnetic resonance (NMR) the species of phosphorus precipitated during the application of these variables was investigated. Standard samples created at 25˚C, with initial phosphorus concentrations of 18 μM, and a growth rate of 9 hours (addition rate of 150 μL min^{-1}) exhibited three ^{31}P NMR peaks, a peak associated with monetite at -1.2 ppm, phosphorate co-precipitated with calcite at 3.1 ppm and an unidentified crystalline phosphate phase at 2.9 ppm. The change in relative intensity, peak position and phosphate uptake was investigated over a variety of conditions. Temperature did not affect the distribution of phosphorus forms, but did change the amount of phosphorus incorporated and the proportion of crystalline monetite formed. Initial phosphorus concentrations, the addition of magnesium, and pH precipitated amorphous calcium phosphate along with proportions of each phosphorus species in the solid.

3.2. Introduction

3.2.1. Overview of Trace and Minor Elements

Phosphate uptake during calcite precipitation has been investigated extensively due to its environmental implications for phosphate mobility and potential use as paleoclimate proxy. Phosphorus concentrations in the environment have dramatically increased due to the application of fertilizers, such as manure and industrial waste [1-2]. Increased phosphorus concentrations in natural waters leads to eutrophication [3]. The use of calcium carbonates for remediation has been studied due to the reactivity of calcite with phosphorus [4-5]. Phosphate uptake processes range from phosphate sorption to the surface of calcite, coprecipitation of phosphate with calcite, to precipitation of calcium phosphates each with a different solubility. By understanding the conditions in which these precipitates form, it is possible to optimize the conditions in the field to precipitate the most stable of phosphorus forms, such as hydroxylapatite [6].

The precipitation of calcium carbonate in cave systems occurs over time from drip water. This solution contains both trace and minor elements that vary in concentration seasonally [7-8]. During precipitation of calcium carbonate, these small component elements such as phosphorus, magnesium and strontium can be included either as structural defects or sorb to the surface. Increased bioactivity is observed during periods of high rainfall, which is positively correlated to the concentration of phosphorus present in speleothems, while the concentrations of magnesium and strontium are inversely related[7, 9]. As phosphorus concentrations change seasonally, the species of phosphorus formed also changes, which can be used to determine the original drip water properties [7-8].

Phosphorus is present in sediments in multiple forms, both organic and inorganic. Sources of phosphorus include decaying plant material, bat guano, and leaching from minerals rich in phosphorus. The largest source of dissolved phosphorus present during speleothem formation comes from leaching of decaying vegetation during autumn and winter storms [10]. Phosphorus is commonly found in the form of phosphate due to the hydrolysis of phosphorus with water.

Calcite is widely distributed in low-temperature geochemical settings such as in caves and in the ocean as tests of marine organisms [10-11]. The broad presence of calcite enables scientists to collect samples from all over the world that correlate to the same geological time period to map out the global climate. In calcium carbonate systems that exhibit seasonal layering, such as corals and speleothems, amounts of mineral precipitated and concentrations of included elements can be used as a paleoproxy [7].

3.2.2. Chemical Form of Phosphorus

An understanding of the chemical form of phosphorus within calcite is necessary for determining the mechanism by which it is removed from solution. Phosphate has a small solubility index and will precipitate at small concentrations in the presence of calcium carbonate. As calcium carbonate precipitates, phosphate can be adsorbed to the active surface sites and occluded by further precipitation of calcium carbonate. Amorphous calcium phosphate may form in solutions of high phosphate concentrations, which over time can change to a crystalline calcium phosphate [6]. Possible calcium phosphates that precipitate in the presence of calcium include hydroxylapatite [12], monetite, and brushite.

The most common and stable calcium phosphate is hydroxylapatite (HAP), $Ca_{10}(PO_4)_6(OH)_2$, the hydroxyl endmember of the apatite group. This mineral is commonly found in bones and calcium carbonate precipitates. Monetite, $CaHPO_4$, is the least stable of crystalline calcium phosphates and is commonly found in limestone caves rich with bat and bird guano. The hydrated form of is brushite, $CaHPO_4 \bullet 2H_2O$, which is commonly found in guano-rich caves.

Calcium phosphates along with other phosphorus species have been identified with analytical techniques such as x-ray diffraction (XRD), fourier transform infrared spesctroscopy (FTIR), and solid state nuclear magnetic resonance (NMR). Previous research with solid state NMR has identified monetite and phosphate coprecipitated with calcite in speleothems [13]. Whereas XRD has identified brushite [14]. Many other speleothems exhibit loosely bound phosphorus that resulted from the oversaturation of calcite in the system accompanied by the co-precipitation of phosphate[15]. It is possible to imitate these systems in the laboratory, enabling scientists to understand the processes that drive the formation of different phosphate species [16-18]. In addition the synthesis of calcium phosphates during calcite precipitation using inorganic material shows that the main phosphate species in speleothem calcite is inorganic in origin, instead of organic phosphorus entrapped in the crystalline calcite [19].

3.2.3. Phosphate Co-precipitation with Calcite

Previous research has investigated the effect of temperature, pH, rate of addition and phosphate concentrations in the starting solution on the incorporation of phosphate in the precipitation of calcium carbonate minerals.

3.2.3.1. Temperature

Changes in temperature affect the total energy in the system, potentially changing the amount of calcite formed and the amount of phosphorus consumed. Griffin and Jurinak studied the effect of temperature on the removal of phosphorus during calcite precipitation. As temperature increased, the amount of phosphorus left in solution decreased, suggesting that more phosphorus was included in the crystalline structure [1].

House and Donaldson (1986) investigated the incorporation of phosphate with calcite from 5 to 35˚C. The amount of phosphate taken up changed with temperature, but the rate of uptake did not affect the total amount of phosphorus coprecipitated. They hypothesized that active surface sites immediately fill with phosphate, preventing the inclusion in the crystal structure leading to surface densities of phosphorus of 0.22 to 0.13 μmole m^{-2}[20]. The rate of precipitation is so fast that complete incorporation is not possible, and a secondary form of phosphate forms through layer growth. A two-component model of adsorption was developed to explain the coprecipitation of phosphate with calcite from 5-25˚C in which PO_4^{3-} or $CaPO_4^-$ and HPO_4^{2-} or $CaHPO_4^0$ describe the sorption isotherms. Phosphate and hydrogen phosphate ions were assumed to adsorb on the surface of calcite replacing both the adsorbed water and partially dehydrating.

$$H_2O(ads) + PO_4^{3-}(aq) = PO_4^{3-}(ads) + H_2O \qquad K_1$$

$$H_2O(ads) + HPO_4^{2-}(aq) = HPO_4^{2-}(ads) + H_2O \qquad K_2$$

3.2.3.2. pH

The pH in natural systems varies depending on the concentration of dissolved CO_2, this can greatly impact the products produced during precipitation of phosphorus with calcite. Ishikawa and Ichinkuni investigated phosphate incorporation in calcite in pH ranges of 7.9-9.5. Their proposed mechanism for the coprecipitation of phosphate with calcite was based on the homogeneous distribution of phosphate within the crystal [21]. House and Donaldson also studied the impact of pH on the uptake of phosphate by calcite with pH ranging from 7 to 9.5. They determined the precipitation of phosphorus with calcite is dependent on the solution pH.

3.2.3.3. Rate of Growth

In order to model conditions in which phosphate can be exposed to calcite, reactants were added at varying rates. House and Donaldson analyzed phosphate coprecipitation with calcite with a batch method, in which all reactants were added at once. Within the first two minutes of the reaction, 80% of the phosphate uptake occurred no matter how long the solution was left with the precipitate [20]. Based on models and scanning force microscopy, the batch method was determined to produce only two phosphorus phases, an amorphous phase of phosphate sorbed to the surface of calcite and HAP [22].

Several studies investigated the incorporation of phosphate with calcite with varying rates of addition of reactants [13, 16-18]. By using the constant addition method it is possible to mimic precipitation from drip water in caves. This method allows the gradual growth of calcite crystals. Speciation data collected on solids synthesized with this method was used to determine

that three phosphorus forms are present, monetite, phosphorus coprecipitated with calcite, and an unidentified form.

3.2.3.4. Phosphorus Concentration

Initial concentrations of phosphate in solution dramatically change the amount of calcite precipitated. Reddy (1977) studied the effect of 1.6 X 10^{-5} M glycerophophate and 2 X10^{-6} M orthophosphate on the rate of calcite seeded crystal growth at 25˚C, pH 8.8. The addition of the phosphate decreased the crystallization rate constants to half that of their values in pure solutions. This effect was explained by Langmuir-type adsorption [23]. The rate constant was defined as:

$$k_0/(k_0-k) = 1 + k_2/k_1 \text{ [additive]}$$

k_0 is the crystal growth rate constant without the additive ion; k_1 and k_2 are adsorption and desorption rate constants for phosphorus[23]. The plot that Reddy (1977) created of $k_0/(k_0-k)$ versus the reciprocal of the additive concentration was linear, indicating that the reaction could be modeled with a Langmuir isotherm. The addition of phosphate reduced the k_2, leading to a stronger equilibrium adsorption of phosphate at the surface. In solutions with a pH of 9.6 and phosphorus concentrations of 1.3 X 10^{-5} to 8.5 X 10^{-5} mol PO_4^{3-} L^{-1} the adsorption of phosphorus on calcite was studied and it was determined that there was a linear relationship between the coprecipitated amount of phosphate and the total amount of phosphate [21]. This observation supported the Langmuir-type adsorption isotherm.

House and Donaldson (1986) studied the adsorption of inorganic phosphate in concentrations below 20 μmol L^{-1}. They found that the rate at which phosphate was removed from solution did not change as initial concentration of phosphate increased. The effect of initial phosphate concentrations was studied by Plant and House (2002) with a range of 0-500 μmol L^{-1} KH_2PO_4. Phosphorus concentrations less than 20 μmol L^{-1} followed the precipitation mechanism previously described. As phosphate concentrations increased above 20 μmol L^{-1} calcite precipitation was inhibited [24]. McDowell et al. (2002) studied the sorption of phosphorus in concentrations of 3.33-36.75 μmoles L^{-1} on calcite and found using X-ray diffraction that mainly that an apatite-like phase and brushite formed [14].

3.2.4. Inclusion of Other Elements

Presence of other dissolved ions such as magnesium, strontium and lead have been shown to affect the precipitation of calcium carbonate and possibly the uptake of phosphate. No natural calcium carbonate system is without other elements present as either structural defects or mineral inclusions. Magnesium, strontium, lead, and cadmium are just a few of the elements that substitute for calcium within the structure, changing the solubility and structure of the mineral [6]. All calcium carbonate systems such as corals, speleothems, and marine sediments contain these elements in small concentrations. Previous research has determined that both strontium and magnesium concentrations are high in speleothems and correlate with seasonal variations [8]. Concentrations of magnesium in samples such as the speleothem from Grotta di Ernesto contain concentrations around 500-1200 μmoles g^{-1}. Whereas strontium concentrations vary from 20-30 μmoles g^{-1}[8].

Concentrations of strontium and magnesium have been shown to vary as rate of rainfall varies, which is used to determine relationships to seasonal climate variations. Strontium concentrations in speleothems are controlled by the variation in cave seepage water and calcite precipitation rates. Portions of speleothem with highest concentrations of strontium correlate to winter and spring seasons. Once this relationship is further understood it can be applied to measuring the seasonal variation of pCO_2 [8, 16]. Correlations between magnesium concentrations and hydro-environmental conditions have been determined. During periods of high rainfall higher concentrations of magnesium were observed in speleothems. This relationship parallels that of phosphorus, enabling scientists to directly study the interaction of magnesium with phosphorus.

The presence of other elements in solution along with phosphorus may inhibit phosphorus uptake during calcite precipitation, the species of phosphorus precipitated and the amount of calcium carbonate formed. Strontium concentrations in sediments have previously shown weak effects on precipitation rates of calcite [16]. Increased concentrations of strontium in speleothems are inverse to those of magnesium and phosphorus, and correlate to periods of high calcite precipitation. Strontium may impede the precipitation of phosphorus with calcite, but further research needs to be conducted to determine if there is a correlation [8].

High concentrations of magnesium inhibit the uptake of phosphorus with calcium carbonates. Previous research has been conducted on seawater and carbonate precipitation, in which magnesium competes with calcium [25]. The addition of magnesium to solutions with phosphate decreases the adsorption of phosphorus on the surface of calcite[26]. Magnesium is also found in fresh water systems, such as caves, at concentrations high enough to impact the formation of calcite and calcium phosphates. Previously, research focused on magnesium versus

calcium ratios to reconstruct past paleotemperatures and no research had been done investigating the effect on uptake of phoshate [8]. Salimi et al. (1985) and Cao and Harris (2008) studied the impact of magnesium on the formation of synthetic hydroxylapatite. Salimi et al. (1985) found that the addition of magnesium not only hindered the formation of HAP but lead to the formation of whitlockite[27]. Contradictory results from Cao and Harris (2008) suggested that ACP formed, because no crystalline phase formed until heat was applied[28]. This result is contrary to the previous theory that magnesium, being classified as a less effective inhibitor, does not cause any change in the chemical character of the substrate precipitated[27, 29]. No solid state NMR data was collected on Cao and Harris (2008) sample to determine whether trace amounts of HAP formed. The technique, X-ray diffraction, they used to analyze the sample only observed ACP, but since phosphorus concentrations are low in the samples it is important to ensure that no other trace amount of crystalline phosphate were present. In addition the concentrations used in experiments reported by Cao and Harris (2008) were high compared to natural systems, but suggest further investigation on the impact of magnesium in polluted systems is needed.

3.2.5. Identifying Phosphorus Species

It is crucial to identify each species of phosphate present to use phosphate species to determine paleoclimate, yet very few studies have successfully accomplished this. Original research on the precipitation of phosphate with calcite determined phosphate species formed from the phosphorus to calcium ratios. Known data on the P/Ca ratios of crystalline phosphates, such as HAP, was compared to those found in the calcite phosphate coprecipitation experiments

to identify each species. Original identification of HAP and phosphate sorbed to the surface of calcite was determined this way by Griffin and Jurnak (1973) [1]. The speciation of phoshate was calculated by House and Donaldson (1986) from the measured pH, temperature, measured total phosphorus and by assuming equilibrium with the calcite solid [20].

Dove and Hochella (1992) used Scanning Force Microscopy (SFM) to observe the precipitation of calcite along with the influence of phosphate on precipitation. Morphological data suggested inhibition of calcite formation was caused by two mechanisms, formation of an amorphous phase and a layered phase which correlated with previous studies [22].

X-ray diffraction (XRD) is the standard method used to characterize predominant species in a solid. But the detection limit of the XRD is around 1%, far above that expected for phosphate/calcite coprecipitation experiments at geochemically relevant phosphate concentrations. The Christmas Island Speleothem has one of the highest concentrations of phosphorus found in natural samples, 3000-6000 μg P g^{-1}, meaning that it is not possible to detect all the phosphorus species present.

One technique has proven its effectiveness in determining trace phosphate species present in solids, solid state NMR. This technique selectively observes one element, such as ^{31}P to detect only the phosphorus forms present in a sample [30]. By observing only one element it is possibly to analyze samples containing phosphorus as low as 2 μmoles dm^{-3}. It is possible to observe other nuclei and their relationship to ^{31}P, providing structural information on the role of phosphorus in solids.

3.2.6. Use of Solid State NMR

Solid State NMR spectroscopy has proven to be a useful technique in identifying the molecular structural environments of phosphorus in natural samples and specifically in phosphate species present in calcium carbonates such as speleothems and corals.

Deep sea corals contain only trace concentrations of phosphorus, 17 to 319 μmoles g^{-1}, which can be used as a paleoproxy. Mason et al. (In Press) was able to use solid state NMR to not only determine all the phosphorus species deep sea corals, but also to determine the concentration of phosphorus and the amounts of each species present matching it to data collected by laser ablation inductively coupled plasma mass spectrometry (LA-ICPMS) [31].

Mason et. al. (2007) determined the form of phosphorus present in speleothems from Grotta di Ernesto to be phosphate incorporated in calcite, crystalline monetite, and an unidentified crystalline phosphate. These data will be used to determine paleoclimate once further research on the processes that drive each species formation are fully understood [13].

Solid state NMR has been used on marine sediments and waters to directly determine the presence of organic phosphorus, whereas previous research to investigate organic phosphorus had to use dissolution experiments to get concentrations of phosphorus high enough for analysis with other techniques [32]. Cade-Menun (2005) also investigated organic phosphorus through solid state NMR on bulk soil, water and other environmental samples to understand the role it has in natural systems[33]. By understanding the forms of phosphorus present in a system it is possible to better understand the phosphorus cycle.

Coprecipitation studies have been analyzed by solid state NMR, in which three species were observed: monetite, phosphate sorbed to the surface of calcite, and an unknown phosphorus

species [13]. Further studies on the sample to characterize the co-precipitated phosphorus with calcite are important for understanding the mechanisms by which dissolved phosphate is removed by calcite precipitation. This chapter continues the analysis of these samples, including exploring different kinetic parameters and analyzing a sample ^{13}C enriched to determine the relationship between calcite and phosphorus. In addition the impact of magnesium on the formation of calcite, phosphate uptake, and phosphate forms precipitated will be investigated.

3.3. Methods

3.3.1. Batch Coprecipitation

Two methods were used for preparation of calcite/phosphate coprecipitates. The first procedure, a batch precipitation method, followed the procedure described by House and Donaldson (1986)[20]. Initial solutions were created with two different concentrations of phosphate, 6.35 and 3.2 μM. All growth solutions contained 2.5 mM $CaCl_2$ and Na_2CO_3, stirring at 700 reps per minute. Reactions were started by the addition of an aged slurry of calcite seeds, 60 mg/g water. Typically the solution turned milky white within five minutes of seed addition. If precipitation was evident before the addition of the seeds, the sample was discarded. To monitor phosphate uptake during precipitation 5 mL samples of the growth solution were taken at 0, 5, 10, 17, 30, 65, 90, 140, 200, 250 and 300 minutes with a plastic syringe fed into the solution through Teflon tubing, filtered through 0.2 μm filters and analyzed for phosphate (see 3.2.3.1). Coprecipitation experiments were conducted at 10 or 25 degrees Celsius with the temperature held constant using a water bath. Table 1 summarizes the conditions for sample synthesis. After 300 minutes of reaction the solids were separated by filtration with 0.2 μm filter paper and dried in an oven at 60˚C overnight.

3.3.2. Constant Addition Method

The second calcium/phosphate coprecipitation method followed Zhong and Mucci (1993) and Tesoriero, Pankow (1996) and Reeder et al. (2000) and consisted of a constant rate of addition of Ca^{2+} and CO_3^{2-} through separate syringes to a seeded solution, with phosphate included with the carbonate[16-18]. Solutions were pumped from a dual syringe pump into a glass beaker containing initially 0.7 L distilled water, 0.007 M $CaCl_2$, 0.007 $NaHCO_3$, and 0.1 M NaCl. Addition of $CaCl_2$ and $NaHCO_3$ to the initial solution was to ensure approximate equilibrium with the calcite seeds. NaCl was added as a background electrolyte. One syringe contained 0.1 M $CaCl_2$ and 0.1 M NaCl; the second contained 0.1 M $NaHCO_3$, 0.1 M NaCl and varying amounts of KH_2PO_4 solution. Tables 2-8 contain the experimental phosphate concentrations, pumping rates, temperatures, and pH used. Temperatures were controlled with a water bath. All experiments were started at a pH of 8.2 except for a few pH-varied experiments. After the addition of the calcite seeds the pH was measured with an Orion pH electrode, and adjusted if necessary with 0.1 M NaOH added drop wise until pH reached the targeted value. Experiments conducted at a pH of 9.4 were kept constant with an automated Metrohm 718 stat titrino titrator with 0.1 M NaOH and Orion pH electrode for the duration of the synthesis. Solutions were open to the air and stirred with a magnetic stir bar at 300 rpm. The pumping rate for standard experiments was 150 μL/min for 9 hrs giving a total addition of 81 mL from each syringe. The reaction was promptly stopped and the solid collected by filtration and dried in an oven at 60˚C overnight. Growth rate experiments were conducted by adjusting the pump rates to add the same volume (81 mL) over periods varying from 0 minutes to 51 hours, see Table 3. A separate ^{13}C-enriched sample was created using sodium hydrogencarbonate 98 atom % ^{13}C with all volumes scaled down by one-fourth of the original synthesis; each syringe contained 20.25

mL solution, and the initial solution in the beaker contained 175 mL. To reduce ^{13}C exchange with atmospheric CO_2, the vessel was sealed during the 4.5 hrs of coprecipitation.

Samples containing magnesium in the initial solution were also created with varying temperature, pumping rate, and pH. All standard experiments were conducted as described above but contained 10 mM $MgSO_4$ in the initial solution. Other experiments were conducted by varying the magnesium concentration from 0.2 mM to 20 mM.

3.3.3. Analytical Methods

3.3.3.1. Phosphate Analysis

Solutions were analyzed for phosphate concentration before and after each experiment to determine phosphate uptake during calcite precipitation. Analysis was done using an Hach Ultraviolet spectrometer to determine phosphorus concentrations remaining in solution. Phosphate concentrations were measured by UV-VIS spectroscopy using Hach Reactive Phosphorus Test 'N Tube^{tm} Vials. Standards were created varying from 1 μM to 100 μM using the same stock K_2PO_4 solution as the solution used for experiments to ensure accuracy. The standard constant addition experiment was repeated three times to monitor reproducibility. The phosphate content of the overgrowths was calculated by difference in total phosphate added from that remaining, as determined from the concentration in solution at the end of the experiment and total solution volume.

3.3.3.2. X-ray Diffraction

Powder X-ray diffraction (XRD) was used to analyze all samples using a Scintag PADX diffractometer using copper radiation operating with a voltage of 45 kV and 25 mA. Samples were scanned from 15˚ to 50˚ 2θ, with a step size of 0.2˚, at a rate of 1 degree per minute. Further analysis with XRD at a slow scan rate was done on one sample from 26 to 27 degrees (2θ) with a step size of 0.00050 per 250 seconds in an attempt to observe reflections from trace amounts of monetite in the sample.

3.3.3.3. NMR Spectroscopy

Most ^{31}P NMR spectra were collected using a Varian Inova 400 MHz Solid State NMR spectrometerunder magic-angle-spinning conditions (MAS) at operating frequencies of 161.8 MHz and 399.8 MHz for ^{31}P and ^{1}H, respectively. Samples were contained in a 7.5 mm (o.d) Si_3N_4 rotor which was spun at rates of 3 and 5 kHz. ^{31}P Single pulse experiments were completed with a relaxation delay of 2 seconds and 6.5 μs pulses ($\pi/2$ = 6.5 μs). Additional single pulse experiments to quantify the relative intensities of phosphate species were collected with a relaxation delay of 1000 seconds, 4 μs pulses ($\pi/2$ = 4 μs), and tppm (time proportional phase modulated) ^{1}H decoupling ($\nu_{1,H}$ = 35 kHz) on a Chemagnetics probe assembly configured for 3.2 mm (o.d.). Ramped CP/MAS experiments were done with contact times of 0.2, 2, and 10 milliseconds. The ^{31}P NMR chemical shifts ($\delta_{P\text{-}31}$) are referenced with respect to 85% phosphoric acid, using hydroxylapatite as a secondary reference set to $\delta_{P\text{-}31}$ = 2.65 ppm. The $^{31}P\{^{1}H\}$ heteronuclear correlation (HETCOR) experiments used a Chemagnetics probe assembly configured for 3.2 mm (o.d.) rotors spinning at 10 kHz with a pulse width of 3 μs, 2 ms contact

time, ramped CP. The F1 spectral window was 50 kHz with 80 hyper complex points collected in T1, each represented 800 acquisitions. The $^{31}P\{^{13}C\}$ rotation echo double resonance (REDOR) data were collected directed ^{31}P excitation at dephasing periods of 1, 2, and 5 ms (corresponding to 8, 16, and 40 rotor periods) with a relaxation delay of 2 seconds, 8 kHz spinning rate, and 10 μs ^{13}C π dephasing pulses. The ^{1}H NMR chemical shifts (δ_{H-1}) are referenced with respect to tetramethylsilane (TMS) using adamantane as a secondary reference set to δ_{H-1} = 2.0 ppm.

3.4. Results and Discussion

3.4.1. Phosphate uptake during $CaCO_3$ precipitation

Data were collected on the amount of phosphate removed from solution and the amount of sample precipitated. These data were used to calculate the approximate P/Ca and P/$CaCO_3$ precipitated, but which could not be determined exactly since no Ca^{2+}(aq) concentrations were determined. The ratios determined for phosphorus to calcium are calculated from the amount of calcium added to the solution and the phosphate taken up, assuming all calcium past solution equilibrium precipitated as $CaCO_3$. This ratio differs from that estimated for P/$CaCO_3$ which is determined from the mass of solid recovered. The aim is to provide an estimate of the phosphorus content in the $CaCO_3$ overgrowths. However, the main focus of this work is the variation in speciation of phosphate in calcium carbonate with crystallization conditions, rather than a detailed study of phosphate uptake.

3.4.1.1. Batch Methods

Final solution phosphorus concentrations, P/Ca and P/calcite ratios in the overgrowths were determined for each experiment (Table 1). All values for molar P/Ca were calculated assuming that all the calcium added after the calcite suspension was equilibrated precipitated as calcite. For sample B.STD the final concentration of phosphate in the solution is 1.16 μM indicating that 82% of the phosphorus was incorporated in the overgrowths, yielding a P/Ca ratio of 2063 (μmol phosphate mol^{-1} calcium) and a P/calcite ratio of 760 μg P g^{-1} calcite, Table 1. X-ray diffraction indicates that all calcium carbonate is in the form of calcite in samples prepared with this method.

As the initial concentration of phosphate in solution increases, more phosphate is included within the solid. Sample B.P3.2 contains 64% of the initial phosphate, with a P/Ca ratio of 814 μmol P mol^{-1} Ca in the overgrowths, and a P/calcite ratio of 289 P/g calcite. The sample B.P9.2 incorporated 66% of the phosphate, giving a P/Ca ratio of 2363 μmol P mol^{-1} Ca, and a P/calcite ratio of 911 μg P/g calcite in the overgrowths, Table 1. The increase in the P/calcite ratio suggests that the limit of the ability of calcite to take-up phosphate was not reached.

A very slight increase in the amount of phosphate incorporated in calcite is observed at the lower temperature. A sample created at 10˚C, B.T10, contains a P/Ca ratio of 2275 μmol P mol^{-1} Ca, and a P/calcite ratio of 839 μg P g^{-1} calcite. The P/calcite ratio is slightly higher than that found for the sample created with the same initial phosphorus concentration but higher temperature, B.STD, suggesting that calcite precipitation is slightly decreased at lower temperatures, consistent with higher calcite solubility at lower temperature. Vmiteq was used to determine if there was any relationship between initial phosphate concentration and the amount

of Ca2+ precipitated (Table 1), a small increase in the amount of Ca^{2+} removed as temperature increased was observed.

Samples created by House and Donaldson (1986) exhibited similar values for phosphate included in the solid, and P/Ca ratios as those synthesized for the present study. Previous results described by House and Donaldson, using similar methods, determined that at 10˚C with a starting phosphate concentration in the initial growth solution of 6.35 μM phosphate yielded a solid with a P/Ca ratio of 2220 μmol P mol^{-1} Ca, probably within experimental uncertainty of value for sample B.T10 (2275). This similarity in results suggests that the samples created in this study for solid state NMR analysis are comparable to those studied by House and Donaldson, so it is reasonable to expect that a similar distribution of phosphorus species should have been formed. Experiments conducted at 25˚C were not reported by House and Donaldson in a way that is comparable to our results due to the lack of defining a key term used in their calculations.

3.4.1.2. Constant Addition Method

Experiments using the constant addition method were analyzed for final phosphate concentration, P/Ca and P/calcite ratios. Phosphate concentrations remaining in solution are below detection limit of the UV-VIS-detected reactive phosphate method in some of the samples; for these cases an average of the range between the detection limit and zero is used to estimate phosphate concentration in the solid. To calculate P/Ca ratios the moles Ca^{2+} was calculated assuming that all calcium added after the calcite suspension was equilibrated precipitated as $CaCO_3$. For co-precipitation experiment CA.STD, the final solid contains 19.13 μmoles phosphate. The precipitated P/Ca ratio in the overgrowths is 2531 (μmoles/moles) or

1167 μg P g^{-1} calcite, Table 2. The predominant precipitate was determined to be calcite by X-ray powder diffraction.

Actual phosphate concentrations in samples created with varying phosphate concentrations in the syringe were not acquired because the concentrations remaining in solution after synthesis are either below or above the detection range of 0.06-5.00 mg/L phosphate. It was not possible to determine a correlation between initial phosphate concentration and P/Ca or P/solid ratios due to the lack of phosphorus data. For sample CA.P.81 no phosphate was detected through UV-VIS spectroscopy (Table 2) . There is an increase in the amount of solid precipitated for sample CA.P.81 versus the standard sample, CA.STD. These data are consistent with previous hypothesis that phosphate inhibits the precipitation of calcium carbonate [1, 23, 34], but is not sufficient enough evidence to prove it. Conventional X-ray powder diffraction patterns exhibit reflections only for calcite. However, based on NMR results presented below (3.3.2) slowly scanned XRD patterns reveal the major reflections for a trace fraction of monetite (Fig. 1, inset). Vminteq was used to determine how Ca^{2+} precipitation varied as initial phosphate concentrations increased, no trend was observed; as temperature increased the solubility index of phosphates increased.

A trend is observed in the amount of phosphate incorporated in the solid as the pumping rate decreased (Table 3). Sample CA.D0 exhibits modest phosphate incorporation, with only 52% of the phosphate taken up. The P/Ca ratio for this samples is 1344 μmol P mol^{-1} Ca, with 2866 μg P g^{-1} calcite. By controlling the growth rate, nearly all of the phosphate is included in the precipitate. As rate decreases, the overall the concentration of phosphorus in the solid increase, yet the apparent P/calcite ratio decreases due to the increased recovery efficiency and an increase in time for calcium carbonate precipitation.

No clear trend is observed in the amount of phosphate taken up by the precipitate with synthesis temperature (Table 4). All four samples incorporated 19 (±.2) μmoles phosphate, nearly all of the 19.4 μmoles of phosphate introduced during synthesis. No correlation is observed in the P/Ca ratio, all values are around 2530 μmolesP /moles Ca. As temperature increases, the apparent ratio of P to calcite decreases from 1869 μg P g^{-1} calcite to 940 μg P g^{-1} calcite for the 10˚C and the 80˚C samples (CA.T10c and CA.T80c, respectively). Temperature previously was shown to affect the amount of calcite precipitated, agreeing with these results [20]. X-ray diffraction data of the 80˚C sample exhibits reflections for aragonite along with calcite (seed crystals), in agreement with previous studies on the synthesis of aragonite coprecipitates (Figure 1b) [31].

One sample (CA.PH9.4) was prepared at elevated pH (9.4). This sample exhibits a slight, but negligible decrease in the amount of phosphate in the precipitate of 18.31 μmoles phosphate compared to samples prepared at pH 8.2 but otherwise identical conditions (Table 5). The P/Ca ratios decreased to 2425 μmol P mol^{-1} Ca and apparent 550 μg P g^{-1} calcite. More solid was recovered at pH 9.4 than at 8.2 suggesting that as pH increases more calcite precipitates consistent with reduced solubility of calcite at higher pH. X-ray diffraction data confirms that only calcite precipitated.

Very few of the experiments conducted following the constant addition method are comparable to the batch method due to the higher phosphate concentrations used in the constant addition method. One sample, CA.D0 (Table 3), was created with the standard amount of phosphate used in the constant addition method, 19.4 μmoles, but added to the initial solution all at once. This sample exhibits a final concentration of phosphate in the solid that relates to the bulk experiments previously discussed. For the batch method sample B.P9.2 (Table 1), the

initial solution contained 9.2 μM phosphate, of which 66% (6.04 μmoles) was taken up by the solid, while constant addition sample, CA.D0, took up a total of 10.15 μmoles phosphate, 52% of the intial 19.4 μmoles. A difference in P/Ca ratios is observed as the sample B.P9.2 has a ratio of 2363 μmol P mol^{-1} Ca and sample CA.D0 has one of 1344 μmol P mol^{-1} Ca. All other constant addition experiments exhibit higher concentrations of phosphate precipitated in the solid, and higher or similar P/Ca ratios than those observed in the batch methods. This difference could be due to the longer reaction periods for the constant addition experiments that allow the phosphate to be adsorbed and encapsulated by the calcite.

3.4.1.3. Constant Addition Method with Mg^{2+}

Samples created with magnesium in solution were analyzed for final dissolved phosphate concentrations, from which P/Ca and P/solid ratios were determined. For some of the samples phosphate concentrations remaining in solution are below detection limit of the UV-VIS-detected reactive phosphate method. For these cases an average of the range between the detection limit and zero was used to estimate phosphate concentration in the solid. To determine P/Ca ratios moles Ca was calculated assuming all calcium added after the calcite suspension was equilibrated precipitated as $CaCO_3$(s). For co-precipitation experiment MCA.STD, virtually all the added phosphate, 19.05 μmoles phosphate is included within the solid. The P/Ca ratio of the overgrowth is 2531 μmol P mol^{-1} Ca or 1819 μg P g^{-1} solid, Table 6. XRD data determined the predominant phase is calcite (Figure 1c).

Changes in the concentration of magnesium in solution alters the amount of calcite precipitated and the amount of phosphate removed from solution (Table 6). Solids were

synthesized with 0.2, 2, 10, and 20 mM magnesium in the initial growth solution and 19.4 μmoles of phosphate added, of which 19.10, 14.96, 19.1 and 11.87 μmoles phosphate respectively were taken up by the precipitate. In solutions containing magnesium concentrations higher than 10 mM, MCA.Mg20, removal of phosphate from solution appears to be inhibited. P/Ca ratios for the 0.2, 2, 10, and 20 mM magnesium solutions are: 2525, 1981, 2520, and 1573 μmol P mol^{-1} Ca or 2217, 1541, 1819 and 2201 μg P g^{-1} solid, respectively (Table 6). Up to 10 mM magnesium inhibits the precipitation calcium carbonate, but not that of phosphate; above this threshold both calcium carbonate formation and phosphate removal appear to be inhibited. Vminteq was used to calculate the amount of Ca^{2+} precipitated with the addition of $MgSO_4$, as Mg2+ concentrations increased, the amount of Ca^{2+} removed from solution dramatically decreased from 0.01384 moles in CA.STD conditions to 0.00665 moles in MCA.STD conditions.

Solids created with varying addition rate exhibit a direct relationship between the amount of phosphate removed from solution and growth rate (Table 7). Batch, 4.5 hr, and 9 hr experiments were conducted, yielding solids containing: 10.15, 11.42, 19.05 μmoles phosphate, respectively from the 19.4 μmoles added during the experiment. No sample precipitated for the batch experiment, while as P/Ca ratios for the 4.5 and 9 hr experiments are 1506 and 2520 μmol P mol^{-1} Ca or 1584 and 1819 μg P g^{-1} calcite, Table 7. Loss of phosphorus in the batch experiments may be caused by the adsorption of phosphate to the surface of the glassware.

Several additional samples were prepared at different temperatures and pH (Table 8). Precipitates formed at 10˚C removed less phosphate to the solid than those synthesized at higher temperatures but much less solid was formed resulting in higher apparent μg P g^{-1} solid. Samples created at 10˚C and 25˚C consist of primarily calcite, where as those synthesized at

80˚C are dominantly aragonite. Phosphate concentrations in the precipitate are as follows for samples MCA.T10c, MCA.STD, MCA.T80c: 4.53, 19.04, and 17.86 μmoles phosphate, respectively. The P/Ca ratio increases as temperature increases from 10˚C to 25˚C, (600 and 2520 μmol P mol^{-1} Ca), and decreased back to 2363 μmol P mol^{-1} Ca for the 80˚C reaction. As temperature increases, the P/solid ratio decrease from 1844 to 979 μg P g^{-1} calcite for the 25 and 80˚C samples, respectively (Table 8). This is due in part to the effect of temperature on calcium carbonate solubility, in which precipitation is favored at higher temperatures. XRD of the samples MCA.T80.c indicates that most of the sample consisted of aragonite, with a trace amount of calcite from the seed material, Figure 2.

One batch sample was created at a pH of 9.4, MCA.PH9.4, for which the phosphate concentration remaining in solution is below the detection limit (Table 8). To calculate the P/Ca and P/calcite ratios the average phosphate concentration between all the phosphate being taken up and the detection limit was used, 19.1 μmoles. This yields 2533 μmole P $mole^{-1}$ Ca, similar to that at pH 8.2, and a decrease in the apparent P/solid ratio of 576 μg P g^{-1} solid owing to the larger amount of solid precipitated.

The addition of magnesium to solution dramatically decreases the amount of phosphate removed from solution and the amount of precipitate in comparison to experiments with only Ca^{2+} and NaCl. The sample CA.D4.5 has 17.3 μmoles phosphate, but with 10 mM Mg^{2+}, MCA.D4.5, contains 11.4 μmoles phosphate. The addition of magnesium to the reactions decreases the amount of solid precipitated from 0.42 g (CA.STD) to 0.24 g (MCA.STD). A similar result is observed in the variable temperature and growth rate experiments. Both Ca^{2+}/NaCl and Mg^{2+} + Ca^{2+}/NaCl experiments exhibit higher amounts of solid precipitate for the pH 9.4 experiments that at pH 8.2, suggesting that pH has more of an effect on precipitation than

the addition of magnesium. Samples created without magnesium remain consistent with a ratio of 2522 μmoles P/mole Ca, where as the sample MCA.T10c decreases to 600 μmoles P/mole Ca. A major difference is observed in P/solid ratios for the 150 μL/min (9hrs) experiments, where CA.STD has 1167 μg P g^{-1} solid and the 10 mM magnesium sample, MCA.STD, has 1819 μg P g^{-1} solid. Both sets of experiments exhibited the similar trends of decreasing P/solid ratios as temperature increased.

3.4.2. Phosphate Distribution from NMR Spectroscopy

3.4.2.1. Batch Methods

The distribution of phosphate in the coprecipitation samples prepared by the batch method was investigated by ^{31}P solid state NMR spectroscopy. For the solid B.STD two main peaks are observed in the single pulse experiments, a broad peak centered at $\delta_{P\text{-}31}$= 3.2 ppm (4.2 ppm full width at half-maximum; FWHM), and an overlapping, narrower peak at $\delta_{P\text{-}31}$= 2.6 ppm (1.0 ppm FWHM); (Figure 3a). The relative intensities of the observed signals were determined from least squares fits of the spectra to a sum of Gaussian curves and are given in Table 9. The relative intensity of the peak at 3.2 ppm is 0.61 and 0.39 for that at 2.6 ppm. A small feature occurs near -1 ppm that could represent a third phosphorus environment, but the intensity is near noise (<1%). In CP/MAS experiments two peaks are observed, one at $\delta_{P\text{-}31}$= 3.2 ppm (4.6 ppm FWHM) that is similar to the broad peak in SP spectra and one at $\delta_{P\text{-}31}$= 2.6 ppm (2.1 ppm FWHM) (Figure 3d) which is much weaker than the narrow peak in the SP spectra. A small fraction near -1 ppm also appears in the CP/MAS spectra of the same position as that in the SP spectrum of this sample. Calcite is the only phase detected by X-ray powder diffraction.

No relationship between the distribution of phosphate species or synthesis temperature and initial phosphate concentration is apparent, because the ^{31}P NMR spectra of all batch samples are essentially the same (Figure 3). Spectra of samples B.P3.2 and B.T10 both contain a broad peak at 3.2 ppm and a narrower peak at 2.6 ppm with relative intensities the same as for sample B.STD within uncertainty (Table 9)

3.4.2.2. Constant Addition Method

For ^{31}P solid state NMR spectra of sample CA.STD (Figure 4) single pulse experiments yield three peaks; a narrow peak at $\delta_{P\text{-}31}$= -1.2 ppm (0.6 ppm FWHM), a broad peak at at $\delta_{P\text{-}31}$= 3.1 (2.6 ppm FWHM), and a sharp peak at at $\delta_{P\text{-}31}$= 2.9 (0.6 ppm FWHM) (Figure 4a). The relative intensities of these peaks were determined by least square fits to a sum of Gaussian curves. The relative intensities for the -1.2, 3.1 and 2.9 ppm peaks are, 0.42, 0.44, and 0.14 respectively. The CP/MAS spectrum of this sample exhibits two peaks, a broad peak at $\delta_{P\text{-}31}$= 3.1 ppm (3.1 ppm FWHM) and a peak at $\delta_{P\text{-}31}$= -1.2 ppm (0.8 ppm FWHM) (Figure 4d) that are similar to those in the corresponding SP spectra. However the narrower SP peak at 2.9 ppm is notably absent in CP spectra (cf. Figure 4a,d).

For the sample prepared with 78 μmoles phosphate (CA.P78), the peak positions in ^{31}P single pulse experiments are similar to those for CA.STD (Figure 4a-b): a narrow peak at $\delta_{P\text{-}31}$= -1.2 ppm (0.6 ppm FWHM) a narrow peak at $\delta_{P\text{-}31}$= 2.9 (0.6 ppm FWHM), and $\delta_{P\text{-}31}$= 3.1 ppm (2.8 ppm FWHM). The relative intensities for the -1.2, 2.9 and 3.1 ppm peaks are, 0.24, 0.24, 0.52 respectively (Table 10). An additional peak may be present in Figure 4b around 2.5 ppm, as observed by the broadening of the spectrum, but cannot be distinguished from the peak at 2.9 and

3.1 ppm. The CP/MAS spectrum (Figure 4d-e) exhibits three peaks, two of which, the broad peak at 3.1 ppm and the narrower peak at -1.2 ppm match those of CA.STD, the third peak a broad peak at at $\delta_{P\text{-}31}$= 2.5-3 ppm (6.3 ppm FWHM) had previously not been observed. The sample prepared with 0.81 μmoles phosphate, CA.P.81, yeilded no detectable NMR signal. Lack of signal for sample CA.P.81 indicates that either no phosphate precipitated in the sample and that the phosphate lost from solution was attracted to the surfaces of the container, or that the concentration of the phosphorus is simply below the detection limit of NMR. Sample CA.P485 yielded much different ^{31}P NMR spectra dominated by a very broad peak at $\delta_{P\text{-}31}$= 2.5-3 ppm (6.3 ppm FWHM) (Figure 4c and 4f) with perhaps only a small peak near -1.2 ppm (<1%) which is apparent only in vertically expanding residuals of fits to a single Gaussian curve.

The ^{31}P Solid State NMR single pulse spectra collected on the varying rate samples exhibit three peaks similar to those observed for sample CA.STD (Figure 5a-c). The relative intensities for the -1.2 (narrow), 3.1 (broad) and 2.9 (narrow) ppm peaks of sample CA.D0 are 0.29, 0.55, and 0.15 respectively (Table 11). There are no significant variations in the peak position and widths of the CP/MAS spectra as rate varies (Figure 5d-f). Sample CA.D0's relative intensity is lower than that of CA.STD for the peak at -1.2 ppm, which is assigned below to crystalline monetite, suggesting that decreased rate favors formation of crystalline calcium phopshate.

For ^{31}P Solid State NMR single pulse and CP/MAS experiments collected on the samples prepared at varying temperature, (10-80 degrees Celsius; Figure 6a-f) a no extreme changes were observed in the peak positions and widths in relation to CA.STD. For CAT10c, only two peaks, 3.1 ppm and -1.2 ppm could be distinguished with relative intensities of 0.54 and 0.46, respectively (Table 12). After 86, SP, acquisitions for sample CA.T10s signal to noise remained

poor, suggesting less phosphorus was precipitated. This is not consistent with the amount of phosphorus to solid ratio explained in the above section, suggesting that phosphate adsorbed to the surface of the glassware. For CA.T80c the relative intensities for the SP -1.2, 3.1 and 2.9 ppm peaks are, 0.56, 0.05, 0.39 respectively (Table 12). Sample CA.T80c was determined to be predominantly aragonite with XRD, yet ^{31}P SP peak positions and intensities did not change in relation to the primarily calcite CA.STD. All samples produce the same CP/MAS peaks observed in CA.STD, 3.1 ppm and -1.2 ppm with the absence of the peak at 2.9 ppm.

A ^{31}P Solid State NMR single pulse spectrum collected on the varying pH solid, CA.PH9.4 differs significantly from those obtained for samples prepared at pH 8.2 (Figure 7). This spectrum can be fit with two peaks, a peak at $\delta_{P\text{-}31}$= 0.38 (2.4 ppm FWHM), and $\delta_{P\text{-}31}$= 3.3 ppm (2.6 ppm FWHM) (Figure 7a-b). The relative intensities for the -2.4, 0.38 and 3.3 ppm peaks are, 0.05, 0.38, 0.57 respectively (Table 13). The peaks at -2.4 ppm and 0.38 ppm are not observed in CA.STD, while as the narrow peak at -1.2 ppm observed in CA.STD is not present at pH 9.4, suggesting that the species of phosphorus precipitated varies with pH. The signal-to-noise ratio was very poor after 86 acquisitions for CA.PH9.4, suggesting that less phosphate was precipitated with the calcite, further research needs to be conducted on this sample. The CP/MAS spectrum varied from that for CA.STD by the additional appearance of a broad peak at $\delta_{P\text{-}31}$= 2.5-3 ppm (6.3 ppm FWHM) (Figure 7c-d).

The principle difference between NMR spectra of the batch method and continuous addition methods is the appearance of three peaks in most single pulse spectra of $\delta_{P\text{-}31}$= -1.2 ppm (0.9-1.2 ppm FWHM), a narrow peak at $\delta_{P\text{-}31}$= 2.9 (0.8-1.1 ppm FWHM), and $\delta_{P\text{-}31}$= 3.1 ppm (3.6-4.1 ppm FWHM). The batch methods only yields two peaks, one which matches the peak at 3.1 ppm which is observed in the continuous addition experiments, and a second peak at

2.6 ppm which exhibits similar properties to those seen at 2.9 ppm in the continuous addition. The peak at 3.1 ppm for both types of synthesis is broad, and allows the exact placement of the narrow peak at 2.6-2.9 to vary. In addition, even though the peak at 2.6 ppm observed in the batch experiments appears slightly in CP/MAS spectra, it is broader and much lower signal-to-noise insinuating that it is similar to the peak at 2.9 ppm.

3.4.2.3. Constant Addition Method with Mg^{2+}

The addition of magnesium in different concentrations is observed to affect number of peaks observed with solid state NMR and the peak positions. At concentrations of 2 mM magnesium and below, MCA.Mg.2 and MCA.Mg2, three peaks similar to those observed in CA.STD, the sample created without magnesium, are present (Figure 8a-c). Spectra for these samples differ from that of MCA.STD in that the narrow peak at -1.3 ppm is observed. The relative intensities for the -1.3, 2.8 and 3.8 ppm peaks are, 0.36, 0.14, 0.5 respectively (Table 14). The CP/MAS spectrum varies from the CA.STD sample with the addition presence of a broad peak at $\delta_{P\text{-}31}$= 2.5-3 ppm (6.3 ppm FWHM) (Figure 8d), but once again contains the -1.2 ppm peak that MCA.STD does not exhibit. Samples precipitated from 20 mM magnesium solutions, MCA.Mg20, yeild SP spectra similar to that of MCA.STD (cf. Figure 8). The relative intensity of the broad peak at 3.6 ppm increases to 0.82 in MCA.Mg20 from the value of 0.72 for MCA.STD. As the concentration of magnesium present in the growth solution increases, the line width increases (c.f. Figure 8a-c). This result could indicate that the phosphate co-precipitating with calcite is more disordered, or that a second broad peak similar to that observed for CA.P78

may be also hidden in the spectra. Figure 9 illustrates a fit of the spectra from sample MCA.Mg20 exhibiting both the peak at 2.9 ppm and 3.1 ppm.

A spectrum was collected for sample MCA.D0 to show changes in speciation as the rate of addition decreases. Single pulse differed from that of MCA.STD mainly due to the additional presence of a peak at $\delta_{P\text{-}31}$= -0.9 (2 ppm FWHM) and corresponding decrease in the intensity of the peak at 2.9 ppm (narrow), (Figure 10). The relative intensities for the -0.9, 3.1 and 2.9 ppm peaks are, 0.08, 0.74, 0.18 respectively (Table 15).

Decrease in synthesis temperature to 10˚C has no affect on peak positions and widths of SP and CP/MAS spectra compared to samples prepared at 25˚C (Figure 11a-b, 11 d-e, Table 16) compared to MCA.STD. Large changes did occur in the 80˚C experiments the spectra of which show three peaks $\delta_{P\text{-}31}$= 3.1 ppm (3.4 ppm FWHM), $\delta_{P\text{-}31}$= 8.5 ppm (1.8 ppm FWHM), and $\delta_{P\text{-}31}$= 5.8 ppm (2.9 ppm FWHM) (Figure 11c,f). For the SP spectrum of MCA.T80c the relative intensities were 0.27, 0.18, and 0.55 for the 11.5, 8.5, and 5.8 ppm peaks, respectively (Table 16). The increase of synthesis temperatures to 80˚C resulted in the formation of five distinct phosphorus environments as indicated by the number of peaks observed in CP/MAS spectra (Figure 11f). More detailed information on this sample was obtained from analysis by $^{31}P\{^{13}C\}$ REDOR, see section 3.3.3.

The solid precipitated at a pH of 9.4 exhibits no change in the peak positions and widths from those observed in the MCA.STD (pH 8.2) in both ^{31}P SP and CP/MAS spectra (Figure 12, Table 16). The peak at 2.9 ppm (narrow) appears less sharp, but least-squares fits yield relative intensities that are comparable to those for MCA.STD: 0.74 for the 3.1 ppm peak and 0.26 for the 2.9 ppm peak. The CP/MAS spectra of MCA.PH9.4 and MCA.STD are nearly identical.

The addition of magnesium at concentrations of 10 mM or higher (eg. MCA.STD), to the constant addition method, CA.STD, removes the ^{31}P SP and CP/MAS peak at -1.1 ppm. When magnesium is added to solution below 10 mM, the peak at -1.1 ppm occurs, yet CP/MAS yield an additional peak at 2.5 ppm. In the experiments with varying temperatures with magnesium, changes in phosphate speciation were observed, while as those in the standard constant addition experiments remained constant.

3.4.3. Relationship of ^{31}P to ^{13}C from REDOR Experiments

The relationship between phosphorus and carbon for phosphate environments represented by the three peaks, at -1.2 ppm, 2.9 ppm, and 3.1 ppm observed for most calcite/phosphate coprecipitates was investigated by ^{31}P{^{13}C} REDOR experiments. Figures 13-15 show ^{31}P{^{13}C} REDOR data sets collected for sample CA.STD.c13 at three different dephasing periods of 1, 2, and 5 ms. Each set consists of a spin echo spectrum (S_0) containing signal from all of the phosphorus species in the sample and a REDOR spectrum (S), which is acquired interleaved with and identical to S_0, except that pulses are applied to the ^{13}C nuclei that cause a decrease in the ^{31}P signal intensity for phosphorus in close spatial proximity to carbon (within about 4 Å). The amount of signal decrease depends on the length of the dephasing period, the ^{31}P-^{13}C distances, and the number of ^{13}C nuclei near phosphorus. The difference spectrum, S_0-S, displays signal only from phosphorus in close spatial proximity to ^{13}C nuclei. The results (Figs. 13-15) show that all three peaks show a significant REDOR effect that increases with dephasing period and that is nearly complete by 5 ms (Fig. 16). This result indicates that all of the peaks correspond to phosphorus that are in close proximity to carbon. Figure 16 shows the relationship

of $\Delta S/S_0$ ($\Delta S = (S-S_0)/S_0$) versus the dephasing periods (dephasing curve); by 5 ms 95% of the -1.2 ppm signal is gone. At 5 ms both the 3.1 ppm and 2.9 ppm peaks show slightly higher relationships with carbon with 84% and 91% remaining respectively.

The $^{31}P\{^{13}C\}$ CP/REDOR results for a ^{13}C-enriched solid, MCA.T80c.C13, provides information on the phosphorus relationship to coprecipitated aragonite. Spectral sets were collect with 0.5, 1, 1.5, 2, 3, and 4 ms dephasing periods, (Figures 17-22). In each set, S_0 closely resembles the $^{31}P\{^{1}H\}$ CP/MAS spectrum of aragonite/phosphate coprecipitate MCA.T80c, (Figure 11f). Figure 23 is a $^{31}P\{^{13}C\}$ REDOR dephasing curve, which shows that for the sharp peaks at 11.3 and 8.0 ppm the REDOR effect is almost complete by 5 ms, yet the peaks 5.5 ppm and 3.1 ppm are only 50-60% dephased. This is consistent with phosphate coprecipitated in the carbonate mineral. The sharp peaks correspond to environments associated with carbonate. While as the peaks at 3.1 and 5.5 ppm correspond to phosphorus in a carbon position of aragonite or calcite, as previously modeled by Mason et. al [31]. One model was created to explain the phosphate system, this fit is not a unique fit due to low resolution and broad peaks and other models may exist. Figure 24 shows the 5 peaks, all well defined, peak positions δ_{P-31}= 11.3 (0.6 ppm FWHM), δ_{P-31}= 10.7 (2.7 ppm FWHM), δ_{P-31}= 8.1 (1.7 pmm FWHM), δ_{P-31}= 6.0 (3.0 ppm FWHM), and δ_{P-31}= 3.1 (3.8 ppm FWHM). The relative intensities for the peaks at 11.3, 10.7, 8.1, 6.0 and 3.1 ppm are 0.08, 0.18, 0.24, 0.33 and 0.17 respectively.

3.4.4. ^{31}P-detected ^{1}H NMR Spectra from HETCOR Experiments

A $^{31}P\{^{1}H\}$ HETCOR spectrum was collected for sample CA.STD to determine the relationship between ^{31}P and ^{1}H to potentially aid in peak assignments. Figure 25 is a 2-dimensional $^{31}P/^{1}H$ contour plot that corresponds to the ^{1}H located near phosphorus. Two peaks

were observed in the ^{1}H dimension, a narrow peak at δ_{H-1}=13.9 ppm and a peak at δ_{H-1}=7.1 ppm. The peak located at 13.9 ppm correlates to the ^{31}P peak observed at -1.1 ppm and the peak at 7.1 ppm corresponds to the ^{31}P peak at 3.1 ppm. Signal to noise is poor due to the low concentration of phosphorus in the sample.

3.4.5. Peak Assignments

Based on ^{31}P and ^{1}H NMR results and XRD the ^{31}P peak at -1.2 ppm can be assigned to monetite. This ^{31}P NMR chemical shift is identical to that reported previously for pure-phase monetite [30]. This peak for the synthetic samples closely resembles that assigned to monetite for the Christmas Island Speleothem (Ch. 2), and exhibits the same reaction to decoupling power as previously observed. Further analysis with slowly scanned XRD was done on the CA.STD sample, from 26 to 27 degrees (2θ) at a step rate of 0.0005˚ per 250 seconds in an attempt to observe major monetite reflections from the sample in a region in which no reflections of calcite and aragonite occur (c.f. Figure 1a inset). The X-ray diffraction result is consistent with the presence of monetite at trace fractions. The ^{1}H cross-peak at δ_{H-1}= 13.9 ppm for the -1.2 ppm ^{31}P peak in $^{31}P\{^{1}H\}$ HETCOR spectra (Figure 26) occurs at the same chemical shift as reported for the acidic protons in the hydrogen phosphate groups of monetite [35]. One complicating factor in the assignment of this peak to monetite is the surprisingly strong $^{31}P\{^{13}C\}$ REDOR effect observed (Figure 16), which indicates that the corresponding phosphorus are in close proximity to carbonate groups. Pure monetite ($CAHPO_4$) should not give a P/C REDOR signal. One possibility is that monetite precipitated under these conditions of high dissolved carbonate concentrations incorporates a significant amount of carbonate as a substitution defect for

phosphate. For example, apatite can contain up to 10-12 wt. percent carbonate. Qualitatively, the approach to nearly 100% REDOR dephasing by 5 ms suggests that the carbonate content would have to be somewhat higher than this fraction, such as that all phosphate groups have several carbonate neighbors. Another possibility is that the monetite crystals are small and encapsulated by calcite. This explanation would likely require that the crystals be nanometer in size, but the relative sharpness of the XRD peaks (Figure 1, inset) seems to argue against this explanation. An understanding of the relationship between phosphate and carbonate in monetite precipitated under these conditions requires further investigation.

The narrow peak at δ_{31P}= 2.9 ppm shows the same characteristics as a peak observed by Mason et al. (2007) and assigned to an unidentified anhydrous calcium orthophosphate. This peak was also observed in the Christmas Island Speleothem (Ch. 2). The small peak width indicates well-ordered phosphate environments, suggesting a crystalline phase. Its presence in single pulse experiments, but absence in CP/MAS spectra suggests that the phosphorus is not within 4Å of a proton [13]. The only similar 31P chemical shift reported in the literature for a phosphate phase giving a single peak is apatite (2.7±.1 ppm), but varieties of this mineral yield strong signals in CP/MAS spectra. A similar narrow peak at 2.6 ppm was observed for samples made by the batch method which likely arises from similar material. In spectra of the batch samples, this peak did appear to give rise to a weak signal by CP/MAS spectra, but which is broader, suggesting that the CP signal arises from more disordered regions. One possibility is that the peak at 2.6 ppm arises from similar, but more disordered form of the phase that is at 2.9 ppm from the constant addition methods, perhaps owing to the more rapid crystallization rate in the batch methods. The difference in chemical shift (2.9 vs. 2.6 ppm) is within uncertainty given the poor signal-to-noise ratios and overlap with the broad peak at 3.1 ppm.

The broad peak located near δ_{31P}= 3.1 ppm matches closely a similar resonance described by Mason et al. in speleothems and corals and in the Christmas Island speleothem described in Chapter 2 [13, 31, 36]. Hinedi et al. [36] observed a similar peak in coprecipitated calcite samples. The $^{31}P\{^{13}C\}$ REDOR results indicate that the peak at 3.1 ppm exhibits a close proximity to carbon, consistent with assignment to phosphate occurring as a substitution defect in calcite. The large width indicates a range of bonding environments expected for defect sites. The occurrence of this peak in CP/MAS spectra indicate that ^{1}H species such as hydroxyl and water molecules help accommodate the substitution of phosphate for carbonate.

The broader peak observed near δ_{31P}= 2.5 ppm for samples prepared with high phosphate content likely corresponds to amorphous calcium phosphate (ACP). Peaks with similar position and width were observed in previous investigations of ACP data [37]. This peak was observed in samples created with higher phosphorus concentrations, CA.P485, and was apparent in some CP/MAS spectra in the absence of the peak at 2.9 ppm. ACP is the predominant species in the samples containing 500 and 1000 μmoles/dm^3 which is caused by an imbalance of the thermal equilibrium. The reaction solution can only hold up to 45 μM phosphate before the solution reaches saturation; vminteq was used to determine the saturation index of different phosphate species and the amount of calcium expected in solution. In solutions containing 78 μM phosphate only 1.52 mmoles of the original 15 mmoles Ca^{2+} remain in solution, with saturation indexes of 0.545 for ACP and 9.32 for HAP, this increases to 2.12 and 11.7 for ACP and HAP, respectively, upon addition of 485 μM. Due to the broad nature of the peak arising from ACP it is hard to determine if small amounts of other phosphate species are present in the sample.

No previous study has reported the peaks at 11.3 ppm and 8.1 ppm For the sample MCA.T80.c. Both peaks are narrow, indicating that they arise from a crystalline phase. The

presence of 50-40% of signal after 5 ms indicates the phosphorus are in close proximity to the carbonate ion, likely meaning that these peaks are a mixed carbonate/phosphate phase. In addition the appearance of both peaks in the CP/MAS spectra means that there are significant amounts of ^{1}H. Previous research on synthetic aragonite/phosphate coprecipitates made at 25˚C, with low concentrations of Mg^{2+} observed similar peaks. This suggests that Mg^{2+} inhibits the precipitation of more stable phosphate phases, along with calcite. Further investigation is require to understand the nature and origin of these phosphate environments.

3.5. Conclusions

^{31}P NMR provided data on the batch experiments that confirmed House and Donald's hypothesis that precipitation was explained by the formation of two phosphorus species, an unidentified crystalline phosphate and phosphate co-precipitated with calcite. Temperature and phosphorus concentration had no affect on the species formed, but on how much phosphorus was consumed by the calcite and how much calcite precipitated.

Use of the constant addition method provided evidence that varying temperature, pH, initial phosphate concentrations and rate of reactant addition changed the amount of phosphate precipitated, the species of phosphate formed, and the degree of crystallization. Initial phosphorus concentrations above 78 μM impede the formation of most crystalline calcium phosphates, with the dominate phosphate species being amorphous calcium phosphate. As reaction temperature increases and experiments in which the rate of reactant added decreases the degree of calcium phosphate crystallization increases and the amount of phosphate consumed by the reaction. Increasing the pH creates a variety of phosphate species that have not been

previously identified by ^{31}P solid state NMR. Further research on the combination of these variables must be conducted to see if there is a combined effect of the variables. Spectra collected on CA.STD with $^{31}P\{^{13}C\}$ CP/REDOR provided evidence that monetite is encapsulated in calcium carbonate, due to the short distance between phosphorus and carbon. Spectra of CA.D0 compared to the batch experiments contain one additional phosphate form, monetite, due to the increase of initial Ca^{2+} of 2.5 mM, for batch, and 25 mM for the constant addition experiments.

The addition of magnesium above 2 mM to the reaction solution impedes the formation of crystalline phosphate as determined by solid state NMR spectroscopy. The dominant phosphorus species present in most of the solids were phosphate co-precipitated with calcite and a phosphorus species previously described as unknown anhydrous calcium orthophosphate. Aragonite samples created at 80˚C with Mg^{2+} yielded new ^{31}P NMR peaks previously not identified, and were determined to be in close proximity to carbonate using $^{31}P\{^{13}C\}$ CP/REDOR. Further ^{31}P research on the effect of magnesium on calcium phosphate precipitation must be investigated.

3.6. References

1. Griffin, R.A. and J.J. Jurinak, *The Interaction of Phosphate with Calcite.* Soil Sci. Soc. Amer. Proc, 1973. **37**: p. 847-850.

2. Sims, J., et al., *Integrating soil phosphorus testing into environmentally best agricultural management practices.* Journ of Environmental Quality, 2000. **29**(60-71).

3. Lehmann, J., et al., *Long-term dynamics of phosphorus forms and retention in mature-amended soils.* Environ. Sci. Technol., 2005. **39**: p. 6672-6680.

4. Houwen, J.A.M.V.D. and E. Valsami-Jones, *The Application of Calcium Phosphate Precipitation chemistry to Phosphorus Recovery: The Influence of Organic Ligands.* Environmental Technology, 2001. **22**(11): p. 1325-1335.

5. Hu, C., et al., *Effects of longterm wastewater application on chemcail properties and phosphorus adsorption capactiy in soils of wastewater land treament systems.* Environ. Sci. Technol., 2005. **39**: p. 7240-7245.

6. Cao, X., et al., *Inhibition of calcium phosphate precipitation under environmentally-relevant conditions.* Science of the Total Environment, 2007. **383**: p. 205-215.

7. Fairchild, I.J., et al., *Annual to sub-annual resolution of multiple trace-element trends in speleothems.* Journal of Geological Society, 2001. **158**(5): p. 831-841.

8. Huang, Y., et al., *Seasonal variation in Sr, Mg and P in modern speleothems (Grotta di Ernesto, Italy).* Chemical Geology, 2001. **175**: p. 429-448.

9. Baldini, J.U., F. McDermott, and I.J. Fairchild, *Structure of the 8200-Year Cold Event Revealed by a Speleothem Trace Element Record.* Science, 2002. **296**(5576): p. 2203-2206.

10. Frisia, S. and A. Borsato, *Developments in Sediments*. Carbonates in Continental Settings, ed. A.J. Van Loon. Vol. 61. 2010, Netherlands: Elsevier.

11. Jimenez-Lopez, C., et al., *Chemical, mineralogical and isotope behavior, and phase transformation during the precipitation of calcium carbonate minerals from intermediate ionic solution at 25 degrees C.* Geochimica et Cosmochimica Acta, 2001. **65**(19): p. 3219-3231.

12. Treble, P.C., J. Chappell, and J.M.G. Shelley, *Complex speleothem growth processes revealed by trance element mapping and scanning electron microscopy of annual layers.* Geochemica et Cosmochimica Acta, 2005. **69**: p. 4855-4863.

13. Mason, H.E., et al., *Phophorus Speciation in Calcite Speleothems Determined from Solid-State NMR Spectroscopy.* Earth and Planetary Science Letters, 2007. **254**: p. 313-322.

14. McDowell, R.W., et al., *Analysis of Potentially Mobile Phosphorus in Arable Soils Using Solid State Nuclear Magnetic Resonance.* J. Environ. Qual., 2002. **31**: p. 450-456.

15. Aydin, I., et al., *Determination of mineral phosphate species in sedimentary phosphate rock in Mardin, SE Anatolia, Turky by sequential extraction.* Microchemical Journal, 2009. **91**: p. 63-69.

16. Tesoriero, A.J. and J.F. Pankow, *Solid solution partitioning of Sr^{2+}, Ba^{2+}, and Cd^{2+} to calcite.* Geochimica et Cosmochimica Acta, 1996. **60**: p. 1053-1063.

17. Zhong, S.J. and A. Mucci, *Calcite precipitation in seawater using a constant addition techinique: a new overalll reaction kinetic expression.* Geochimica et Cosmochimica Acta, 1993. **57**: p. 1409-1417.

18. Reeder, R.J., et al., *Uranyl incorporation into calcite and aragonite: XAFS and luminescence studies.* Environ. Sci. Technol., 2000. **34**: p. 638-644.

19. Sykes, G.A., M.J. Collins, and D.I. Walton, *The significance of a geochemically isolated intracrystalline organice fraction within biominerals.* Org. Geochem., 1995. **23**(11/12): p. 1059-1065.

20. House, W.A. and L. Donaldson, *Adsorption and Coprecipitation of Phosphate on Calcite.* Journal of Colloid and Interface Science, 1986. **112**(2): p. 309-324.

21. Ishikawa, M. and M. Ichikuni, *Coprecipitation of phosphate with calcite.* Geochemical Journal, 1981. **15**: p. 283-288.

22. Dove, P.M. and F.J. Hochella, *Calcite precipitation mechanisms and inhibition by orthophosphate: In situ observations by Scanning Force Microscopy.* Geochimica et Cosmochimica Acta, 1993. **57**: p. 705-714.

23. Reddy, M.M., *Crystallization of calcium carbonate in the presence of trace concentrations of phosphorus-containing anions.* Journal of Crystal Growth, 1977. **41**: p. 287-295.

24. Plant, L.J. and W.A. House, *Precipitation of calcite in the presence of inorganic phosphate.* Colloids and Surfaces, 2002. **203**: p. 143-153.

25. Mucci, A., *Growth kinetics and composition of magnesium calcite overgrowths precipitated from seawater: Quantitative influence of orthophosphate ions.* Geochemica et Cosmochimica Acta, 1986. **50**: p. 2255-2265.

26. Millero, F., et al., *Adsorption and Desorption of Phosphate on Calcite and Aragonite in Seawater.* Aquatic Geochemistry, 2001. **7**: p. 33-56.

27. Salimi, M.H., J.C. Heughebaert, and G.H. Nancollas, *Crystal Growth of Calcium Phosphates in the Presence of Magnesium Ions.* Langmuir, 1985. **1**: p. 119-122.

28. Cao, X. and W. Harris, *Carbonate and Magnesium Interactive Effect on Calcium Phosphate Precipitation.* Environ. Sci. Technol., 2008. **42**: p. 436-442.

29. Meyer, H.J., *The influence of Impurities on the growth rate of calcite.* Journal of Crystal Growth, 1984. **66**: p. 639-646.

30. Aue, W.P., et al., *Solid-State Phosphorus-31 Nuclear Magnetic Resonance Studies of Synthetic Solid Phases of Calcium Phosphate: Potential Models of Bone Mineral.* Biochemistry, 1984. **23**: p. 6110-6114.

31. Mason, H.E., et al., *Phosphate defects and apatite inclusions in coral skeletal aragonite revealed by solid-state NMR spectroscopy.* Geochemica et Cosmochimica Acta, In review.

32. Clark, L.L., E.D. Ingall, and R. Benner, *Marine Organic Phosphorus Cycling: Novel Insights From Nuclear Magnetic Resonance.* American Journal of Science, 1999. **2999**: p. 724-737.

33. Cade-Menun, B., *Characterizing phosphorus in environmental and agricultural samples by 31P nuclear magnetic resonance spectroscopy.* Talanta, 2005. **66**: p. 359-371.

34. House, W.A., *Inhibition of Calcite Crystal Growth by Inorganic Phosphate.* Journal of Colloid and Interface Science, 1987. **119**(2): p. 505-511.

35. Yesinowski, J.P. and H. Eckert, *Hydrogen Environments in Calcium Phosphates: ^{1}H MAS NMR at High Spinning Speeds.* J. Am. Chem. Soc., 1987. **109**: p. 6274-6282.

36. Hinedi, Z.R., et al., *A ^{31}P and ^{1}H MAS NMR study of phosphate sorption onto calcium carbonate.* Journal of Colloid and Interface Science, 1992. **152**(1): p. 141-160.

37. Tropp, J., N.C. Blumenthal, and J.S. Waugh, *Phosphorus NMR study of solid amorphous calcium phosphate.* J. Am. Chem. Soc., 1983. **105**(1): p. 22-26.

3.7. Figures

Figure 1. X-ray powder diffraction (XRD) of selected phosphate/$CaCO_3$ coprecipitated samples. a) CA.P78; b) CA.T80c; c) MCA.STD; d) MCA.Mg.2. Spectra were collected from 15 to 50˚ 2θ with a step size of 0.01. Inset shown from 26-27 degrees from sample CA.P78 analyzed at 250 seconds per step. Reflections are assigned to calcite (C), aragonite (A), and monetite (M).

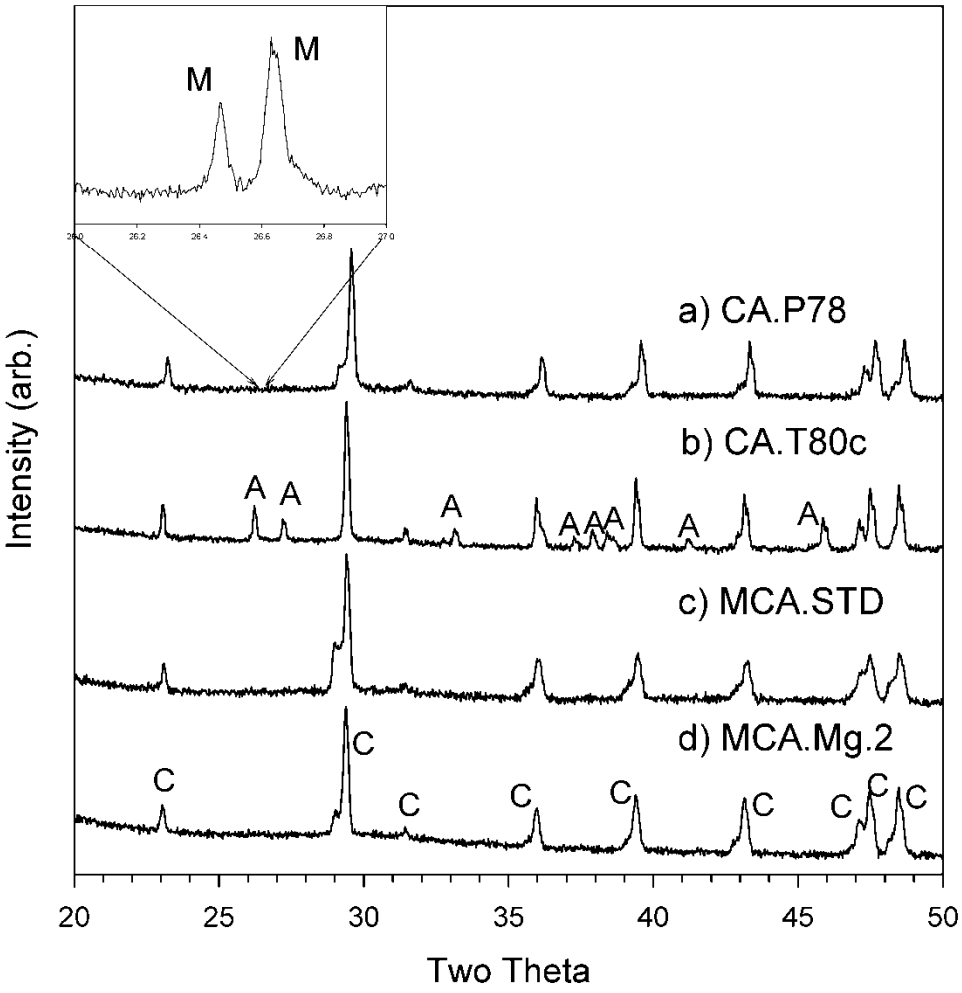

Figure 2. X-ray powder diffraction patterns of 80˚C 10mM Magnesium sample from 15 to 50˚ 2θ with a step size of 0.01. a) MCA.T80c; b) MCA.T80c.13c.

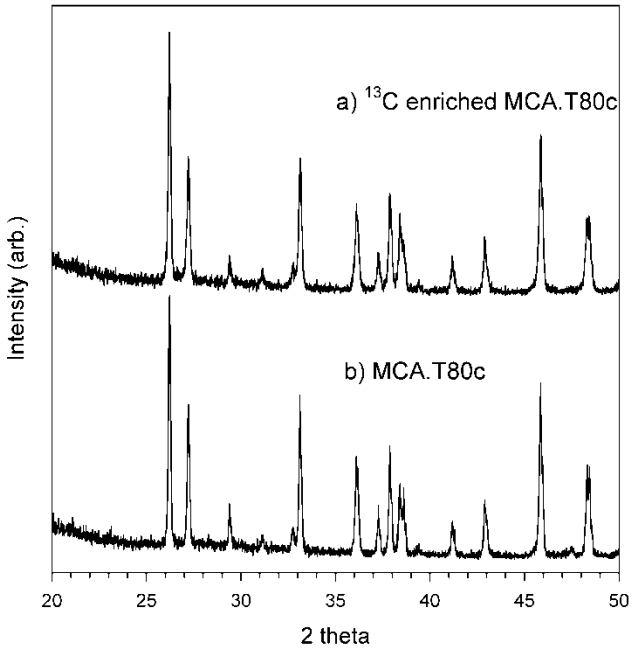

Figure 3. Center band region of ^{31}P SP and CP/MAS NMR spectra of calcite/phosphate coprecipitate samples synthesized by the batch method. a) SP, B.STD; b) SP, B.T10; c) SP, B.P3.2; d) CP, B.STD; e) CP, B.P3.2. Spectra were collected at a spin rate of 3 kHz, a 2 s pulse delay, 2 ms contact time for (from bottom to top) 76096, 77832, 110336, 54144, 58752 acquisitions.

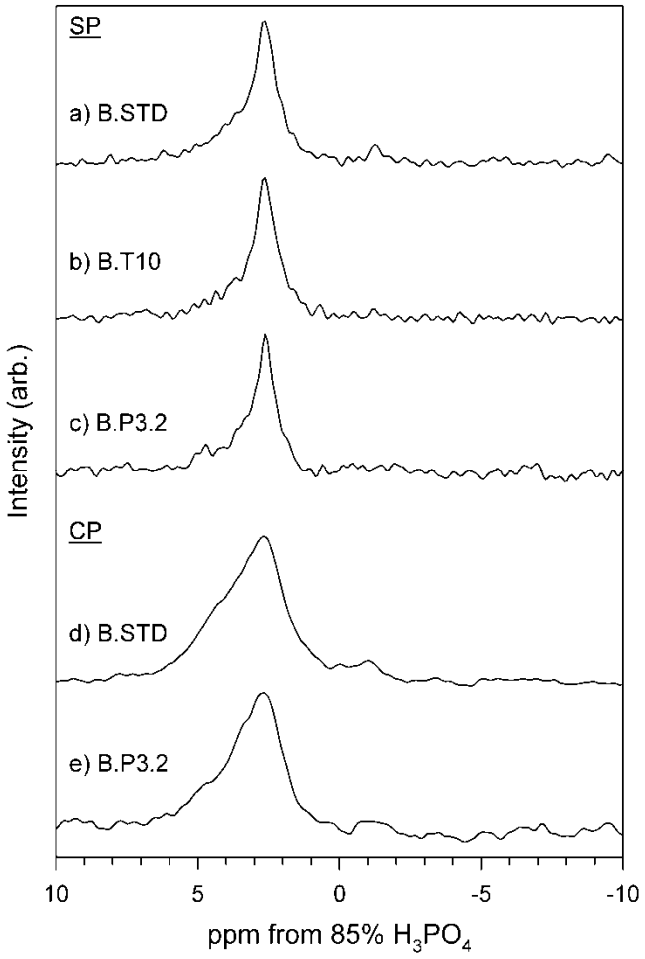

Figure 4. ^{31}P SP MAS and $^{31}P\{^{1}H\}$ CP/MAS NMR spectra of phosphate/$CaCO_3$ coprecipitate samples with varying phosphate addition (See Table 2). a) SP, CA.STD; b) SP, CA.P78; c) SP, CA.P485; d) CP, CA.STD; e) CP, CA.P78; f) CP, CA.P485. SP spectra were collected at a spin rate of 8 kHz, 1000 s relaxation delay and decoupling frequency of 35 kHz; CP spectra were collected with a contact time of 2 ms, 8 kHz spin rate and 2 s pulse delay. SP spectra represent 86 acquisitions; CP spectra represent (from bottom to top) 21144, 13864, 21776 acquisitions.

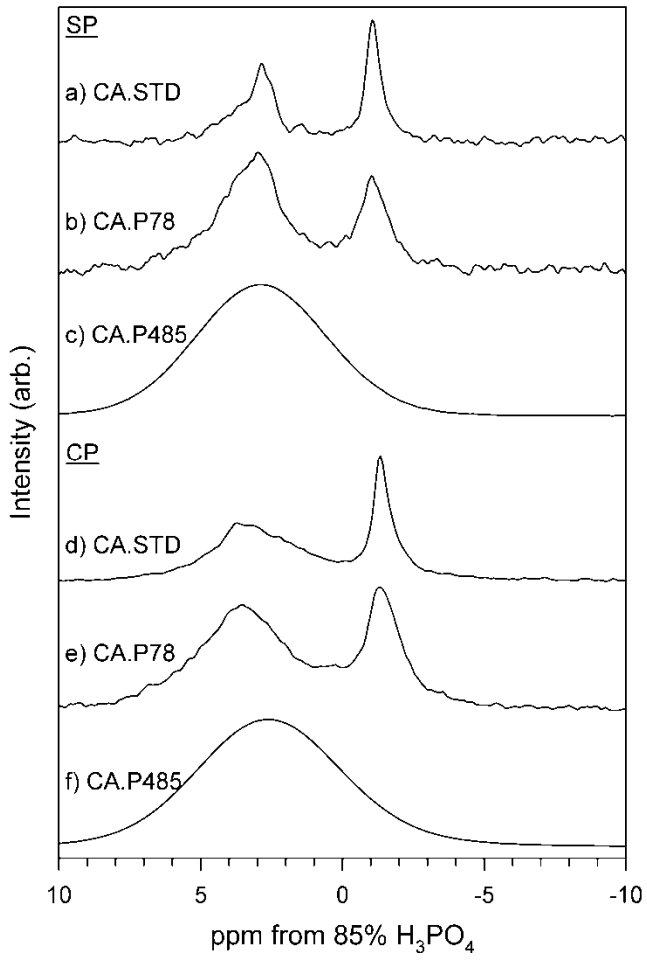

Figure 5. ^{31}P SP MAS and $^{31}P\{^{1}H\}$ CP/MAS NMR spectra of phosphate/$CaCO_3$ coprecipitate samples with varying rate (See Table 3). a) SP, CA.RI; b) SP, CA.STD; c) SP, CA.R26.6; d) CP, CA.RI; e) CP, CA.STD; f) CP, CA.R26.6. Spectra were collected at a spin rate of 8 kHz, 1000 s pulse delay and decoupling frequency of 35 kHz, CP spectra were collected with a 2 ms contact time, 8 kHz spin rate and 2 s pulse delay. SP spectra represent 86 acquisitions, CP spectra represent (from bottom to top) 5376, 3478, 5192.

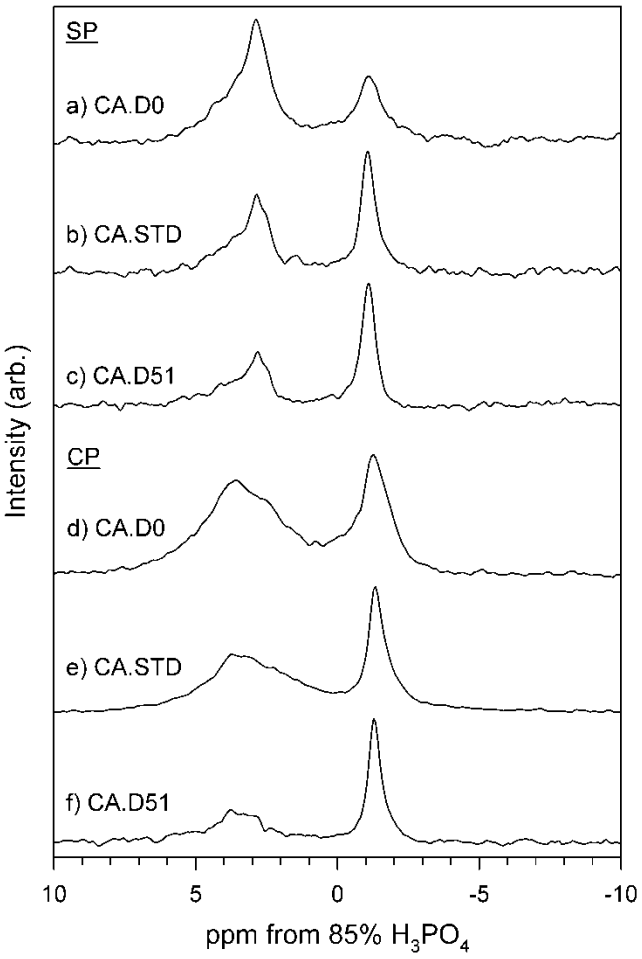

Figure 6. ^{31}P SP MAS and $^{31}P\{^{1}H\}$ CP/MAS NMR spectra for phosphate/$CaCO_3$ coprecipitate samples with varying temperature (See Table 4). a) SP, CA.T10c; b) SP, CA.STD; c) SP, CA.T80c; d) CP, CA.T10c; e) CP, CA.STD; f) CP, CA.T80c. Each SP spectrum was collected at a spin rate of 8 kHz , 35 kHz decoupling frequency and a 1000 s relaxation delay; CP was collected with a 2 s pulse delay, 2 ms contact time and 8 kHz spinning rate. SP spectra represent 86 acquisitions and CP (from bottom to top) 7352, 21144, 7336 acquisitions.

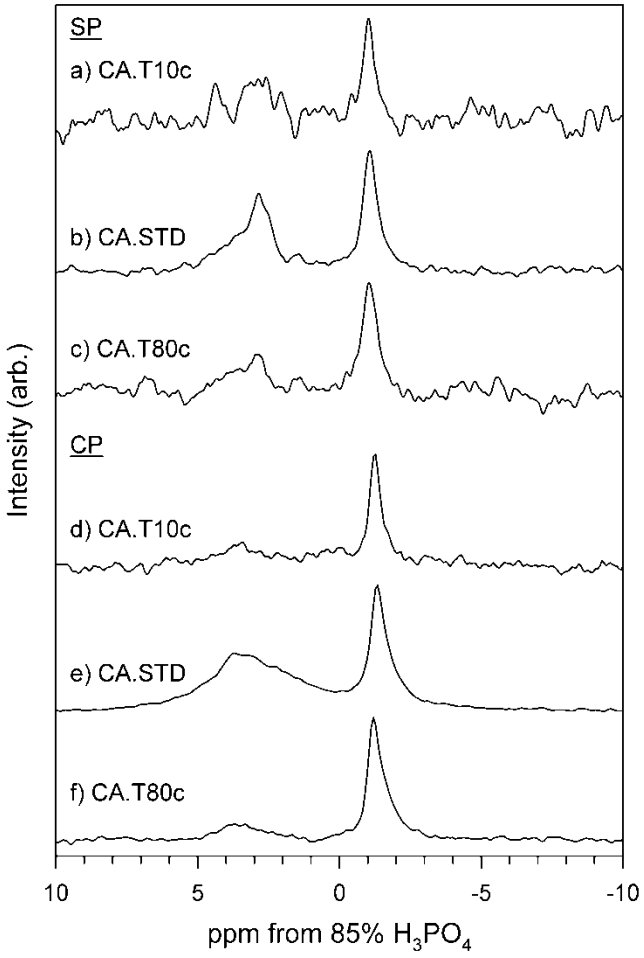

Figure 7. ^{31}P SP MAS and $^{31}P\{^{1}H\}$ CP/MAS NMR spectra of phosphate/$CaCO_3$ coprecipitate samples with varying pH (See Table 5). a) SP, CA.PH9.4; b) SP, CA.STD; c) CP, CA.PH9.4; d) CP, CA.STD. Spectra were collected at a spin rate of 8 kHz, 1000 s relaxation delay, 35 kHz decoupling frequency; CP were collected with 2 s relaxation delay, 2 ms contact time and 8 kHz spinning rate. SP spectra represent 86 acquisitions, CP spectra represent (from bottom to top) 21144 and 45136 acquisitions.

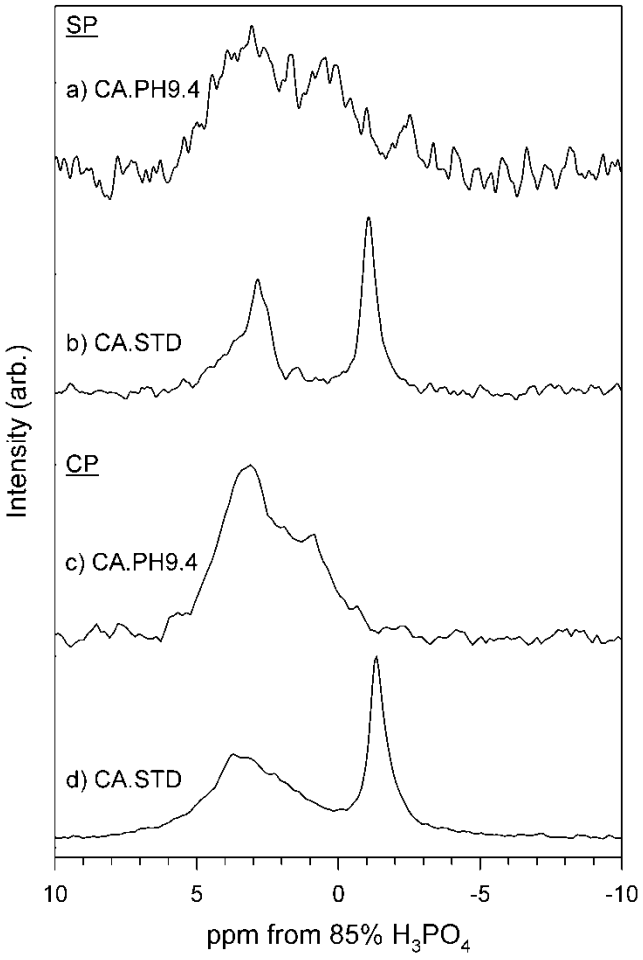

Figure 8. ^{31}P SP MAS and $^{31}P\{^{1}H\}$ CP/MAS NMR spectra of phosphate/$CaCO_3$ coprecipitate samples with varying magnesium concentrations in the initial growth solution (See Table 6). a) SP, CA.STD; b) SP, MCA.Mg.2; c) SP, MCA.STD; d) SP, MCA.Mg20; e) CP, CA.STD; f) CP, MCA.Mg.2; g) CP, MCA.STD; h) CP, MCA.Mg20. SP spectra were collected at a spin rate of 8 kHz, 35 kHz decoupling frequency and 1000 s relaxation delay; CP spectra were collected with a 2 s relaxation delay, 2 ms contact time, and 8 kHz spinning speed. SP spectra represent 86 acquisitions, CP spectra represent (from bottom to top) 5576, 15360, 6760 acquisitions.

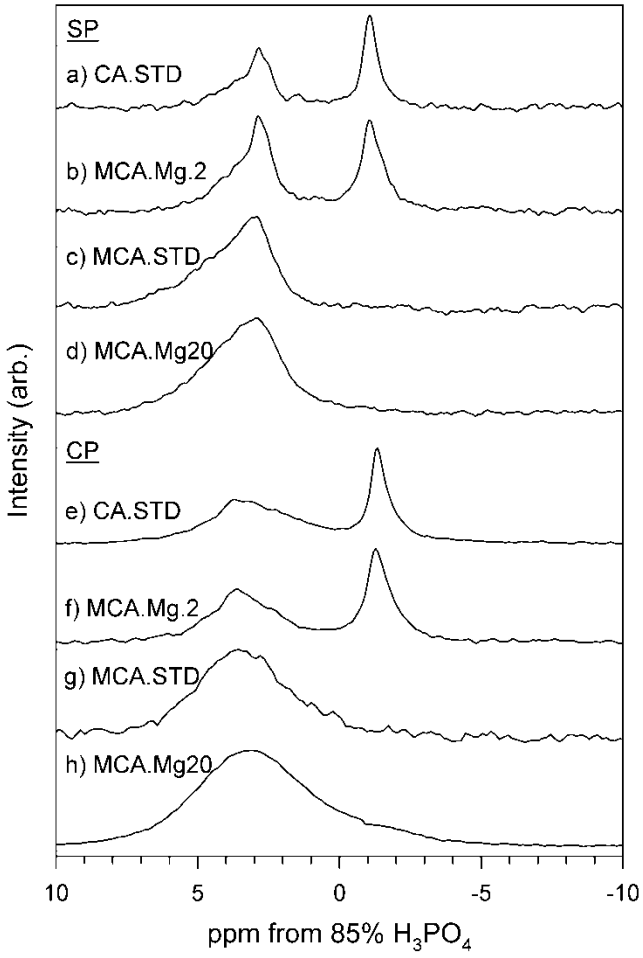

Figure 9. ^{31}P SP MAS NMR spectrum individual curve and the least squares fit corresponding to the principle phosphate environments: $\delta_{P\text{-}31}$= 3.1 (3.5 ppm FWHM) and $\delta_{P\text{-}31}$=2.9 (0.6 ppm FWHM) a) MCA.STD; b) MCA.Mg20

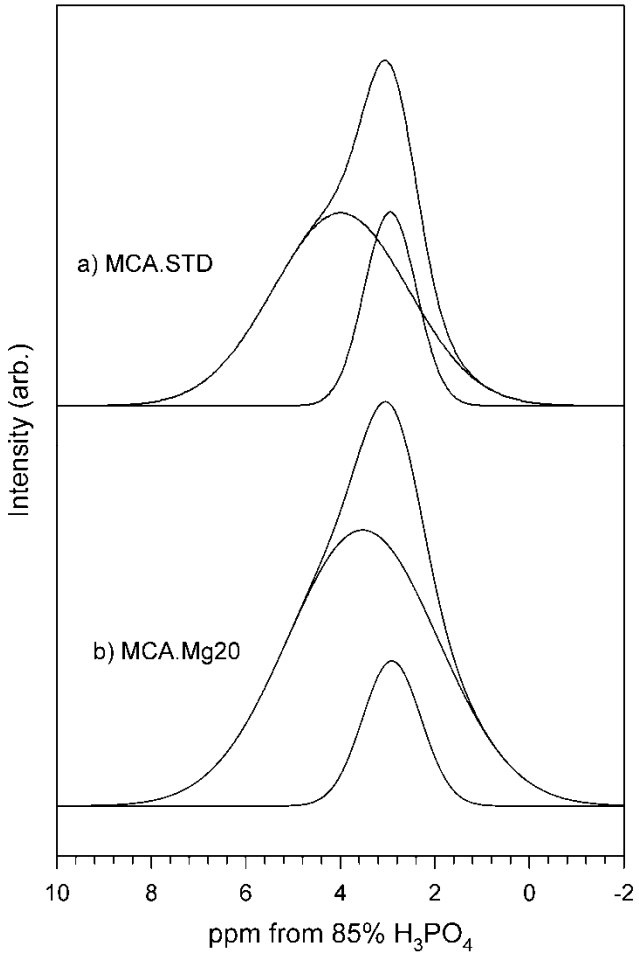

Figure 10. ^{31}P SP MAS NMR spectra of phosphate/$CaCO_3$ coprecipitate samples with Mg^{2+} and varying rate of addition (See Table 7). a) SP, MCA.D); b) SP, MCA.STD. SP spectra were collected at a spin rate of 8 kHz, 35 kHz decoupling frequency, and 1000 s relaxation delay. SP spectra represent 86 acquisitions.

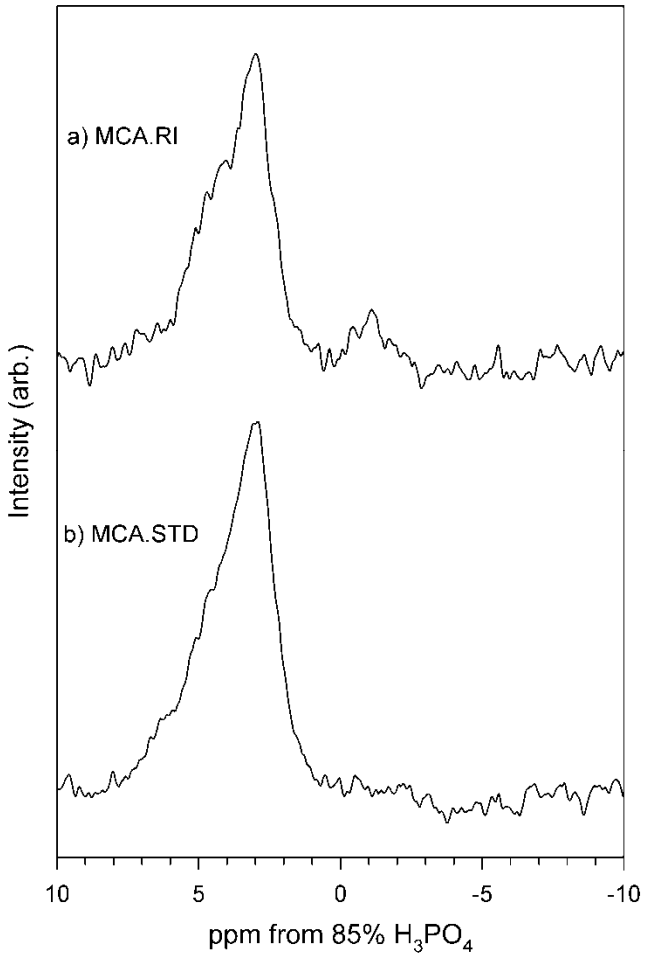

Figure 11. ^{31}P SP MAS and $^{31}P\{^{1}H\}$ CP/MAS NMR NMR spectra of phosphate/$CaCO_3$ coprecipitate samples with varying temperature and magnesium (See Table 8). a) SP, MCA.T10c; b) SP, MCA.STD; c) SP, MCA.T80c; d) CP, MCA.T10c; e) CP, MCA.STD; f) CP, MCA.T80c. SP spectra were collected at a spin rate of 8 kHz, 35 kHz decoupling frequency, and 1000 s relaxation delay; CP spectra were collected with 2 s relaxation delay, 2 ms contact time and 8 kHz spinning speed. SP spectra represent 86 acquisitions, CP spectra represent (from bottom to top) 58072, 15360, 80000 acquisitions.

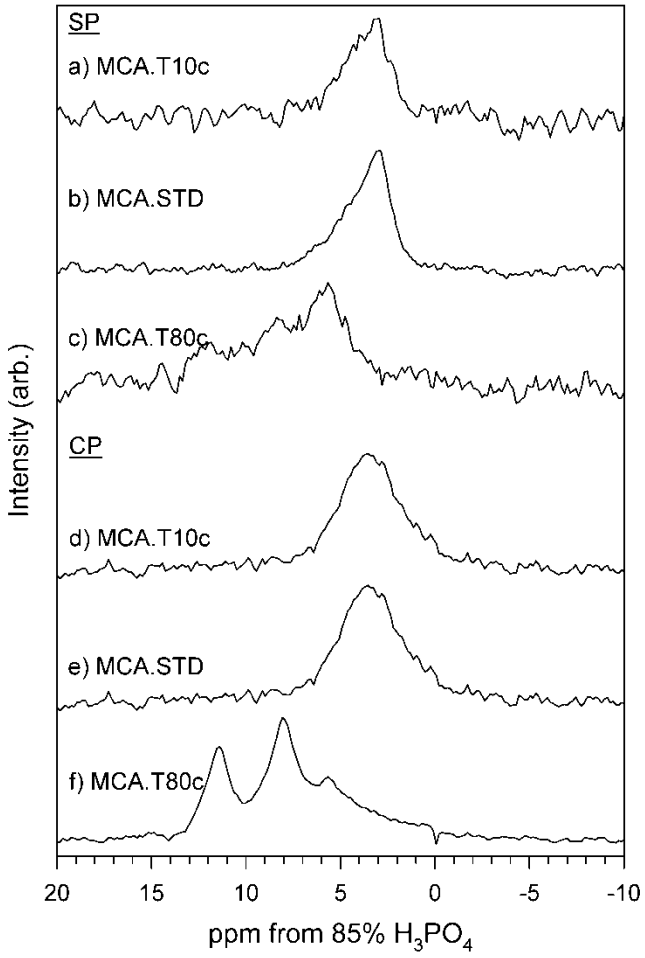

Figure 12. ^{31}P SP MAS and $^{31}P\{^{1}H\}$ CP/MAS NMR spectra of phosphate/$CaCO_3$ coprecipitate samples with varying pH (See Table 8). a) SP, MCA.PH9.4; b) SP, MCA.STD; c) CP, MCA.PH9.4; d) CP, MCA.STD. SP spectra were collected at a spin rate of 8 kHz, 35 kHz decoupling frequency and 1000 s relaxation delay; CP spectra were collected with 2 s relaxation delay, 2 ms contact time and 8 kHz spinning speed. SP spectra represent 86 acquisitions, CP spectra represent (from bottom to top) 15360 and 59992 acquisitions.

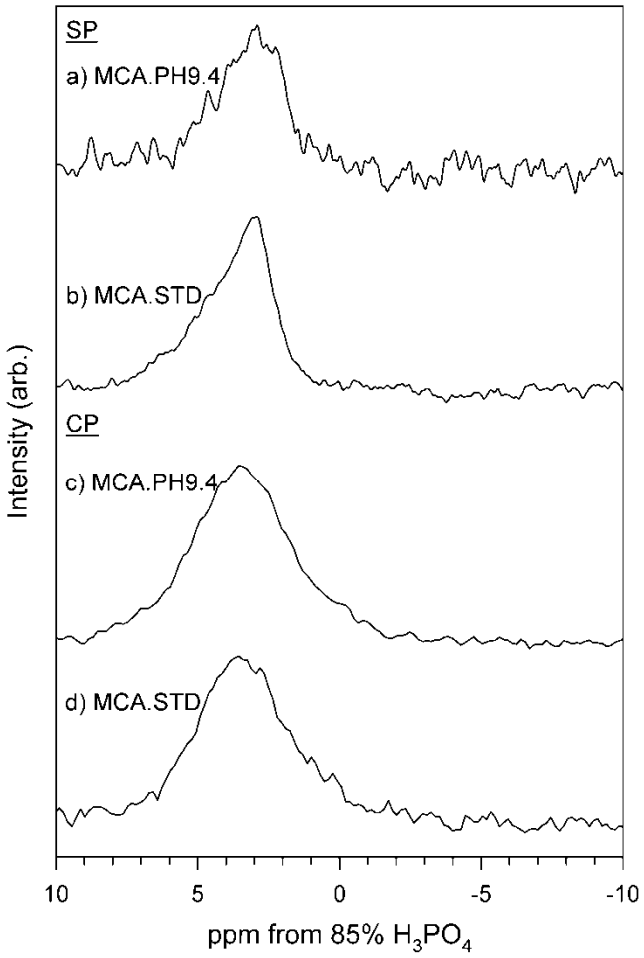

Figure 13. $^{31}P\{^{13}C\}$ CP/REDOR NMR spectral set for sample CA.STD.c13 calcite/phosphate coprecipitate. Collected at 8 kHz spinning rate, 2 ms contact time, 2 s relaxation delay, 31392 acquisitions and 1 ms dephasing time (8 rotor periods).

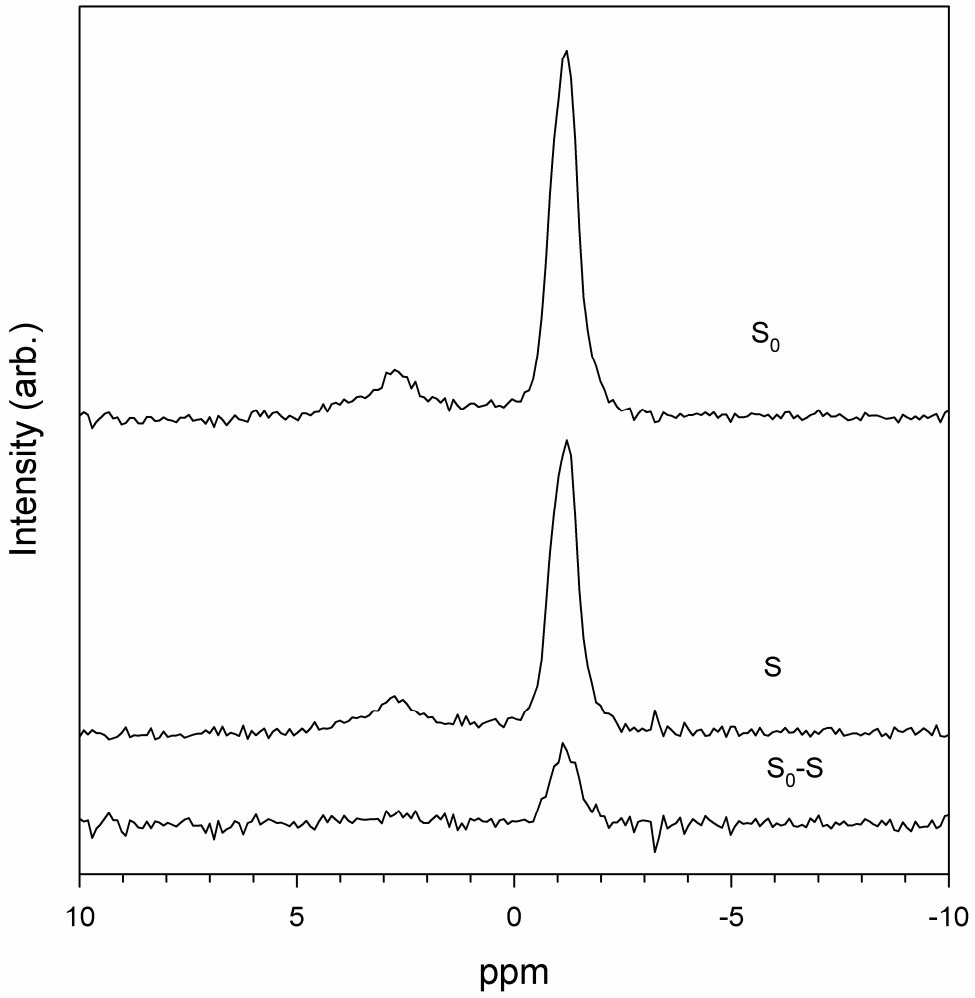

Figure 14. $^{31}P\{^{13}C\}$ CP/REDOR NMR spectral set for sample CA.STD.c13 calcite/phosphate coprecipitate. Collected at 8 kHz spinning rate, 2 ms contact time, 2 s relaxation delay, 42520 acquisitions and 2 ms dephasing time (16 rotor periods).

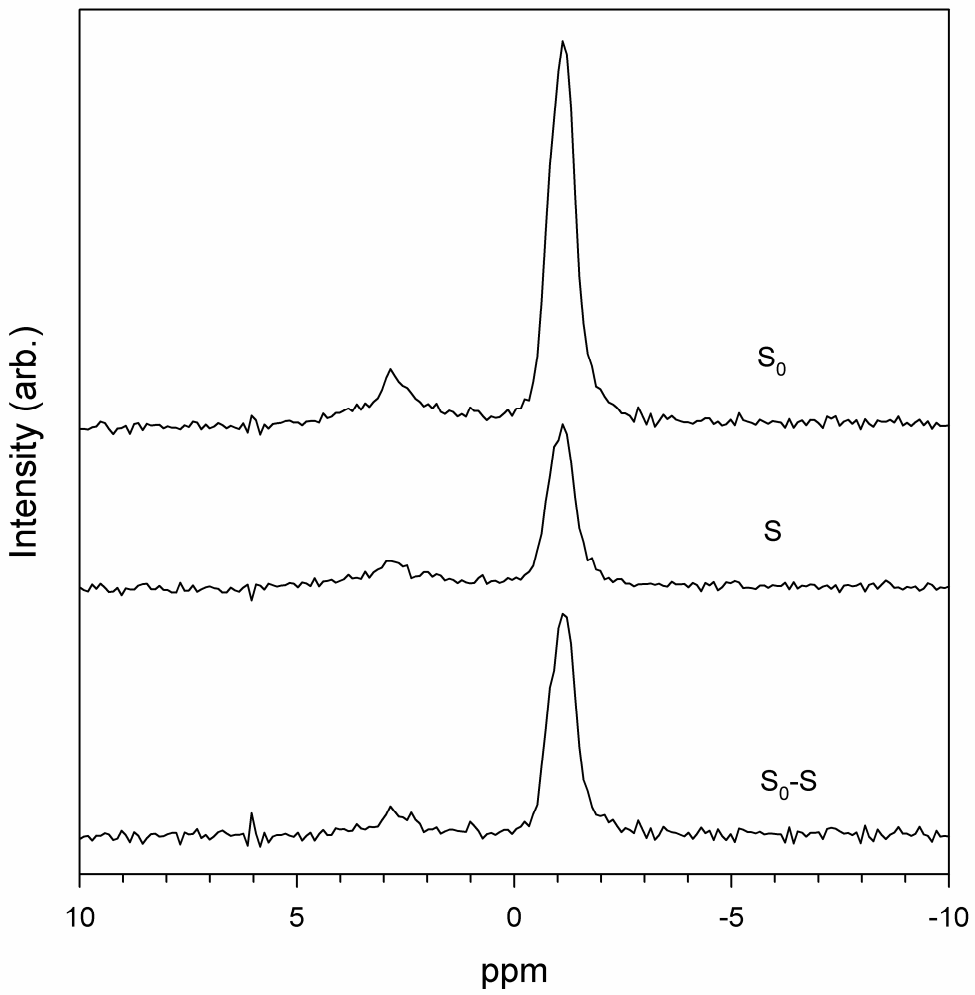

Figure 15. $^{31}P\{^{13}C\}$ CP/REDOR NMR spectral set for sample CA.STD.c13 calcite/phosphate coprecipitate. Collected at 8 kHz spinning rate, 2 ms contact time, 2 s relaxation delay, 109988 acquisitions and 5 ms dephasing time (40 rotor periods).

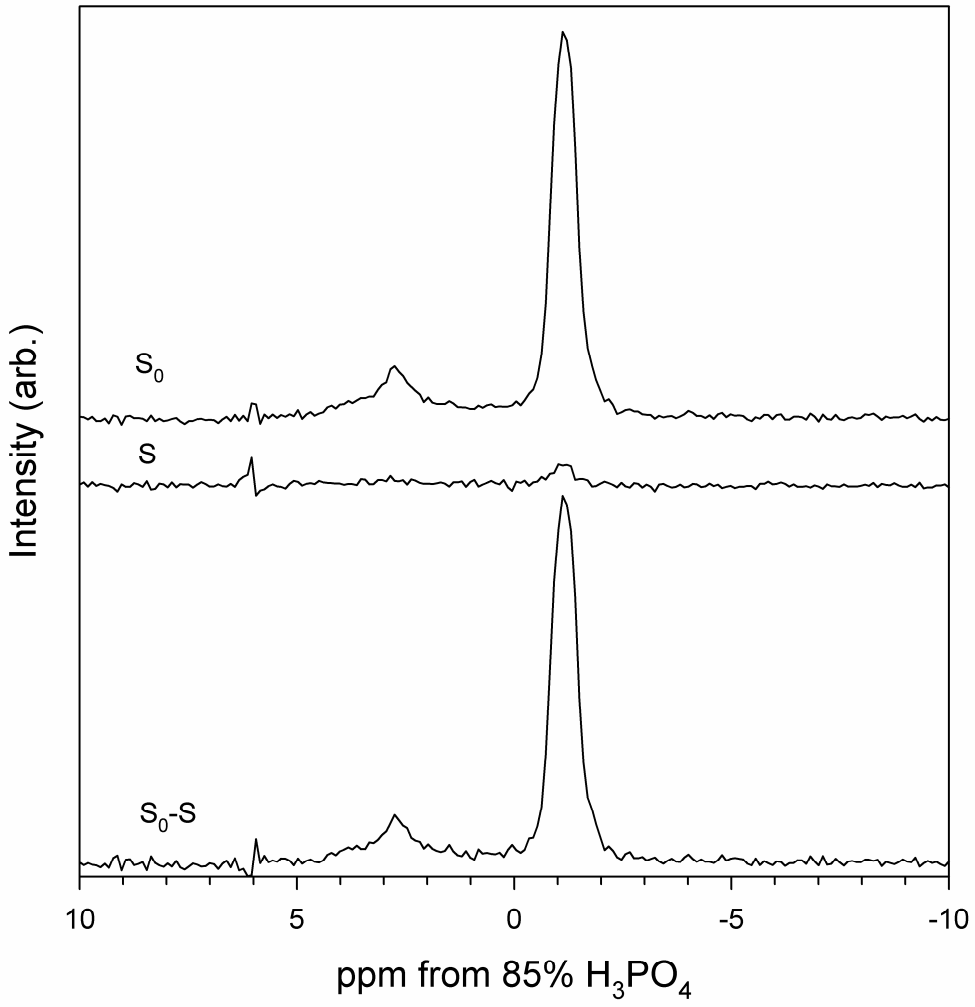

Figure 16. $^{31}P\{^{13}C\}$ CP/REDOR Dephasing curve for sample CA.STD.c13 calcite/phosphate coprecipitate.

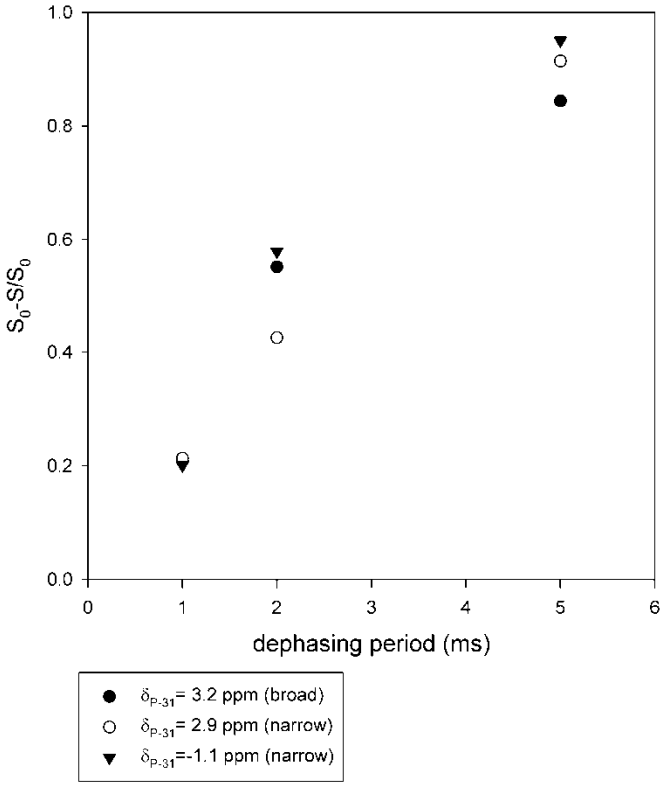

Figure 17. $^{31}P\{^{13}C\}$ CP/REDOR NMR spectral sets for sample MCA.STD.c13 aragonite/phosphate coprecipitate. Collected at 8 kHz spinning rate, 2 ms contact time, 2 s relaxation delay, 35117 acquisitions and 0.5 ms dephasing time (4 rotor periods).

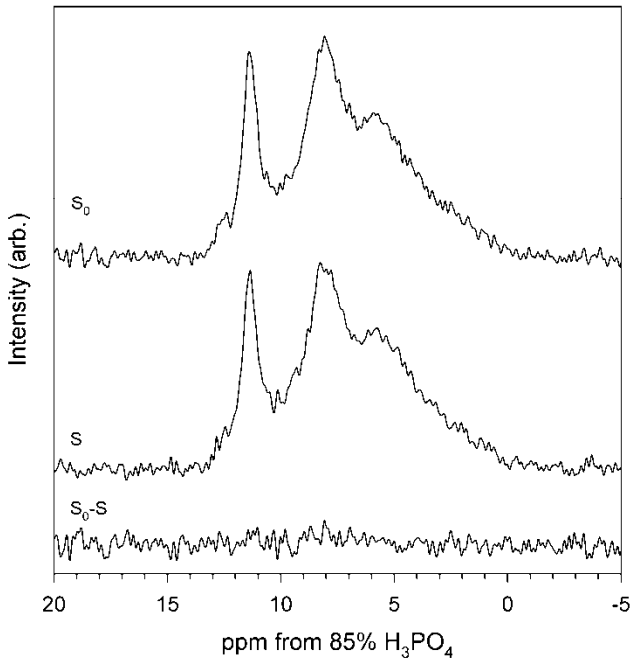

Figure 18. $^{31}P\{^{13}C\}$ CP/REDOR NMR spectral set for sample MCA.STD.c13 aragonite/phosphate coprecipitate. Collected at 8 kHz spinning rate, 2 ms contact time, 2 s relaxation delay, 27064 acquisitions and 1 ms dephasing time (8 rotor periods).

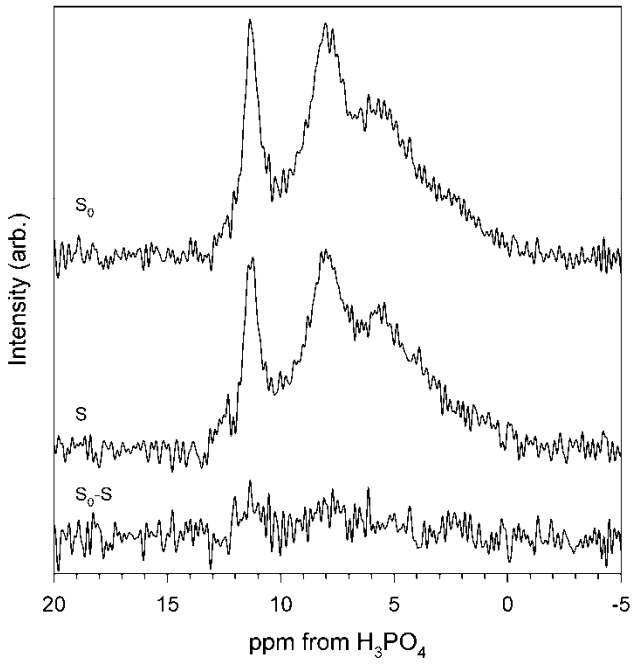

Figure 19. $^{31}P\{^{13}C\}$ CP/REDOR NMR spectral set for sample MCA.STD.c13 aragonite/phosphate coprecipitate. Collected at 8 kHz spinning rate, 2 ms contact time, 2 s relaxation delay, 21792 acquisitions and 1.5 ms dephasing time (12 rotor periods).

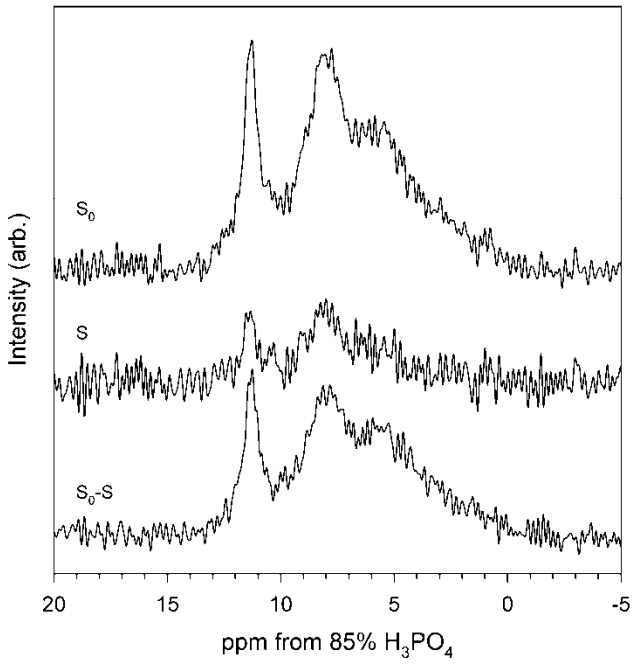

Figure 20. $^{31}P\{^{13}C\}$ CP/REDOR NMR spectral set for sample MCA.STD.c13 aragonite/phosphate coprecipitate. Collected at 8 kHz spinning rate, 2 ms contact time, 2 s relaxation delay, 16892 acquisitions and 2 ms dephasing time (16 rotor periods).

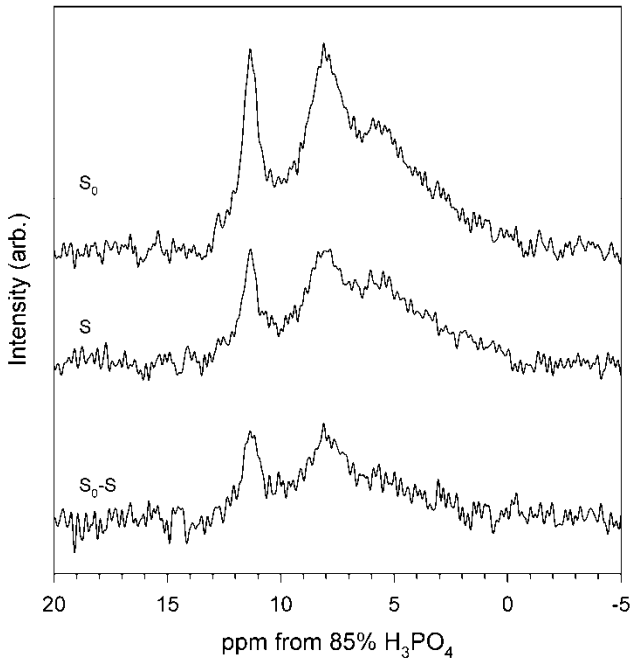

Figure 21. $^{31}P\{^{13}C\}$ CP/REDOR NMR spectral set for sample MCA.STD.c13 aragonite/phosphate coprecipitate. Collected at 8 kHz spinning rate, 2 ms contact time, 2 s relaxation delay, 25852 acquisitions and 3 ms dephasing time (24 rotor periods).

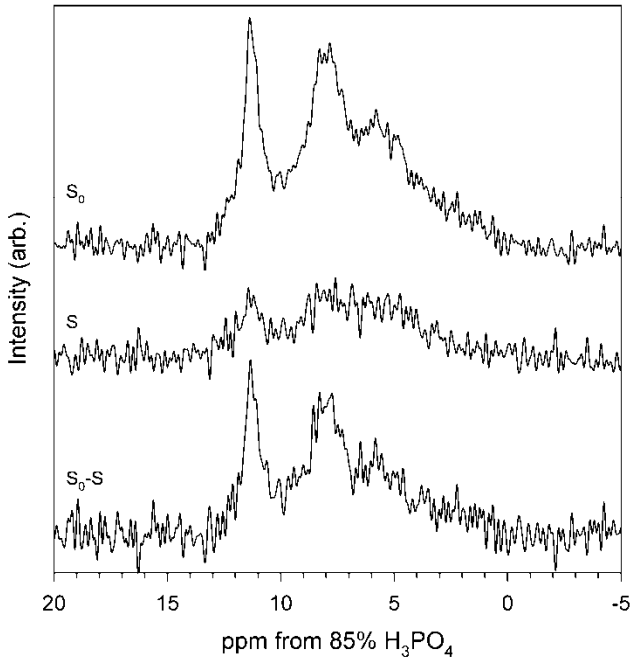

Figure 22. $^{31}P\{^{13}C\}$ CP/REDOR NMR spectral set for sample MCA.STD.c13 aragonite/phosphate coprecipitate. Collected at 8 kHz spinning rate, 2 ms contact time, 2 s relaxation delay, 23320 acquisitions and 4 ms dephasing time (32 rotor periods).

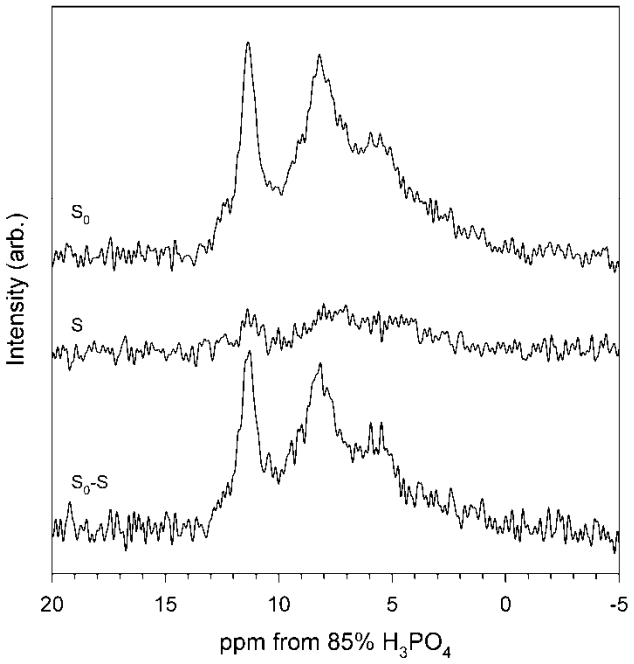

Figure 23. $^{31}P\{^{13}C\}$ CP/REDOR Dephasing Curve for sample MCA.STD.c13 aragonite/phosphate coprecipitate.

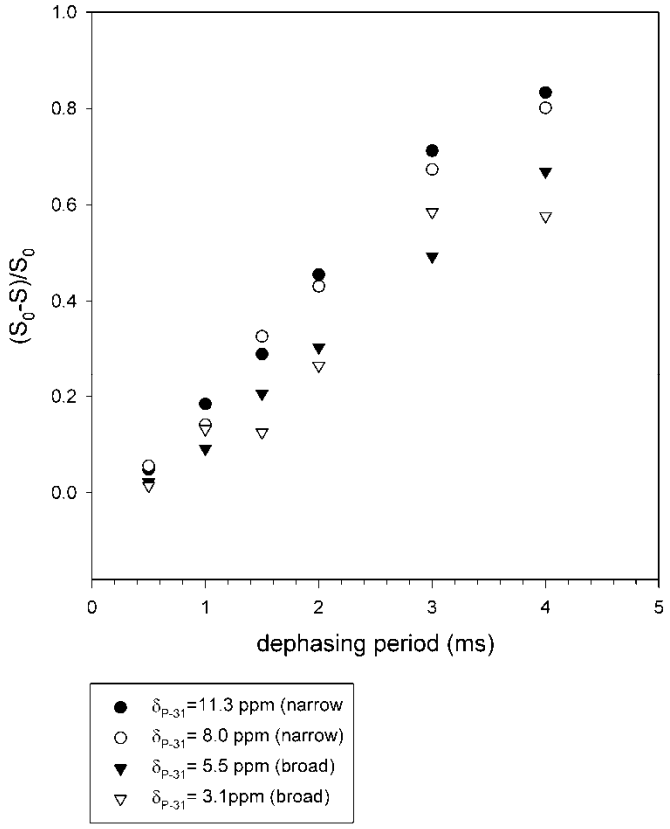

Figure 24. Least square fit of $^{31}P\{^{13}C\}$ CP/REDOR S_0 spectrum of MCA.STD.c13 aragonite/phosphate coprecipitate, with a sum of Gaussian curves corresponding to model 1. corresponding to 27064 acquisitions at a relaxation delay of 2 s. a) Observed spectrum, the same as that in Figure 18a; b) fitted spectral profile c) individual components corresponding to peaks at: $\delta_{P\text{-}31}$= 11.4, 0.6 ppm FWHM, $\delta_{P\text{-}31}$= 10.7, 2.6 ppm FWHM, $\delta_{P\text{-}31}$= 6.0, 3.1 ppm FWHM, $\delta_{P\text{-}31}$= 3.0, 4.0 ppm FWHM, $\delta_{P\text{-}31}$= 8.2, 1.7 ppm FWHM d) residuals, corresponding to (a)-(b).

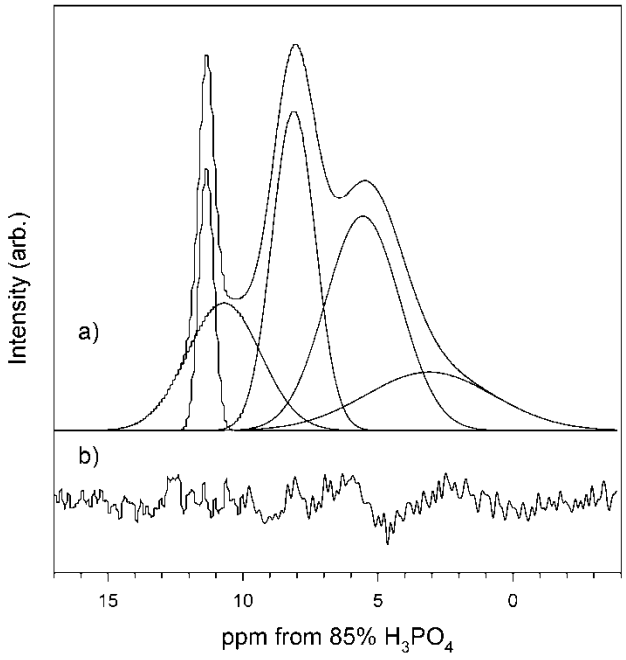

Figure 25. $^{31}P\{^{1}H\}$ HETCOR spectrum of the Ca.STD sample. The Spectrum was collected at a spin rate of 10 kHz, ^{31}P pulse width of 4 μs and ^{1}H pulse width of 3 μs and a pulse delay of 2 s for 800 acquisitions for each point in the t_1. The F1 spectral window was 50 kHz with 80 hyper complex points. The spectrum at the top of the 2D plot corresponds to ^{31}P, the spectrum on the right side corresponds to the ^{1}H.

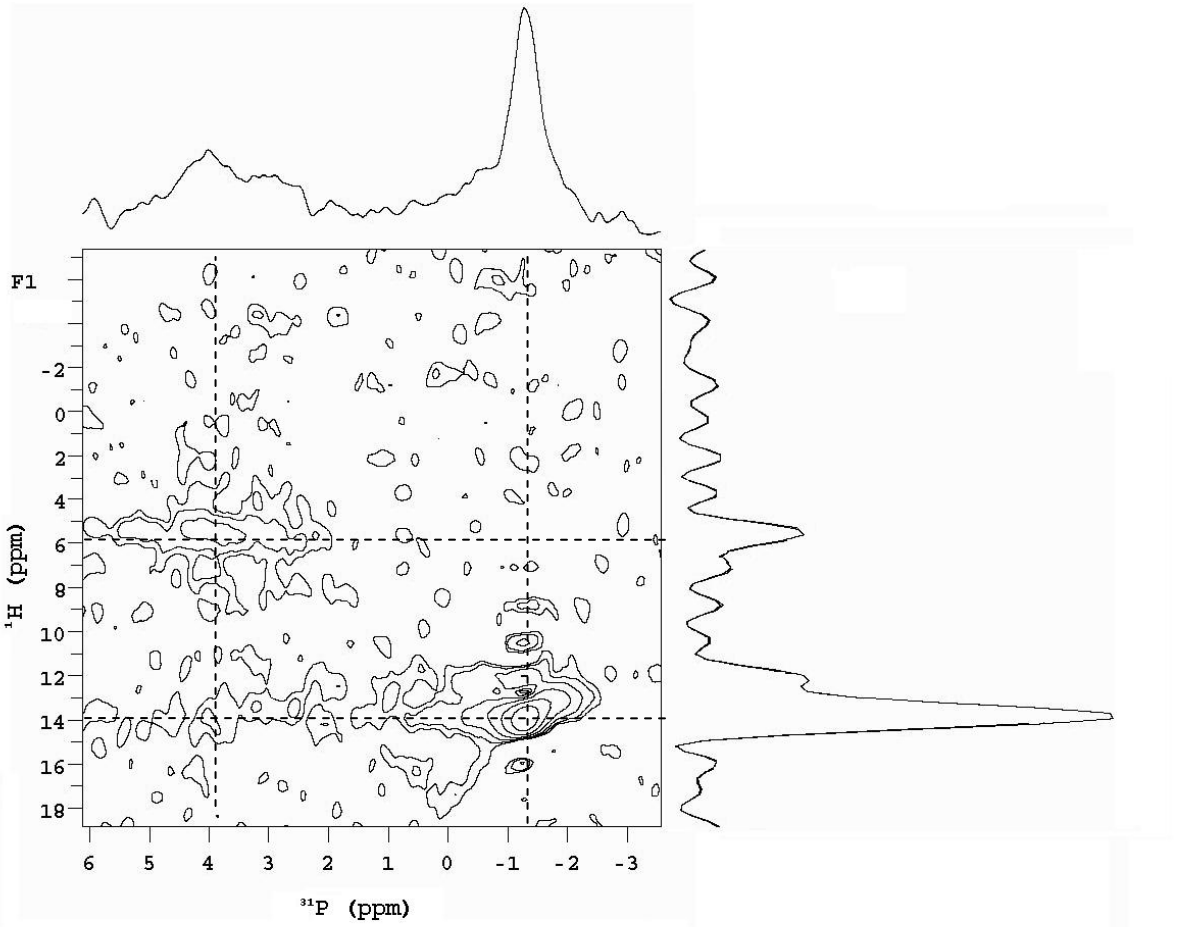

3.8. Tables

Table 1: Synthesis conditions for batch method calcite/phosphate coprecipitation experiments. All samples were synthesized in 2 L of solution, except for B.P9.2 which was synthesized in 1 L. Standard deviations are estimated from largest deviation observed with actual samples from the batch method.

Sample	Initial P Concentration (µM)	Concentration P in solution at 300 min (µM)	P in Solid (µmole)	Solid precipitated (g) (±20%)	Starting Ca^{2+} (moles)	µmole P $mole^{-1}$ Ca added to solution (± 20%)	µg P g^{-1} Solid (± 20%)	Vminteq Calculated Ca^{2+} Precipitated in Reaction (moles)
10˚C								
B.T10	6.35	0.63	11.44	0.42	0.050	2275	839	0.00046
25˚C								
B.P3.2	3.20	1.16	4.08	0.44	0.050	814	289	0.00098
B.STD	6.35	1.16	10.38	0.42	0.050	2063	760	0.00098
B.P9.2	9.20	0.32	6.04	0.21	0.025	2363	911	0.00098

Table 2: Synthesis conditions for preparation of calcite/phosphate coprecipitates using the constant addition method with varying phosphate concentrations. All experiments were conducted at 25˚C, with a pumping rate of 150µL/min for 9 hr (total of 81 mL from each syringe), pH 8.2 and 0.7 L initial solution volume. Entries with b.d.l. mean below detection limit of 0.06 mg L^{-1}, a.d.l. means above detection limit of 5.0 mg L^{-1}. Values of standard deviation listed with value are calculated from a mean, all other standard deviations are estimated from largest deviation observed with actual samples. Symbols for product determined by XRD C (calcite) and A (aragonite) some samples were not analyzed by XRD and dashes are placed in the box instead.

Sample	PO_4 added (µmoles)	Ca^{2+} added to syringe (moles)	Solid recovered (g) (± 20%)	PO_4 remaining in Solution (µmole L^{-1}) (± 20%)	% P in solid (± 20%)	µmole P $mole^{-1}$ Ca added to solution (± 20%)	µg P g^{-1} Solid (± 20%)	Product determined by XRD	Vminteq Calculated Ca^{2+} Precipitated in Reaction (moles)
CA.P.81	0.81	0.076	0.74	b.d.l	0.00	-	-	-	0.01348
CA.STD	19.40	0.076	0.51 ± 0.02	b.d.l	98.5 ± 3.6	2531	1167	C	0.01384
CA.P78	77.60	0.076	0.19	a.d.l	-	-	-	C	0.01348
CA.P485	485.10	0.076	0.14	a.d.l	-	-	-	-	0.01344

Table 3: Synthesis conditions for preparation of calcite/phosphate coprecipitates using the constant addition method with varying rates of addition. All experiments were conducted at 25˚C, Volume of solution pumped a total of 81 mL from each syringe, pH 8.2, 19.4 µmoles phosphate and 0.7 L initial solution volume. Entries with b.d.l. mean below detection limit of 0.06 mg L^{-1}. Values of standard deviation listed with value are calculated from a mean, all other standard deviations are estimated from largest deviation observed with actual samples. Symbols for product determined by XRD C (calcite) and A (aragonite) some samples were not analyzed by XRD and dashes are placed in the box instead.

Sample	Duration (hr) (syringe volume-81 mL)	Ca^{2+} added to syringe (moles)	Solid recovered (g) (± 20%)	PO_4 remaining in Solution (µmole L^{-1}) (± 20%)	% P in solid (± 20%)	µmole P $mole^{-1}$ Ca added to solution (± 20%)	µg P g^{-1} Solid (± 20%)	Product determined by XRD
CA.D0	0	0.076	0.11	10.74	52.33	1344	2866	-
CA.D1	1	0.076	0.21	b.d.l	98.5 ± 3.6	2531	2808	-
CA.D4.5	4.5	0.076	0.32 ± 0.04	2.42 ± 0.5	89.2 ± 2.3	2291	1665	-
CA.STD	9	0.076	0.51 ± 0.02	b.d.l	98.5 ± 3.6	2531	1167	C
CA.D51	51	0.076	0.66	3.16	85.98	2209	786	-
CA.D9.2w	9 hr sit 2 weeks	0.076	0.62	b.d.l	98.5 ± 3.6	2534	961	-

Table 4: Synthesis conditions for preparation of calcite/phosphate coprecipitates using the constant addition method with varying temperatures. All experiments were conducted with a pumping rate of 150 µL/min for 9 hr (total of 81 mL from each syringe), pH 8.2, 19.4 µmoles phosphate and 0.7 L initial solution volume. Entries with b.d.l. mean below detection limit of 0.06 mg L^{-1}. Values of standard deviation listed with value are calculated from a mean, all other standard deviations are estimated from largest deviation observed with actual samples. Symbols for product determined by XRD C (calcite) and A (aragonite).

Sample	Temperature (˚C)	Ca^{2+} added to syringe (moles)	Solid recovered (g) (± 20%)	PO_4 remaining in Solution (µmole L^{-1}) (± 20%)	% P in solid (± 20%)	µmole P $mole^{-1}$ Ca added to solution (± 20%)	µg P g^{-1} Solid (± 20%)	Product determined by XRD
CA.T10c	10	0.076	0.31	0.63	97.20	2522	1869	C
CA.STD	25	0.076	0.51 ± 0.02	b.d.l	98.5 ± 3.6	2531	1167	C
CA.T40c	40	0.076	0.43	b.d.l	98.5 ± 3.6	2533	1367	C
CA.T80c	80	0.076	0.62	0.63	97.20	2498	940	A+ C (m)

Table 5: Synthesis conditions for preparation of calcite/phosphate coprecipitates using the constant addition method with varying pH. All experiments were conducted at 25˚C, with a pumping rate of 150 µL/min for 9 hr (total of 81 mL from each syringe), 19.4 µmoles phosphate and 0.7 L initial solution volume. Entries with b.d.l. mean below detection limit of 0.06 mg L^{-1}. Values of standard deviation listed with value are calculated from a mean, all other standard deviations are estimated from largest deviation observed with actual samples. Symbols for product determined by XRD C (calcite) and A (aragonite).

Sample	pH	Ca^{2+} added to syringe (moles)	Solid recovered (g) (± 20%)	PO_4 remaining in Solution (µmole L^{-1}) (± 20%)	% P in solid (± 20%)	µmole P $mole^{-1}$ Ca added to solution (± 20%)	µg P g^{-1} Solid (± 20%)	Product determined by XRD
CA.STD	8.2	0.076	0.51 ± 0.02	b.d.l	98.5 ± 3.6	2531	1167	C
CA.PH9.4	9.4	0.076	1.03	1.26	94.39	2425	550	C

Table 6: Synthesis conditions for preparation of calcite/phosphate coprecipitates using the constant additions method with varying Mg^{2+} concentrations. All experiments were conducted at 25˚C, with a pumping rate of 150 µL/min for 9 hr (total of 81 mL from each syringe), pH 8.2, 19.4 µmoles phosphate added and 0.7 L initial solution volume. Entries with b.d.l. mean below detection limit of 0.06 mg L^{-1}. Values of standard deviation listed with value are calculated from a mean, all other standard deviations are estimated from largest deviation observed with actual samples. Symbols for product determined by XRD C (calcite) and A (aragonite) some samples were not analyzed by XRD and dashes are placed in the box instead.

Sample	Mg (mmole)	Ca^{2+} added to syringe (moles)	Solid recovered (g) (± 20%)	PO_4 remaining in Solution (µmole L^{-1}) (± 20%)	% P in solid (± 20%)	µmole P $mole^{-1}$ Ca added to solution (± 20%)	µg P g^{-1} Solid (± 20%)	Product determined by XRD	Vminteq Calculated Ca^{2+} Precipitated in Reaction (moles)
MCA.Mg.2	0.2	0.076	0.2672	b.d.l	98.6 ± 0.07	2525	2217	C	0.00922
MCA.Mg2	2	0.076	0.3006	4.44	77.09	1981	1541	-	0.00091
MCA.STD	10	0.076	0.32573	b.d.l	98.6 ± 0.07	2520	1819	C	0.00665
MCA.Mg20	20	0.076	0.1671	7.53	61.21	1573	2201	-	-

Table 7: Synthesis conditions for preparation of calcite/phosphate coprecipitates using the constant addition method with Mg^{2+} and varying rates of addition. All experiments were conducted at 25˚C, with a pumping rate of 150 µL/min for 9 hr (total of 81 mL from each syringe), pH 8.2, 10 mM $MgSO_4$ in the initial solution, 19.4 µmoles phosphate added and 0.7 L initial solution volume. Entries with b.d.l. mean below detection limit of 0.06 mg L^{-1}. Values of standard deviation listed with value are calculated from a mean, all other standard deviations are estimated from largest deviation observed with actual samples. Symbols for product determined by XRD C (calcite) and A (aragonite) some samples were not analyzed by XRD and dashes are placed in the box instead.

Sample	Pumping Time (hr)	Ca^{2+} added to syringe (moles)	Solid recovered (g) (± 20%)	PO_4 remaining in Solution (µmole L^{-1}) (± 20%)	% P in solid (± 20%)	µmole P $mole^{-1}$ Ca added to solution (± 20%)	µg P g^{-1} Solid (± 20%)	Product determined by XRD
MCA.D0	0	0.076	-	9.25	52.32	1344	-	-
MCA.D4.5	4.5	0.076	0.22326	7.98	58.86	1506	1584	C
MCA.STD	9	0.076	0.32573	b.d.l	98.6 ± 0.07	2520	1819	C

Table 8: Synthesis conditions for preparation of calcite/phosphate coprecipitates using the constant addition method with Mg^{2+} and varying temperature and pH. All experiments were conducted with 81 mL of solution pumped from each syringe, 10 mM $MgSO_4$ in the initial solution, 19.4 μmoles phosphate added and 0.7 L initial solution volume. Entries with b.d.l. mean below detection limit of 0.06 mg L^{-1}. Values of standard deviation listed with value are calculated from a mean, all other standard deviations are estimated from largest deviation observed with actual samples. Symbols for product determined by XRD C (calcite) and A (aragonite) some samples were not analyzed by XRD and dashes are placed in the box instead.

Sample	Pumping Time (hr)	Temperature (˚C)	pH	Ca^{2+} added to syringe (moles)	Solid recovered (g) (± 20%)	PO_4 remaining in Solution (μmole L^{-1}) (± 20%)	% P in solid (± 20%)	μmole P $mole^{-1}$ Ca added to solution (± 20%)	μg P g^{-1} Solid (± 20%)	Product determined by XRD
MCA.T10c	9	10	8.2	0.076	0.1328	14.87	23.35	600	1056	-
MCA.STD	9	25	8.2	0.076	0.32573	b.d.l	98.6 ± 3.6	2520	1844	C
MCA.T80c	9	80	8.2	0.076	0.5652	1.54	17.86	2363	979	A + C (m)
MCA.T80c.D0	0	80	8.2	0.076	0.5894	b.d.l	98.6 ± 0.07	2531	1005	A + C (m)
MCA.PH9.4	0	25	9.4	0.076	1.0283	b.d.l	98.6 ± 0.07	2533	576	-

Table 9: Peak intensities for ^{31}P single-pulse (SP) NMR spectra of calcite/phosphate coprecipitates synthesized using the batch method. Estimated values for standard deviation are calculated from four independent fits.

			Relative Intensities (±0.04)	
Sample	Initial Phosphate Concentration (μM)	Temperature (˚C)	3.2 ppm (broad)	2.6 ppm (narrow)
B.T10	6.35	10	0.61	0.39
B.STD	6.35	25	0.61	0.39
B.P3.2	3.2	25	0.62	0.38

Table 10: ^{31}P single pulse NMR Peak positions and intensities for calcite/phosphate coprecipitates with varying phosphate concentrations. All samples were prepared at 25˚C, with a 150µL/min pumping rate for 9 hr (total of 81 mL from each syringe), pH 8.2 and 0.7 L initial solution volume.

		Relative Intensities (±0.04)			
Sample	µg P g^{-1} Solid (± 20%)	-1.2 ppm (narrow)	2.9 ppm (narrow)	3.1 ppm (broad)	2.5 ppm (broad)
CA.P.81	-	-	-	-	-
CA.STD	1167	0.42	0.14	0.44	-
CA.P78	-	0.24	0.24	0.52	-
CA.P485	-	0.002	-	-	0.998

Table 11: ^{31}P single pulse NMR Peak positions and intensities for calcite/phosphate coprecipitates with varying rates of addition. All samples were prepared at 25˚C, volume of solution pumped 81 mL from each syringe, pH 8.2, 19.4 µmoles phosphate added and 0.7 L initial solution volume.

		Relative Intensities (±0.04)		
Sample	µg P g^{-1} Solid (± 20%)	-1.2 ppm (narrow)	2.9 ppm (narrow)	3.1 ppm (broad)
CA.T10c	1869	0.46	-	0.54
CA.STD	1167	0.42	0.14	0.44
CA.T80c	940	0.56	0.05	0.39

Table 12: ^{31}P single pulse NMR Peak positions and intensities for calcite/phosphate coprecipitates with varying temperatures. All samples were prepared with a pumping rate of 150 µL/min for 9 hr (total of 81 mL from each syringe), pH 8.2, 19.4 µmoles phosphate added and 0.7 L initial solution volume.

		Relative Intensities (±0.04)		
Sample	µg P g^{-1} Solid (± 20%)	-1.2 ppm (narrow)	2.9 ppm (narrow)	3.1 ppm (broad)
CA.T10c	1869	0.45	0.13	0.43
CA.STD	1167	0.42	0.14	0.44
CA.T80c	940	0.56	0.05	0.39

Table 13: ^{31}P single pulse NMR Peak positions and intensities for calcite/phosphate coprecipitates with varying pH. All samples were prepared at 25˚C, with a pumping rate of 150 µL/min for 9 hr (total of 81 mL from each syringe), 19.4 µmoles phosphate added and 0.7 L initial solution volume.

		Relative Intensities (±0.04)			
Sample	µg P g^{-1} Solid (± 20%)	-1.2 ppm (narrow)	2.9 ppm (narrow)	3.1 ppm (broad)	0.38 ppm (broad)
CA.STD	1167	0.42	0.14	0.44	-
CA.PH9.4	550	-	-	0.42	0.58

Table 14: ^{31}P single pulse NMR Peak positions and intensities for calcite/phosphate coprecipitates with Mg^{2+} using varying magnesium concentrations. All samples were prepared at 25˚C, with a pumping rate of 150 µL/min for 9 hr (total of 81 mL from each syringe), pH 8.2, 19.4 µmoles phosphate added and 0.7 L initial solution volume.

		Relative Intensities								
		Broad			Narrow			Narrow		
Sample	µg P g^{-1} Solid (± 20%)	δ_P	Width	Relative Intensity	δ_P	Width	Relative Intensity	δ_P	Width	Relative Intensity
CA.STD	1167	3.1	2.6	0.44	2.9	0.6	0.14	-1.2	0.6	0.42
MCA.Mg.2	2217	3.8	2.8	0.5	2.8	0.7	0.14	-1.3	0.6	0.36
MCA.STD	1819	3.7	2.8	0.72	2.8	0.6	0.28	-	-	-
MCA.Mg20	2201	3.8	2.8	0.82	2.8	0.7	0.18	-	-	-

Table 15: ^{31}P single pulse Peak positions and intensities for calcite/phosphate coprecipitates with Mg^{2+} using varying rates of addition. All samples were prepared at 25˚C, volume of solution pumped 81 mL from each syringe, pH 8.2, 10 mM Mg^{2+} in initial solution, 19.4 µmoles phosphate added and 0.7 L initial solution volume.

		Relative Intensities (±0.04)		
Sample	µg P g^{-1} Solid (± 20%)	-1.3 ppm (narrow)	2.8 ppm (narrow)	3.8 ppm (broad)
MCA.D0	-	0.08	0.18	0.74
MCA.STD	1819	-	0.28	0.72

Table 16: ^{31}P single pulse peak positions and intensities for calcite/phosphate coprecipitates with Mg^{2+} using varying temperatures and pH. All samples were prepared with a volume of solution pumped 81 mL from each syringe, 10 mM Mg^{2+} in initial solution, 19.4 μmoles phosphate added and 0.7 L initial solution volume.

		Relative Intensities (±0.04)					
Sample	μg P g^{-1} Solid (± 20%)	-1.3 ppm (narrow)	2.8 ppm (narrow)	3.8 ppm (Broad)	11.5 ppm (narrow)	8.5 ppm (narrow)	5.8 ppm (broad)
MCA.T10c	1056	-	0.27	0.73	-	-	-
MCA.STD	1844	-	0.28	0.72	-	-	-
MCA.T80c	979	-	-	-	0.27	0.18	0.55
MCA.PH9.4	576	-	0.26	0.74	-	-	-

Bibliography

1. Aue, W.P., et al., Solid-State Phosphorus-31 Nuclear Magnetic Resonance Studies of Synthetic Solid Phases of Calcium Phosphate: Potential Models of Bone Mineral. Biochemistry, 1984. 23: p. 6110-6114.

2. Aydin, I., et al., Determination of mineral phosphate species in sedimentary phosphate rock in Mardin, SE Anatolia, Turky by sequential extraction. Microchemical Journal, 2009. 91: p. 63-69.

3. Baldini, J.U., F. McDermott, and I.J. Fairchild, Structure of the 8200-Year Cold Event Revealed by a Speleothem Trace Element Record. Science, 2002. 296(5576): p. 2203-2206.

4. Belton, P.S., R.K. Harris, and P.J. Wilkes, Solid-state 31P NMR studies of synthetic inorganic calcium phosphates. J. Phys. Chem. Solids, 1988. 49: p. 21-27.

5. Brasier, A.T., Searching for travertines, calcretes and speleothems in deep time: Processes appearances, predictions and the impact of plants. Earth-Science Reviews, 2011. 104: p. 213-239.

6. Brooks, R., L.M. Clark, and E.F. Thurston, Calcium Carbonate and Its Hydrates. Philosophical Transactions of the Royal Society of London. Series A, Mathematical and Physical Sciences, 1950. 243(861): p. 145-167.

7. Bryant, J.D., et al., Oxygen isotope partitioning between phosphate and carbonate in mammalian apatite. Geochemica et Cosmochimica Acta, 1996. 60(24): p. 5145-5148.

8. Cade-Menun, B., Characterizing phosphorus in environmental and agricultural samples by 31P nuclear magnetic resonance spectroscopy. Talanta, 2005. 66: p. 359-371.

9. Cao, X. and W. Harris, Carbonate and Magnesium Interactive Effect on Calcium Phosphate Precipitation. Environ. Sci. Technol., 2008. 42: p. 436-442.

10. Cao, X., et al., Inhibition of calcium phosphate precipitation under environmentally-relevant conditions. Science of the Total Environment, 2007. 383: p. 205-215.

11. Carr, H.Y. and E.M. Purcell, Effects of Diffusion on Free Precession in Nuclear Magnetic Resonance Experiments. Physical Review, 1954. 94(3): p. 630-638.

12. Clark, L.L., E.D. Ingall, and R. Benner, Marine Organic Phosphorus Cycling: Novel Insights From Nuclear Magnetic Resonance. American Journal of Science, 1999. 2999: p. 724-737.

13. de Groot, C.J., Some remarks on the presence of organic phosphates in sediments. Hydrobiologia, 1990. 207: p. 303-309.

14. de Groot, C.J. and H.L. Golterman, Sequential fractionation of sediment phosphate. Hydrobiologia, 1990. 192: p. 143-148.

15. de Groot, C.J. and H.L. Golterman, Sequential fractionation of sediment phosphate. Hydrobiologia, 1990. 192: p. 143-148.

16. Dolgaleva, I.V., et al., Modeling the Effect of pH on the Calcite Dissolution Kinetics. Theoretical Foundations of Chemical Engineering, 2005. 39(6): p. 614-621.

17. Dove, P.M. and F.J. Hochella, Calcite precipitation mechanisms and inhibition by orthophosphate: In situ observations by Scanning Force Microscopy. Geochimica et Cosmochimica Acta, 1993. 57: p. 705-714.

18. Economou, E.D. and T.C. Vaimakis, Benefication of Greek Calcareous Phosphate Ore Using Acetic Acid Solutions. Ind. Eng. Chem. Res., 1997. 36: p. 1491-1497.

19. Economou, E.D., T.C. Vaimakis, and E.M. Papmichael, Kinetics of Dissolution of the Carbonate Minerals of Phosphate Ores Using Dilute Acetic Acid Solutions. Journal of Colloid and Interface Science, 1998. 201: p. 164-171.

20. Eichele, K., HBA32, in WinSolids. 1995.

21. Elliott, H.A. and G.A. Brown, Comparative evaluation of NTA and EDTA for extractive decontamination of Pb-polluted soils. Water, Air & Soil Pollution, 1989. 45: p. 361-369.

22. Fairchild, I.J., et al., Annual to sub-annual resolution of multiple trace-element trends in speleothems. Journal of Geological Society, 2001. 158(5): p. 831-841.

23. Fairchild, I.J. and P.C. Treble, Trace elements in speleothems as recorders of environmental change. Quaternary Science Reviews, 2009. 28: p. 449-468.

24. Feng, J., et al., NMR Spectroscopy of Citrate in Solids: Cross-Polarization Kinetics in Weakly Coupled Systems. Magnetic Resonance in Chemistry, 2008. 46: p. 408-417.

25. Feng, J., et al., Observation of bicarbonate in calcite by NMR spectroscopy. Am. Mineral, 2006. 91: p. 957-960.

26. Fredd, C.N. and H.S. Fogler, The Influence of chelating Agents on the Kinetics of Calcite Dissolution. Journal of Colloid and Interface Science, 1998. 204: p. 187-197.

27. Fredd, C.N. and H.S. Fogler, The kinetics of calcite dissolution in acetic acid solutions. Chemical Engineering Sciences, 1998. 53(22): p. 3863-3874.

28. Frisia, S. and A. Borsato, Developments in Sediments. Carbonates in Continental Settings, ed. A.J. Van Loon. Vol. 61. 2010, Netherlands: Elsevier.

29. Fulmer, M.T., et al., Measurements of the solubilities and dissolution rates of several hydroxyapatites. Biomaterials, 2002. 23: p. 751-755.

30. Glimcher, M.J., et al., Recent studies of bone minerals: Is the amorphous calcium phosphate theory valide? J. Crystal Growth, 1981. 53: p. 100-119.

31. Golterman, H.L., Fractionation of sediment phosphate with chelating compounds: a simplification, and comparison with other methods. Hydrobiologia, 1996. 335: p. 87-95.

32. Griffin, R.A. and J.J. Jurinak, The Interaction of Phosphate with Calcite. Soil Sci. Soc. Amer. Proc, 1973. 37: p. 847-850.

33. Hahn, E.L., Spin Echoes. Phys. Rev., 1950. 80(4): p. 580-601.

34. Harris, D.C., Quatitiatve Chemical Analysis. 6 ed, ed. J. Fiorillo. 2003, New York: W.H. Freeman and Company. 744.

35. Hartmann, P., J. Vogel, and B. Schnabel, The Influence of Short-Range Geometry on the 31P Chemical-Shift Tensor in Protonated Phosphates. Journal of Magnetic Resonance, Series A, 1994. 111(1): p. 110-114.

36. Hartmann, S.R. and E.L. Hahn, Nuclear Double Resonance in the Rotating Frame. Phys. Rev., 1962. 128(5): p. 2042-2053.

37. Hayashi, S. and K. Hayamizu, High-Resolution Solid-State 31P NMR of Alkali Phosphates. Bull. Chem. Soc. Jpn., 1989. 62: p. 3061-3068.

38. Herzfeld, J. and A.E. Berger, Sideband intensities in NMR spectra of samples spinning at magic angle. J. Chem. Phys., 1980. 73(12): p. 6021-6030.

39. Hieltjes, A.H.M. and L. Lijklema, Fractionation of Inorganic Phosphates in Calcareous Sediments. Journal of Environ Qual., 1980. 9: p. 405-407.

40. Hill, C.A., Mineralogy of Kartchner Caverns, Arizona. Journal of Cave and Karst Studies, 1999. 61(2): p. 73-78.

41. Hinedi, Z.R., et al., A 31P and 1H MAS NMR study of phosphate sorption onto calcium carbonate. Journal of Colloid and Interface Science, 1992. 152(1): p. 141-160.

42. House, W.A., Inhibition of Calcite Crystal Growth by Inorganic Phosphate. Journal of Colloid and Interface Science, 1987. 119(2): p. 505-511.

43. House, W.A. and L. Donaldson, Adsorption and Coprecipitation of Phosphate on Calcite. Journal of Colloid and Interface Science, 1986. 112(2): p. 309-324.

44. Houwen, J.A.M.V.D. and E. Valsami-Jones, The Application of Calcium Phosphate Precipitation chemistry to Phosphorus Recovery: The Influence of Organic Ligands. Environmental Technology, 2001. 22(11): p. 1325-1335.

45. Hu, C., et al., Effects of longterm wastewater application on chemcail properties and phosphorus adsorption capactiy in soils of wastewater land treament systems. Environ. Sci. Technol., 2005. 39: p. 7240-7245.

46. Huang, Y., et al., Seasonal variation in Sr, Mg and P in modern speleothems (Grotta di Ernesto, Italy). Chemical Geology, 2001. 175: p. 429-448.

47. Hunt, C.P., et al., Effect of citraate-bicarbonate-dithionite treatment on fine-grained magnetite and maghemite. Earth and Planetary Science Letters, 1995. 130: p. 87-94.

48. Ishikawa, M. and M. Ichikuni, Coprecipitation of phosphate with calcite. Geochemical Journal, 1981. 15: p. 283-288.

49. Jeppsson, L., R. Anehus, and D. Fredholm, The Optimal Acetate Buffered Acetic Acid Technique for Extracting Phosphatic Fossils. Journal of Paleontology, 1999. 73(5): p. 964-972.

50. Jimenez-Lopez, C., et al., Chemical, mineralogical and isotope behavior, and phase transformation during the precipitation of calcium carbonate minerals from intermediate ionic solution at 25 degrees C. Geochimica et Cosmochimica Acta, 2001. 65(19): p. 3219-3231.

51. Kallay, N., et al., Calorimetric Investigation of Kinetics of Solid Phase Dissolution: Calcium Carbonate Dissolution in Aqueous EDTA Solution. Journal of Colloid and Interface Science, 1997. 188: p. 68-74.

52. Kanel, J.D. and J.W. Morse, The chemistry of orthophosphate uptake from seawater on to calcite and aragonite. Geochimica et Cosmochimica Acta, 1978. 42: p. 1335-1340.

53. Karageorgiou, K., M. Paschalis, and G.N. Anastassakis, Removal of phosphate species from solution by adsorption onto calcite used as natural adsorbent. Journal of Hazardous Marterials, 2007. A139: p. 447-452.

54. Koch, P.L., Isotopic reconstruction of past continental environments. Annual Review of Earth and Planetary Sciences, 1998. 26: p. 573-613.

55. Koch, P.L., N. Tuross, and M.L. Fogel, The Effects of Sample Treatment and Diagenesis on the Isotopic Integrity of Carbonate in Biogenic Hydroxylapatite. Journal of Archaelogical Science, 1997. 24: p. 417-429.

56. Koch, P.L., J.C. Zachos, and D.L. Dettman, Stable isotope stratigraphy and paleoclimatology of the Paleogene Bighorn Basin (Wyoming, USA). Paleogeography, Paleoclimatology, Palaeoecology, 1995. 115(1-4): p. 61-69.

57. Kolodziejski, W. and J. Klinowski, Kinetics of cross-polarization in solid-state NMR: A guide for chemists. Chemical Reviews, 2002. 102: p. 613-628.

58. Koutsoukos, P.G. and G.H. Nancollas, Crystal Growth of Calcium Phosphates-Epitaxial Considerations. Journal of Crystal Growth, 1981. 53: p. 10-19.

59. Krueger, H.W., Exchange of carbon with biological apatite. Journal of Archaelogical Science, 1991. 18: p. 355-361.

60. LaVigne, M., et al., Skeletal P/Ca tracks upwelling in Gulf of Panama coral: Evidence for a new seawater phosphate proxy. Geophysical Research Letters, 2008. 35(L05604).

61. Lee-Thorp, J.A. and J.v.d.M. Nikolaas, Aspects of the chemistry of modern and fossil biological apatites. Journal of Archaelogical Science, 1991. 18(3): p. 343-354.

62. Lehmann, J., et al., Long-term dynamics of phosphorus forms and retention in mature-amended soils. Environ. Sci. Technol., 2005. 39: p. 6672-6680.

63. Lucotte, M. and B. D'Anglejan, A comparison of several methods for the determination of iron hydroxides and associated orthophoshates in estuarine particulate matter. Chem. Geol., 1985. 48: p. 257-264.

64. Mason, H.E., et al., Phophorus Speciation in Calcite Speleothems Determined from Solid-State NMR Spectroscopy. Earth and Planetary Science Letters, 2007. 254: p. 313-322.

65. Mason, H.E., et al., Phosphorus speciation in calcite speleothems determined from solid-state NMR spectroscopy. Earth and Planetary Science Letters, 2007. 254(3-4): p. 313-322.

66. Mason, H.E., et al., Phosphate defects and apatite inclusions in coral skeletal aragonite revealed by solid-state NMR spectroscopy. Geochemica et Cosmochimica Acta, In review.

67. McDowell, R.W., et al., Analysis of Potentially Mobile Phosphorus in Arable Soils Using Solid State Nuclear Magnetic Resonance. J. Environ. Qual., 2002. 31: p. 450-456.

68. Mehra, O.P. and M.L. Jackson, Iron oxide removal from soils and clays by a dithionite-citrate system buffered with sodium bicarbonate. Clays Clay Miner., 1960. 7: p. 317-327.

69. Meyer, H.J., The influence of Impurities on the growth rate of calcite. Journal of Crystal Growth, 1984. 66: p. 639-646.

70. Millero, F., et al., Adsorption and Desorption of Phosphate on Calcite and Aragonite in Seawater. Aquatic Geochemistry, 2001. 7: p. 33-56.

71. Montagna, P., et al., Phosphorus in cold-water corals as a proxy for seawater nutrient chemistry. Science, 2006. 312: p. 1788-1791.

72. Morse, J.W. and R.S. Arvidson, The dissolution kinetics of major sedimentary carbonate minerals. Earth-Science Reviews, 2002. 58: p. 51-84.

73. Mucci, A., Growth kinetics and composition of magnesium calcite overgrowths precipitated from seawater: Quantitative influence of orthophosphate ions. Geochemica et Cosmochimica Acta, 1986. 50: p. 2255-2265.

74. Murphy, T.P., K.J. Hall, and I. Yesaki, Coprecipitation of Phosphate with Calcite in a Naturally Eutrophic Lake. Limnology and Oceanography, 1983. 28(1): p. 58-69.

75. Papassiopi, N., S. Tambouris, and A. Kontopoulos, Removal of heavy metals from calcareous contaminated soils by EDTA leaching. Water, Air & Soil Pollution, 1997. 109(1-4): p. 1-15.

76. Plant, L.J. and W.A. House, Precipitation of calcite in the presence of inorganic phosphate. Colloids and Surfaces, 2002. 203: p. 143-153.

77. Pourpoint, F., et al., Calcium Phosphates and Hydroxyapatite: Solid-State NMR Experiments and First-Principles Calculations. Applied Magnetic Resonance, 2007. 32: p. 435-457.

78. Reddy, M.M., Crystallization of calcium carbonate in the presence of trace concentrations of phosphorus-containing anions. Journal of Crystal Growth, 1977. 41: p. 287-295.

79. Reeder, R.J., et al., Uranyl incorporation into calcite and aragonite: XAFS and luminescence studies. Environ. Sci. Technol., 2000. 34: p. 638-644.

80. Rothwell, W.P., J.S. Waugh, and J.P. Yesinowski, High-Resolution Variable-Temperature 31P NMR of Solid Calcium Phosphates. Journal of the American Chemical Society, 1980. 102(8): p. 2637-2644.

81. Ruttenberg, K.C., Development of a sequential extraction method for different forms of phosphorus in marine sediments. Limnology and Oceanography, 1992. 37(7): p. 1460-1482.

82. Saavedra, C., et al., Effects of Tillage on Phosphorus Release Potential in a Spanish Vertisol. Soil Sci. Soc. Am. J., 2007. 71 p. 56-63.

83. Salimi, M.H., J.C. Heughebaert, and G.H. Nancollas, Crystal Growth of Calcium Phosphates in the Presence of Magnesium Ions. Langmuir, 1985. 1: p. 119-122.

84. Sheikh, M.S., et al., Reduction of dietary phosphorus absorption by phosphorus binders. A theoretical, in vitro, and in vivo study. The Journal of Clinical Investigation, 1989. 83(1): p. 66-73.

85. Shen, G.T. and E.A. Boyle, Determination of lead, Cadmium and other trace metals in annually-banded corals. chemical Geology, 1988. 67(1-2): p. 47-62.

86. Sims, J., et al., Integrating soil phosphorus testing into environmentally best agricultural management practices. Journ of Environmental Quality, 2000. 29(60-71).

87. Sykes, G.A., M.J. Collins, and D.I. Walton, The significance of a geochemically isolated intracrystalline organice fraction within biominerals. Org. Geochem., 1995. 23(11/12): p. 1059-1065.

88. Tesoriero, A.J. and J.F. Pankow, Solid solution partitioning of Sr2+, Ba2+, and Cd2+ to calcite. Geochimica et Cosmochimica Acta, 1996. 60: p. 1053-1063.

89. Tessier, A., P.G.C. Campbell, and M. Bisson, Sequential extraction procedure for the speciation of particulate trace metals. Anal. Chem., 1979. 51: p. 844-851.

90. Treble, P.C., J. Chappell, and J.M.G. Shelley, Complex speleothem growth processes revealed by trance element mapping and scanning electron microscopy of annual layers. Geochemica et Cosmochimica Acta, 2005. 69: p. 4855-4863.

91. Tropp, J., N.C. Blumenthal, and J.S. Waugh, Phosphorus NMR study of solid amorphous calcium phosphate. J. Am. Chem. Soc., 1983. 105(1): p. 22-26.

92. Tseng, Y.-H., et al., High resolution 31P NMR study of octacalcium phosphate. Solid State Nuclear Magnetic Resonance, 2004. 26(2): p. 99-104.

93. Turner, B.L., N. Mahieu, and L.M. Condron, Phosphorus-31 Nuclear Magnetic Resonance Spectral Assignments of Phosphorus Compounds in Soil NaOH-EDTA Extracts. Soil Sci. Soc. Am. J., 2003. 67: p. 497-510.

94. Williams, J.D.H., H. Shear, and R.L. Thomas, Availability to Scenedesmus quadricauda of different forms of phosphorus in sedimentary materials from the Great Lakes. Limnology and Oceanography, 1980. 25(1): p. 1-11.

95. Yesinowski, J.P. and H. Eckert, Hydrogen Environments in Calcium Phosphates: 1H MAS NMR at High Spinning Speeds. J. Am. Chem. Soc., 1987. 109: p. 6274-6282.

96. Zhong, S.J. and A. Mucci, Calcite precipitation in seawater using a constant addition techinique: a new overalll reaction kinetic expression. Geochimica et Cosmochimica Acta, 1993. 57: p. 1409-1417.